REPORT DOCUMENTATION PAGE

Form Approved
OMB NO. 0704-0188

Public Reporting burden for this collection of information is estimated to average 1 hour per response, including the time for reviewing instructions, searching existing data sources, gathering and maintaining the data needed, and completing and reviewing the collection of information. Send comment regarding this burden estimates or any other aspect of this collection of information, including suggestions for reducing this burden, to Washington Headquarters Services, Directorate for information Operations and Reports, 1215 Jefferson Davis Highway, Suite 1204, Arlington, VA 22202-4302, and to the Office of Management and Budget, Paperwork Reduction Project (0704-0188,) Washington, DC 20503.

1. AGENCY USE ONLY (Leave Blank)	2. REPORT DATE	3. REPORT TYPE AND DATES COVERED
	2001	Final Progress 01 May 1998 to 30 April 2001

4. TITLE AND SUBTITLE
Final Progress Report on Wide-band Optical True-Time Delay and Adaptive Beamforming

5. FUNDING NUMBERS
DAAG55-98-1-0244

6. AUTHOR(S)
Wm. Randall Babbitt

7. PERFORMING ORGANIZATION NAME(S) AND ADDRESS(ES)
Physics Department, EPS 264
Montana State University
Bozeman, MT 59717-3840

8. PERFORMING ORGANIZATION REPORT NUMBER **WRB01-001**

9. SPONSORING / MONITORING AGENCY NAME(S) AND ADDRESS(ES)
U. S. Army Research Office
P.O. Box 12211
Research Triangle Park, NC 27709-2211

10. SPONSORING / MONITORING AGENCY REPORT NUMBER
37769.1-PH-DPS

11. SUPPLEMENTARY NOTES
The views, opinions and/or findings contained in this report are those of the author(s) and should not be construed as an official Department of the Army position, policy or decision, unless so designated by other documentation.

12 a. DISTRIBUTION / AVAILABILITY STATEMENT
Approved for public release; distribution unlimited.

20011113 107

13. ABSTRACT (Maximum 200 words)

The focus of the research under this ARO DEPSCoR grant is to explore and develop the inherent capabilities of optical coherent transient technology for creating true-time-delays up to several microseconds on signals with wide bandwidths far in excess of a gigahertz on optical waveforms. Coherent transient technology has the advantages that the delays are programmable with amplitude sensitive processing being performed simultaneously. The research effort explores the issues of implementing an optical coherent transient technology in the multi-gigihertz regime and works towards developing an adaptive beamforming system architecture that utilizes optical coherent transient technology. Progress includes development of chirped lasers and linear frequency chirped programming methods on bandwidths of more than 2 GHz, analysis of the continuous programming continuous processing dynamics and spectral filtering effects of the processing material, development of frequency stabilized Ti:Sapphire lasers and diode lasers for use in the evaluations. Also, initial evaluations of the adaptive beamforming architectures were carried out at CU. The thrust of our efforts went into development of multi-GHz OCT technologies, which allows final development of wide-band adaptive beamforming demonstrations.

14. SUBJECT TERMS	15. NUMBER OF PAGES
Optical Coherent Transients, Spatial-Spectral Holography, Spectral Holeburning True-Time Delay, Adaptive Beamforming, Phased Array Radar, Phased Array Communication, Optical Correlation, Optical processing	137
	16. PRICE CODE

17. SECURITY CLASSIFICATION OR REPORT	18. SECURITY CLASSIFICATION ON THIS PAGE	19. SECURITY CLASSIFICATION OF ABSTRACT	20. LIMITATION OF ABSTRACT
UNCLASSIFIED	UNCLASSIFIED	UNCLASSIFIED	UL

NSN 7540-01-280-5500

Standard Form 298 (Rev.2-89)
Prescribed by ANSI Std. 239-18
298-102

MEMORANDUM OF TRANSMITTAL

U.S. Army Research Office
ATTN: AMSRL-RO-BI (TR)
P.O. Box 12211
Research Triangle Park, NC 27709-2211

☐ Reprint (Orig + 2 copies)

☐ Technical Report (Orig + 2 copies)

☐ Manuscript (1 copy)

☒ Final Progress Report (Orig + 2 copies)

☐ Related Materials, Abstracts, Theses (1 copy)

CONTRACT/GRANT NUMBER: DAAG55-98-1-0244

REPORT TITLE: FINAL PROGRESS REPORT ON WIDE-BAND OPTICAL TRUE-TIME DELAY AND ADAPTICE BEAMFORMING

is forwarded for your information.

SUBMITTED FOR PUBLICATION TO (applicable only if report is manuscript):

Sincerely,

Wm. Randall Babbitt

Physics Department, EPS 264
Montana State University
Bozeman, MT 59717-3840

FINAL PROGRESS REPORT

(1) Foreword

The objective of our research effort is to study and develop an optical coherent transient true-time delay (OCT TTD) based adaptive beamforming system architecture capable of operating on signals with bandwidth in excess of a gigahertz. This work has been fulfilled by the joint effort of two research teams at Montana State University (MSU) and University of Colorado (UC through subcontract). The following materials present the final report of the project.

(2) Table of Contents

Statement of the problem studied	3
Summary of the most important results:	3
Broadband OCT TTD (MSU)	3
Photon echo adaptive array processing (CU)	12
Educational and Industrial Interactions	13
Publications and technical reports	14
Report of inventions (Patents Applications)	15
List of all participating scientific personnel	18
Bibliography	18
Appendices	19

(3) List of Appendixes and Illustrations

Appendixes

1. Interim report
2. Robert D. Peters " Programming high bandwidth true-time delays in an optical coherent transient material," graduate research report, Department of Physics, Montana State University (2001)
3. Randy Reibel, "Spectral filtering of amplitude or phase modulated carriers," graduate project report, Department of Physics, Montana State University (2000)
4. K. D. Merkel, W. R. Babbitt, K. E. Anderson, K. H. Wagner, "Variable-time-delay optical coherent transient signal processing," Opt. Lett. 24, 1386-1388 (1999).
5. Manuscript: Randy Reibel, Zeb Barber, Mingzhen Tian and Wm. Randy Babbitt, "Temporally overlapped linear frequency chirped programming for true-time delay amplification," submitted to Opt. Lett.
6. CU subcontract final report.

Illustrations

Figure 1. (a) Linear frequency chirped programming and (b) temporally overlapped linear frequency chirped programming
Figure 2. Measured echo delays vs. frequency offset for several chirp durations
Figure 3. (a) A chirped scan over a TTD grating created using the TOLFC method
(b) A zoom of a section of the grating showing the frequency spacing of the TTD.
Figure 4. (a) Experimental and (b) simulation results of grating accumulation dynamics with TOLFC's.
Figure 5. The simulated effects of a Gaussian filter such as the Tm:YAG 793 nm transition.
Figure 6. Experimental data showing PM signals turned into AM signals via the Tm:YAG 793 nm transition.
Figure 7. Simulated results for an airy transmissive filter acting to convert PM to AM.
Figure 8. Experimental PM to AM conversion shown using a 3.0 mm thick etalon.
Figure 9. Spectral gratings recorded and probed with un-stabilized (upper traces) and stabilized laser (lower traces).

(4) Statement of the problem studied

In this three-year project, we studied the application of optical coherent transient (OCT) processes to true-time-delay (TTD) and adaptive beamforming (ABF). We concentrated our demonstration in Tm^{3+}:YAG, an inhomogeneously broadened processing material which has the desired properties for advanced TTD and ABF systems. We proposed and studied several multi-gigahertz programming schemes and found a very attractive solution for programming broadband TTD gratings. This approach uses accumulated programming with two temporally overlapped, frequency offset, linear frequency chirps. In addition, we studied 1) the material dynamics for continuously programmed continuous processing, 2) the spectral filtering effects for amplitude and phase-modulated (AM and PM) RF signals, and 3) the delay range, delay resolution and bandwidth limitations. In order to meet the demands for high bandwidth programming, novel laser sources and amplification schemes were developed, which may have applications beyond OCT. A chirped external cavity diode laser (CECDL) with the capability of linear frequency chirps of more than 2 GHz within 1μs was developed and demonstrated. To achieve the required laser frequency stability for accumulated programming of TTD gratings, we designed and implement a frequency stabilization system for our cw Ti:Sapphire laser, which incorporated the locking of a regenerative spectral hole burned into the inhomogeneously broadened medium.

(5) Summary of the most important results:

Broadband OCT TTD (MSU)

We developed a novel TTD technique that will be used as the backbone for an adaptive beamforming system. This technique utilizes several desirable properties of linear frequency chirps, including the ability to program with temporally overlapped optical beams. This technique builds on the original work done on linear frequency chirps (LFCP's) by Dr. Kris Merkel in our lab at low bandwidths,[1] which was the first demonstration of programming TTD gratings with chirps. The benefits of this programming

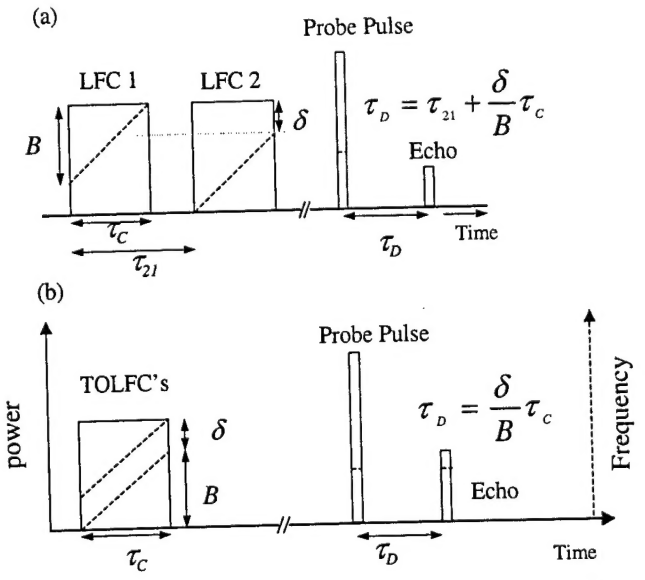

Figure 1. (a) Linear frequency chirped programming and (b) temporally overlapped linear frequency chirped programming. β, τ_c, δ and τ_d are chirp bandwidth, chirp time, frequency offset and delay, respectively.

technique include lower programming powers, picosecond timing resolutions, and the ability to use frequency tuning to directly control the delay of the signal. Figure 1 (a) shows how one can use LFCP's to program a spectral grating. We expanded upon this technique by removing the time delay from the LFCP's to create the TOLFC's shown in Fig. 1(b). In this method, the frequency offset then directly controls the time delay of the output echo signal.[2] Benefits of this approach include, 1) the ability to program with chirp lengths longer than the coherence time of the crystal, which elevates the restrict requirements on the chirp rate of the laser source, 2) greatly simplifies the optical architecture, 3) relaxes of the laser stability requirements for accumulation of spectral gratings, and 4) enables control of broadband spectral structure with narrow band acousto-optic modulators by frequency offset. To extend the TOLFC technique to higher bandwidth (greater than 1 GHz), several major achievements were made as described below. Each section references more detailed discussion in the references or appendices of this report.

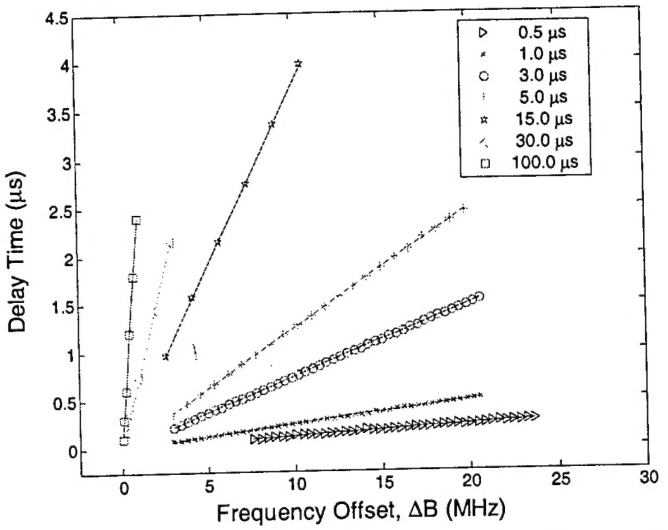

Figure 2. Measured echo delays vs. frequency offset for several chirp durations, τ_C, with solid lines as the expected delay time. Note in particular the data for τ_C = 30 and 100 μs, times which are longer than the homogeneous decay time of the material and allow for long delays.

i. Development of programming architecture with temporally overlapped linear frequency chirped pulses [2,3]

Using a linear frequency chirped laser source enables us to access a broad bandwidth with relatively low optical powers to program efficient OCT TTD gratings. 50 mW outputs from a diode laser focused to a 70μm-diameter spot can produce sufficient processing efficiency with a single programming sequence at a chirp rate of 1GHz/10μs.[Appendix 2] This technique was used to produce these efficient TTD gratings and figure 2 shows the time delays of associated echoes versus the frequency offset, δ . The ability of this technique of programming the medium with chirped pulse durations beyond the 15μs coherence time is shown for the 30 and 100μs chirp lengths. This allows broader bandwidths to be efficiently written into the medium without the need for extremely fast chirp rates and promises to be the technique of choice for extremely wide bandwidth gratings. All of these features combine to make this approach a promising one for a practical adaptive beamforming system. Thus the research effort at MSU has been focused on developing this technology.

ii. Development and characterization of Chirped laser source (Appendices 1, 2)

A chirped external cavity diode laser (CECDL) has been developed, consisting of an anti-reflection coated diode laser, a grating in Littrow configuration with the diode and an electro-optical crystal in between for frequency tuning. (Figures 9, 10 in Appendix 2) The characterization of tuning range, and linearity of chirps has been done with static measurements and real-time measurements with planar and con-focal Fabry-Perrot cavities.[4] (Figures 12,13 in Appendix 2). The latest results confirmed a stable linear chirp of 2.4GHz for as short as 1μs. This laser is a compact and highly tunable source with a rugged design. This technology has the potential to be transferred to the market place as a low-cost, reliable laser source and our collaborators in MSU's Spectrum Lab are in the process of analyzing this possibility.

iii. Demonstration of broadband programming with CECDL (Appendix 2)

In order to fully realize any adaptive beamforming system, we needed a direct method to program high bandwidth gratings. We followed the approach we demonstrated at low bandwidths using the TOLFC method, described in section *i*. The TOLFC TTD programming was first demonstrated with the CECDL on chirps with 450MHz of bandwidth. Echoes were

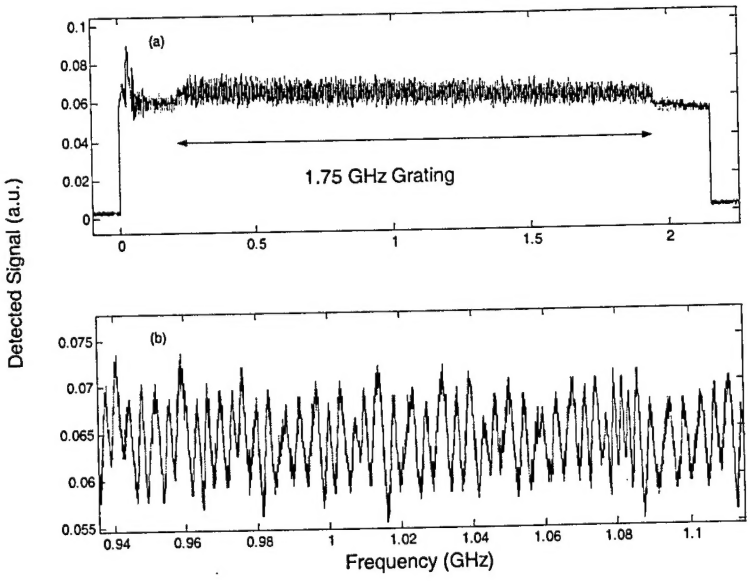

Figure 3. (a) A chirped scan over a TTD grating. This grating was created using the TOLFC method described in section *i*. (b) A zoom of a section of the grating showing the frequency spacing of the TTD.

observed by scattering a 50ns pulse off of the TTD gratings created by the chirps. The delay was tuned from 0.1μs to 0.7μs by frequency offset. This frequency offset was controlled with a low bandwidth 125MHz AOM and the echo delay shows good linearity with the frequency offset as expected by the theory.(figure 17 in Appendix 2). A further enhancement of

programming bandwidth to 1.2 GHz was then demonstrated. (figure 20 in Appendix 2) This conclusively demonstrated that the chirped laser could produce efficient high bandwidth gratings for TTD applications and was the first successful demonstration of broadband true-time delay gratings using a CECDL. In another experiment, we scanned over the TTD grating created with a slower chirp from the CECDL. This allowed a direct view of the spectral grating and is shown in figure 3. Here we see that the laser can indeed chirp and create gratings with bandwidths in excess of 1 GHz.

iv. TTD delay range, resolution, bandwidth limit

It was important to get a handle on the delay resolution that the TTD approach would provide for an adaptive beamforming TTD system. Along with the CECDL results above, working under a separate grant, our team was able to show broadband TTD using a 4Gbit/s 6 bit code. These results are described in reference.[5] Table 1 shows a summary of the expected values of maximum delay, delay resolution and bandwidth for OCT TTD echoes in Tm:YAG and the values achieved throughout that project.

	Maximum delay (μs	Delay resolution	Bandwidth (GHz)
Estimate[6]	1	Sub-ps	10 GHz
Achieved[5, Appendix 2]	0.7	7 ps*	3GHz*

* measurement limited.

v. Dynamics of continuous programming and continuous processing (narrow band chirp accumulation, MT OL and MT HBRS'99, TOLFC Accumulation RR-OL)

The nature of the accumulation of TTD grating allows the processing ability being maintained or refreshed, which enables the continuously programmed continuous processing. The dynamics of the accumulation was studied with brief pulse programming on the entire available bandwidth (17 GHz)[5] and on narrow band 40MHz with TOLFC's.[Appendix 5] The broad band results shows the echo efficiency at a regular level can be reached and maintained with 30 ps pulses at an intensity significantly lower than the damage threshold of the material.[5]

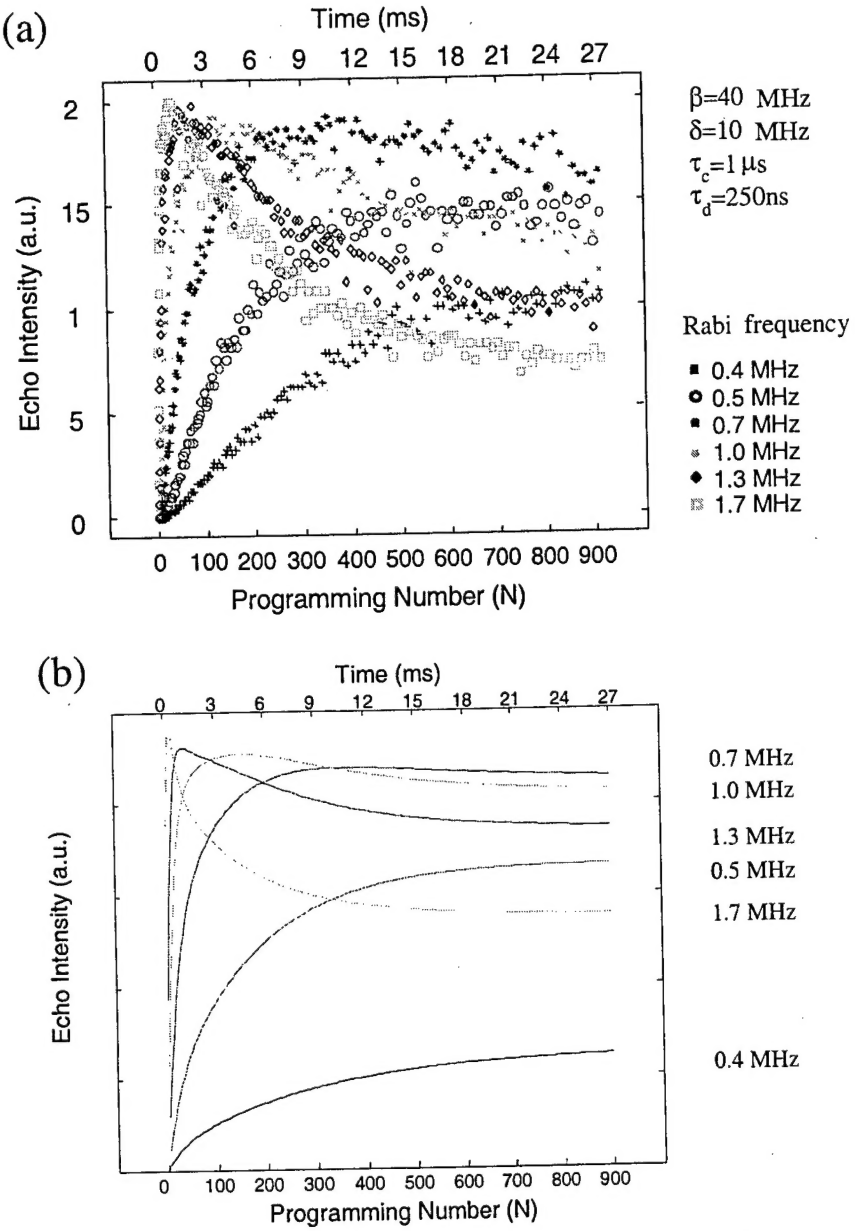

Figure 4 Experimental (a) and simulation (b) results of grating accumulation dynamics with TOLFC's. The repetition rate is 30KHz.

To demonstrate accumulation using the TOLFC method, we first used the frequency stabilized Ti:Sapphire laser described in section *vii* as the laser source. This laser has been locked using a regenerative spectral hole giving a laser jitter of approximately a few kHz.[7] By attenuating the optical power, we chose a series of weak programming strengths that would show the dynamics of the accumulated gratings. The programming pulses are characterized by an individual LFC's Rabi frequency, which were Ω = 0.4, 0.5, 0.7, 1.0, 1.3, and 1.7 MHz for this experiment.

Following the standard approach for accumulation, we repeated programming TOLFC's with a repetition time, τ_r, of 31 μs, for N times. After the N programming sequences, the grating was probed using a 50 ns brief pulse as in the single shot experiments. Figure 4(a) details the echo peak power as a function of N for the set of weak programming pulses. Here, τ_C = 1 μs and δ=10 MHz giving a delay time for the echo of τ_D = 250 ns. As can be seen from the figure, the various gratings accumulate quite well. Because of the population relaxation dynamics, the larger programming strengths, $\Omega > 0.9$ MHz, are too strong and saturate the medium leading to inefficient gratings. The weaker programming strengths, $\Omega < 0.65$ MHz, are not strong enough to accumulate an efficient grating before population decay wipes them out. Between these two regimes the best accumulation can be found such as the $\Omega = 0.72$ MHz programming strength. Figure 4(b) shows an example simulation using the experimental parameters. The simulation program uses an integration routine to simulate the effects of propagation through the medium using the coupled Maxwell-Bloch equations. This simulator has been specifically developed to handle these situations and as can be seen verifies the experimental results.

We also accumulated gratings using the original injection locked ECDL laser system. For these experiments, another set of Rabi frequencies had to be chosen as the systems intensities and spot size were slightly different. The results were similar to the locked laser results discussed above indicating that indeed the injection locked laser could produce efficient accumulated gratings. As the lasers ability to accumulate a grating rests directly on the lasers stability and the programmed τ_D, we changed the time delay to discover the largest τ_D we could accumulate reasonably well. We found that τ_D 's < 250 ns accumulated quite well however the results were noisier than the frequency stabilized laser results. These accumulation results will have a direct impact upon our ability to use affordable non-stabilized external cavity diode laser systems to program efficient high bandwidth gratings.

vi. Broadband spectral filtering PM signal (Appendix 3)

As higher bandwidths are reached, the inhomogeneous broadening of the material can actually influence the spectrum of processed signals. The Tm:YAG crystal has a Gaussian absorption profile centered at 793nm with a full width of half maximum of 17GHz. When the RF signals to be processed are detuned from the peak of the transition and their bandwidth exceeds a few GHz, the spectral filtering effects of the material have to be taken into account in addition to the TTD spectral gratings. This is a complicated form of bandwidth limiting a signal and we have worked on a computer simulator that allows us to simulate the expected echo output from broadband spectral gratings. In this work, two TTD experiments were simulated. In a TTD experiment, as the delay is varied one hopes to see the phase relationship

$$\phi_M = \omega_M \tau_D .$$

Here ϕ_M is the phase shift of the echo with respect to the original waveform, ω_M is a broadband modulation frequency, and τ_D is the time delay. There are two experimental arrangements that

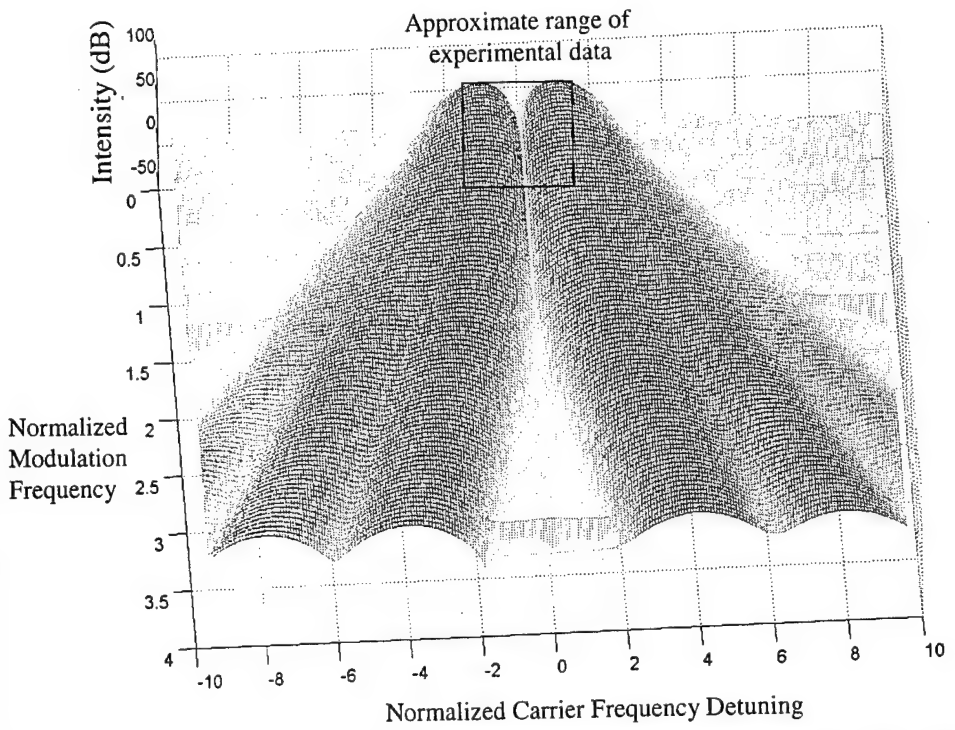

Figure 5. The simulated effects of a Gaussian filter such as the Tm:YAG 793 nm transition. The black box shows the approximate region of the experimental data. Normalized frequencies are in units of half-width-1/e-maximum of the filter.

were simulated to test whether spectral filtering from the guassian filters could in anyway effect this phase relationship. The first arrangement changes the phase relationship by varying ω_M over bandwidths comparable to the inhomogeneous broadening of the transition. This is a very realistic approach to TTD and gives insight into how broadband signals, such as complex shaped radar transmissions, will be affected by this spectral filtering. The simulated results for this experimental case shows that although the filter can limit the bandwidth of the signals, no spurious effects due to higher orders will effect this phase relationship. This is shown in figures 7 and 8 of appendix 3. Thus, TTD applications can be pushed to the very bandwidth limits dictated by the inhomogeneous transition without fear of harmful beam steering effects. The second arrangement was to pick a static ω_M and vary the time delay, τ_D. These results also, showed that the phase relationship given above is maintained for various τ_D's even when ω_M is well beyond the FWHM of the transition (see for example figure 9 in appendix 3). It is important to note however, that the signal strength does decrease in this situation.

In order to push to higher bandwidths of TTD, there has been a significant focus on using integrated optics modulators for both amplitude and phase modulation, AM and PM respectively. The desired intention is that broadband signals, which would be fed into an adaptive beamforming system must be created using electrical sources and then modulated onto optical carriers. These modulators have the desired bandwidths needed to achieve the goals set

forth in this project. However, due to the waveguide nature of these devices, and the 793 nm optical frequency, these devices are prone to photorefractive damage. This meant that the light traveling through these modulators must be kept to low powers, usually less than 10 mW input which gives approximately 1 mW output due to the insertion loss of the modulator. Since the OCT process needs relatively large optical powers (~100mW) we needed to boost the optical power after output from the integrated optics modulators. We have directly studied this problem through other funding sources to achieve amplification of broadband signals at 793nm. This has been done using two approaches that are described in reference 8, and in reference 9. These two techniques were enabling technologies that allowed the following experiments on spectral filtering to be done under this grant. These experiments also gave us much needed experience working with integrated optics modulators and this knowledge has now been transferred to the adaptive beamforming system team.

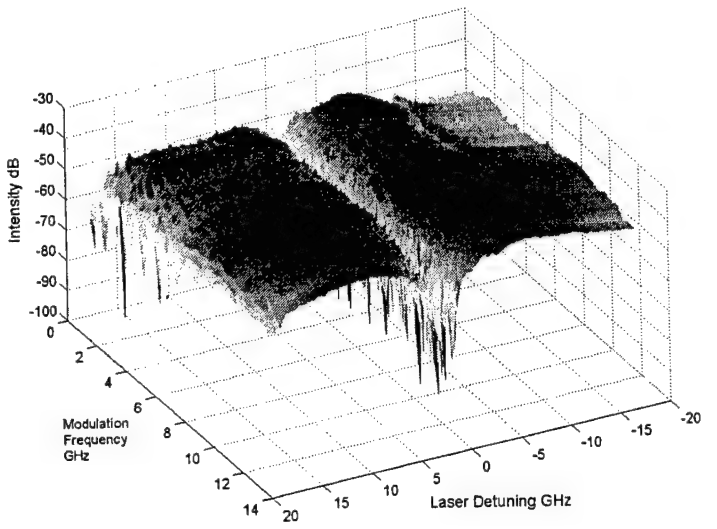

Figure 6. Experimental data showing PM signals turned into AM signals via the Tm:YAG 793 nm transition. The results match the simulated results quite well.

One of the benefits that spectral filtering has is that it can simplify the processing architecture for an adaptive beamforming system. This is done by detuning the spectral filter to reduce one of the phase sidebands created by a phase modulator. This has the effect of turning PM signals into AM signals while the signals are simultaneously delayed. The conversion from PM to AM depends on the modulation depth, the carrier frequency detuning, and the RF frequency. The Tm:YAG medium can act in two different ways, either as an absorptive filter (no echoes) or as a

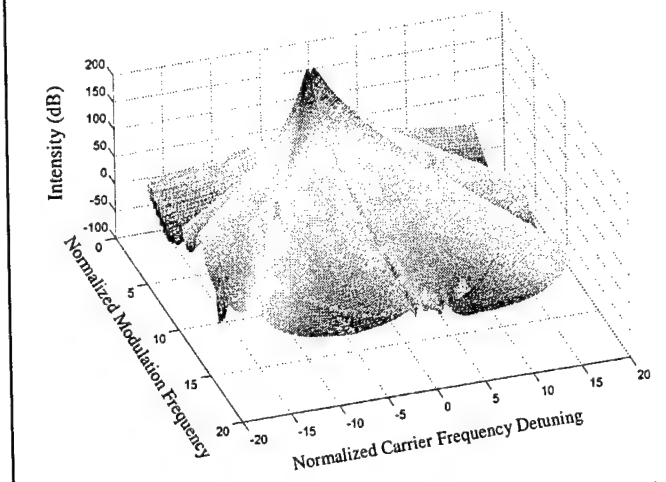

Figure 7. Simulated results for an airy transmissive filter acting to convert PM to AM. Normalized frequencies are in units of FWHM of the filter.

transmissive filter (TTD echoes). We studied the first type of filter and its ability to turn PM into AM by using the medium itself and the above described simulator. In the following experiments, the parameters that are varied are the modulation frequency of the PM signal and the carrier frequency of the optical carrier. By varying these parameters we studied the AM induced by the filtering action and plotted the expected intensity of the AM beat. Figure 5 plots the simulated effects of a guassian absorptive filter and details the range over which the experimental data was taken. Figure 6 shows the experimental results taken by using the integrated optics phase modulator to produce a signal on an optical carrier and passing the carrier through the Tm:YAG crystal and using it as an absorptive filter.

Along with the absorptive filtering, we did a proof of concept experiment showing the results of a transmissive filter. It would be ideal to show the TTD spectral filtering on actual echoes however this would require essentially the completed adaptive beamforming setup. In order to adequately study the effects and get a handle on what to expect experimentally for echoes, we used instead an etalon as a transmissive filter. Several etalons with different free spectral ranges were chosen. We then did essentially the same experiment as described above for the guassian absorptive filter except etalons have an airy function as their spectral shape and this causes significant changes in the expected shape of the PM to AM conversion. Figure 7 shows the simulated results for PM to AM conversion again using the simulator described above for an airy transmissive filter. In figure 8 the experimental results taken using a 3mm thick, 700MHz FWHM, are shown. Again the results match well with the simulated results. By using these results, we can effectively make a system that uses the filtering aspects of the medium to convert PM to AM.

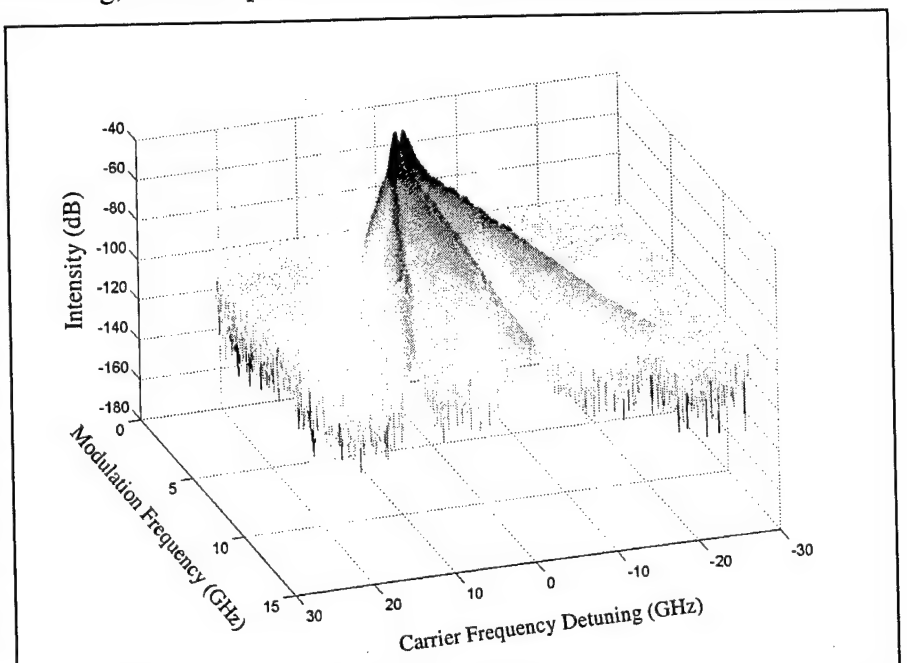

Figure 8. Experimental PM to AM conversion shown using a 3.0 mm thick etalon. Again simulation and experiment match well.

vii. Development of stabilized Ti: Sapphire laser (Appendix 2)

To provide a frequency stabilized laser source for the study on the accumulation dynamics a cw Ti:Sapphire laser was stabilized by Pound-Drever-Hall method, [**ref**] with a regenerative spectral hole in Tm:YAG as a narrow frequency reference. The locking method, setup and characterization are described in Appendix 2(page 13-20). The frequency stability better than 13kHz over a time period of 640μs has been achieved compared to the frequency jitter of 420kHz for the laser only locked to its external cavity. Figure 8 shows the performance of the laser before and after lock. We use two 200ns pulses with time separation of 1μs to program a spectral grating, and then chirp the laser over 10MHz within 30 μs across the grating 500 μs after the grating was created. By monitoring the transmission of a frequency scanned laser pulse, we use the grating structure to measure the shifts in the laser frequency between

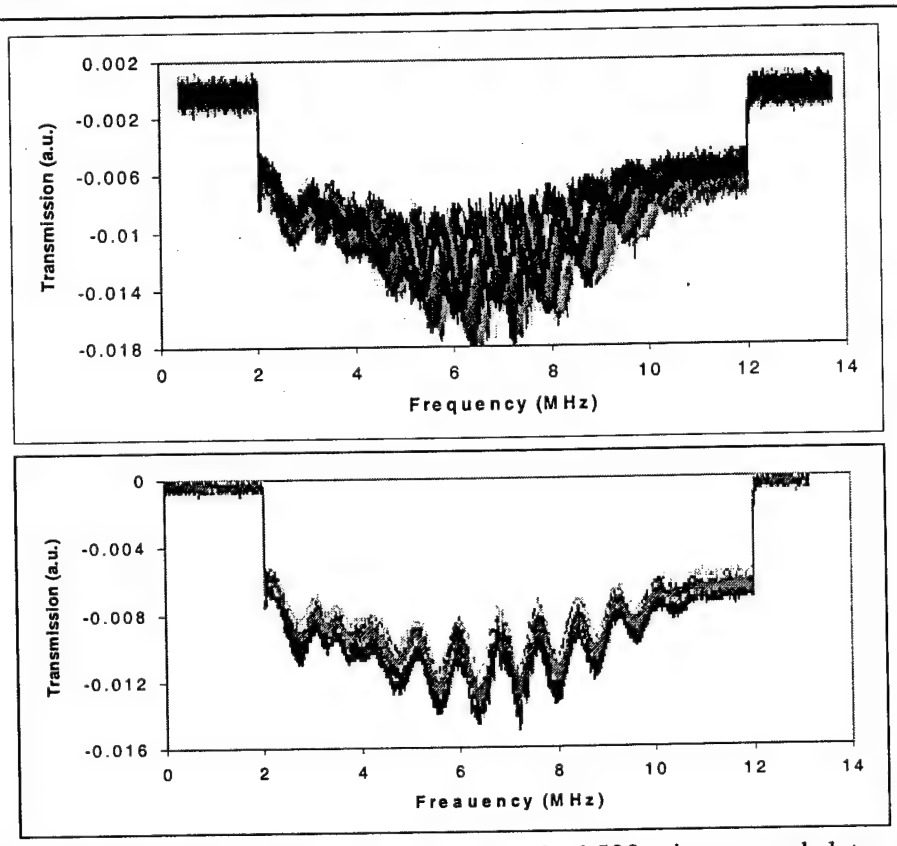

Figure 8. Spectral gratings recorded and probed 500 microseconds later with un-stabilized (upper traces) and stabilized laser (lower traces).

programming of the grating and readout. Figure 8 shows 33 recordings (upper traces) for un-stabilized laser and 43 recordings (lower traces) for the stabilized.

Photon echo adaptive array processing (CU)(Appendix 5)

viii. *Investigation into the implementation of adaptive beam former using OCT's (Appendix 5)*

We have worked though the theory to show the response to be consistent with what is required by the Least Mean Squared(LMS) algorithm and published a paper with the results (see publication list). In addition, we have built computer simulations of the system that allow us to investigate different algorithms for performing within an OCT material.

ix. *Investigation and design novel processing architecture using OCT's. (Appendix 5)*

Optical signal processing using OCT promises to significantly enhance phase array antenna adaptive beam forming due to the large potential processing bandwidths (>17GHz) and time-bandwidths product (>10^5). We investigated the design of a novel processing architecture, which can take full advantage of the utility of these spatial-spectral holographic recording devices in their application to phase array beamforming. We have built state-of-art OCT laboratory capable of demonstrating high bandwidth optical signal processing. In addition, we have further developed our facilities in the area of laser stabilizaton. We have built a Pound-Drever-Hall frequency locking system using a confocal Fabry-Perot cavity as a reference.

x. *Dispersion compensation. (Appendix 5)*

We have extended our work on OCT phase array beamforming to solve the problems of modal dispersion in multimode fiber. The technique will enable encoding information on different spatial modes of a multimode fiber that allows multiplexing up to 10^4. Thus, the capacity in fiber communication systems will be increased dramatically. We have designed and analyzed a multiple channel dispersion compensation system.

Education and industrial connections

Along with the major achievements described above, this work has met its other goals as outlined in the education and industrial interaction sections. This grant has directly supported the research of 4 Graduate and 3 undergraduate students (3 graduate and 2 undergraduate students received direct salary support). One of these students, Ken Anderson at CU, has received his Ph.D. and another student, Robert Peters at MSU, has received his Masters degrees working on this project. Randy Reibel, a graduate student at MSU working with the project, has gained valuable experience while assisting and then leading vital experiments for the adaptive beamforming and steerable array project. The undergraduates worked closely with the graduate students and post-doctoral, receiving valuable training in optics and rf. During this project the joint team worked with professionals nationwide. A strong cooperation has been built with local industries at Bozeman, Montana, such as ADVR and SciMat. We have contracted their work in various ways to assist the goals of this project. Through technology transfer to and from Spectrum Lab at MSU, the CECDL work has advanced to the stage that is will be pursued as a commercial product. Overall, adaptive beamforming and TTD has benefited from the generous support of ARO under this grant. With the technological challenges that this grant helped

overcome, we are confident that a fully functional adaptive beamforming OCT system for phased array radar antennas will be refined in the near future.

(6) Publications and technical reports

(a). Papers published in peer-reviewed journals

[1] K. D. Merkel, W. R. Babbitt, K. E. Anderson, K. H. Wagner, "Variable-time-delay optical coherent transient signal processing," Opt. Lett. **24**, 1386-1388 (1999).

[2] K. D. Merkel and W. R. Babbitt, "Continuous waveform variable true-time delay by optical coherent transients," Optics Comm. 180, 103-110 (2000).

(b) Papers published in non-peer-reviewed journals or in conference proceedings

[1] K. D. Merkel* and W. R. Babbitt, "Continuously programmed optical coherent transient continuous signal processor" 1999 Optics in Computing OSA Topical Meeting, Snowmass, CO, April 12-16, 1999.

[2] K. H. Wagner*, K. E. Anderson, W. R. Babbitt, and K. D. Merkel, "Optical coherent transient true-time-delay beam-forming processor" 1999 Optics in Computing OSA Topical Meeting, Snowmass, CO, April 12-16, 1999.

[3] K. D. Merkel* and W. R. Babbitt, "Frequency-tuned continuous true-time delay by optical coherent transient technology," in Conference on Lasers and Electro-Optics, 1999 OSA Technical Digest Series (Optical Society of America, Washington, DC, 1999) pp 171. Baltimore, MD, May 24-28, 1999.

[4] W.R. Babbitt, "Multidimensional signal processing with spatio-spectral holography," Proceedings of the SPIE, Optical science, Engineering and Instrumentation, Denver, CO, July 18-23, 1999 Vol. 3802, paper 3802-32 (1999).

[5] K. H. Wagner*, K. Anderson, W.R. Babbitt, and K. D. Merkel, "Multidimensional photon echo processing," (Invited Paper) Proceedings of the SPIE, Optical Science, Engineering, and Instrumentation, Denver, CO, July 18-23, 1999, Vol. 3804, paper 3804-03 (1999).

[6] K. Merkel, K. S. Repasky, and W.R. Babbitt, "Design issues in continuously programmed coherent transient processors," Proceedings of the SPIE, Optical Science, Engineering, and Instrumentation, Denver, CO, July 18-23, 1999, Vol. 3802, paper 3802-43 (1999).

[7] K.H. Wagner, K.E. Anderson, W.R. Babbitt, and K.D. Merkel, "Multidimensional photon echo processing," (Invited Paper) Proceedings of the SPIE, Optical Science, Engineering, and Instrumentation, Denver, CO, July18-23, 1999, Algorithms, device, and systems for optical information processing II, Vol. 3804, paper 3804-03 (1999).

[8] K. D. Merkel, K. Repasky, and W. R. Babbitt* "Demonstration of a continuously programmed optical coherent transient processor," presented at 6th Int. Meeting of Hole Burning and Related Spectroscopies: Science and Applications (HBRS'99), September 18-23, 1999, Hourtin, France.

[9] K. D. Merkel, Z. Cole, and W. R. Babbitt "Programmable variable time delay signal correlator based on six-wave mixing optical coherent transients," poster presentation at 6th Int. Meeting of Hole Burning and Related Spectroscopies: Science and Applications (HBRS'99), Sept. 18-23, 1999, Hourtin, France.

[10] K. D. Merkel*, Z. Cole, and W. R. Babbitt, "Signal correlator with programmable variable time delay based on optical coherent transients," IEEE Lasers and Electro-Optics Society 1999 Annual Meeting, Nov. 8-11, 1999, San Francisco, CA.

[11] Z. Cole*, K.D. Merkel, and W.R. Babbitt, "Atomic coherence state phase conjugation in optical coherent," presented at Conference on Lasers and Electro-Optics, 2000 OSA Technical Digest Series (OSA, Washington, DC, 2000) San Francisco, CA, May 7-12, 2000.

[12] M. Tian, R. Reibel, and Wm. R. Babbitt, "Broadband true-time-delay with optical coherent transients," CLEO'2001 (Baltimore, May 2001).

(c) Papers presented at meetings, but not published in conference proceedings

[1] K.E. Anderson, K.H. Wagner, "Multidimensional Photon echo Optical Processing", OSA Optics in Computing 1997-Post deadline paper.

[2] K.E. Anderson, K.W. Wagner, "Multidimensional Optical Signal Processing Architectures Utilizing Photon Echo", Spectral Holeburning 1998 Annual Conference.

[3] K.E. Anderson, K.W. Wagner, " Spatial-Temporal Dispersion Compensation for High Bandwidth Communications", OSA Annual Meeting 1999, talk, Santa Clara, CA (9/28/99).

[4] K.E. Anderson, K.W. Wagner, " Spatial-Temporal Dispersion Compensation Utilizing Photo Echo", Spectral Holeburning 1999 Annual Conference.

[5] K.E. Anderson, K.W. Wagner, "System Issues in Simultaneous Space-Time Coherent Transient Optical Signal Processing ", Spectral Holeburning 2000 Annual Conference.

[6] K.E. Anderson, "Optical Data Storage", Undergraduate class lecture series in Magnetic Data Storage 2000.

[7] R. D. Peters, P. B. Sellin, K. S. Repasky, and W. R. Babbitt; "Frequency stabilization of a Ti: Sapphire laser to a non-persistent spectral hole in Tm:YAG," Spectral Hole Burning Workshop 2000; July 10, 2000.

[8] Mingzhen Tian, Randy Reibel, and W. Randall Babbitt 'Broadband True-Time Delay and Correlation Using Accumulated Photon Echo' OpTeC'2000 (Aug. 2000, Bozeman).

[9] Wm. R. Babbitt, " Optical coherent transient correlators: Science and applications," PQE'2001 (Snowbird, UT, Jan. 2001).

[10] M. Tian, R. Reibel, and Wm. R. Babbitt, "Multi-gigahertz true-time-delay with optical coherent transient," American Physical Society Annual Meeting, (Seattle, WA, March 2001).

[11] Z. Barber, R. Reibel, M. Tian, W. R. Babbitt, "Application of Phase Modulated Optical Signals to Inhomogeneously Broadened Materials", American Physical Society Annual Meeting, (Seattle, WA, March, 2001)

[12] R. Reibel, Z. Barber and W. R. Babbitt, "Amplification of High Bandwidth Phase Modulated Signals at 793 nm", American Physical Society Annual Meeting, (Seattle, WA, March, 2001)

[13] Ken E. Anderson, K.W. Wagner, "Chromatic and Polarization Mode Dispersion Compensation Using Spectral Holography", OFC 2001, Anaheim CA, Mar 2001.

[14] Joe Fischer, Zeb Barber, Randy, Reibel, Mingzhen Tian, and Randy Babbitt, "Linear Phase Chirp Programming for OCT's," Optec2001, (Bozeman, MT, August, 2001).

[15] R.Reibel, Z. Barber, M. Tian and W. R. Babbitt, Z. Cole and K. D. Merkel, "Amplification of High Bandwidth Phase Modulated Signals at 793 nm," Optec2001 (Bozeman, MT, August, 2001).
[16] Wm. R. Babbitt "Optical coherent transient devices," OpTeC2001 (Bozeman, MT, August, 2001).
[17] R. Reibel, Z. Barber, M. Tian, W. R. Babbitt, "Temporally Overlapped Linear Frequency Chirp Programming for True Time Delay Applications," HBRS'01 , (Taipei, Taiwan, November, 2001).
[18] M. Tian, R. Reibel, Z. Barber, W. R. Babbitt, "Broadband true-time delay in Tm:YAG," HBRS'01, (Taipei, Taiwan, November, 2001).
[19] Ken E. Anderson and Kelvin H. Wagner, "Demonstration of Chromatic Dispersion Compensation Using Spectral Holography," HBRS'01 , (Taipei, Taiwan, November, 2001).

(d) Manuscripts submitted, but not yet published

[1] Ken Anderson, "Multidimensional optical signal processing using coherent transient spatial-spectral holography," Thesis for Ph. D. at University of Colorado (2001).
[2] Randy Reibel, Zeb Barber, Mingzhen Tian and Wm. Randy Babbitt, "Temporally overlapped linear frequency chirped programming for true-time delay," submitted to Opt. Lett.
[3] F. Schlotta, K. Wagner, J.Bregman, Correlation Based Array Imaging with Photo Echo, to be submitted to Applied Optics.

(e) Technical reports submitted to ARO

None

(7) List of all participating scientific personnel showing any advanced degrees earned by them while employed on the project

MSU

PI: Prof. Wm. Randall Babbitt,
Research scientists: Dr. Kristian Merkel, Dr. Mingzhen Tian,
Graduate Students: Robert Peters, M.Sc earned 2001, Jinjun Xia,
Undergraduate Students: Joe Fisher.

CU

Prof. Kelvin Wagner
Graduate student: Ken Anderson, Ph.D. earned 2001
Undergraduate student: Eric Hoyte, BS earned, MS in progress.

The work on the chirped laser was done in collaboration with Prof. John Carlsten and Dr. Kevin Repasky, also of the MSU Physics Department.

(8) **Report of inventions (Patents Applications)**

[1]. K.E. Anderson, K.D. Merkel, W.R. Babbitt, K.H. Wagner, "Method and Apparatus for Variable Time Delay Optical Coherent Transient Signal Processing", Patent Pending, #60/152,611.

[2]. K.E. Anderson, "Spatial-Temporal Linear Compensator", Patent Pending , #60/123.346.

[3]. K.E. Anderson, K.W. Wagner, "Method of Polarization Mode Dispersion Compensation using dispersive element and spatial holography", Patent Application in Progress.

[4]. K.E. Anderson, " Polarization Mode Dispersion Compensation using spectral decomposition and Polarization Rotation", Patent Application in Progress.

[5]. K.E. Anderson, "Simulataneous Polarization Mode Dispersion Compensation and wavelength routing", Patent Application in Progress.

(9) **Bibliography**

[1]. K. D. Merkel and W. R. Babbitt, "Chirped-pulse programming of optical coherent transient true-time delays," Opt. Lett **23**, 528-30 (1998).

[2]. Randy Reibel, Zeb Barber, Mingzhen Tian and Wm. Randy Babbitt, "Temporally overlapped linear frequency chirped programming for true-time delay amplification," submitted to Opt. Lett.

[3]. R. Reibel, Z. Barber, M. Tian, W. R. Babbitt, "Temporally Overlapped Linear Frequency Chirp Programming for True Time Delay Applications," HBRS, (Taipei, Taiwan, November, 2001).

[4]. K. Repasy and J. L. Carlsten, " Simple method for measuring frequency chirps with a Fabry-Perot interferometer," Appl. Opt. **39** 5500-5504 (2000); K. Repasky, G. W. Switzer, and J. L. Carlsten, "Design and performance of a frequency chirped external cavity diode laser," to be published.

[5]. M. Tian, R. Reibel, and W.R.Babbitt "Demonstration of optical coherent transient true-time delay at 4 Gbit/s", Opt. Lett. **26**, 1143 (2001).

[6]. K. D. Merkel, and W. R. Babbitt, "Optical coherent transient true-time delay regenerator," Opt. Lett. **21**, 1102 (1996).

[7]. K. D. Merkel, R. D. Peters, P. B. Sellin, K. S. Repasky and W. R. Babbitt, "Accumulated programming of a complex spectral grating," Opt. Lett **25**, 1627-9 (2000).

[8]. R. Reibel, Z. Barber, M. Tian, W. R. Babbitt, Z. Cole , and K. Merkel, "Amplification of high bandwidth phase modulated signals at 793nm," submitted to J. Opt. Soc. Am. B (2001).

[9]. K. D. Merkel and R. Krishna Mohan, "Thulium doped fiber amplifier at 77 K around 794 nm," Optical Society of America TOPS v. 44, (2000)

[10]. Randy Reibel, "Spectral filtering of amplitude or phase modulated carriers," graduate project report, Department of Physics, Montana State University (2000)

[11]. N. M. Strickland, P. B. Sellin, Y. Sun, J. L. Carlsten, and R. L. Cone, "Laser Frequency stabilization using regenerative spectral hole burning," Phys. Rev. B **62** 1473-1476 (2000).

(10) Appendixes

[1]. Interim report

[2]. Robert D. Peters " Programming high bandwidth true-time delays in an optical coherent transient material," graduate research report, Department of Physics, Montana State University (2001)
[3]. Randy Reibel, "Spectral filtering of amplitude or phase modulated carriers," graduate project report, Department of Physics, Montana State University (2000)
[4]. K. D. Merkel, W. R. Babbitt, K. E. Anderson, K. H. Wagner, "Variable-time-delay optical coherent transient signal processing," Opt. Lett. **24**, 1386-1388 (1999)..
[5]. Manuscript: Randy Reibel, Zeb Barber, Mingzhen Tian and Wm. Randy Babbitt, "Temporally overlapped linear frequency chirped programming for true-time delay amplification," submitted to Opt. Lett.
[6]. CU subcontract final report.

Appendix 1

1999 Interim report

REPORT DOCUMENTATION PAGE

Form Approved
OMB NO. 0704-0188

Public Reporting burden for this collection of information is estimated to average 1 hour per response, including the time for reviewing instructions, searching existing data sources, gathering and maintaining the data needed, and completing and reviewing the collection of information. Send comment regarding this burden estimates or any other aspect of this collection of information, including suggestions for reducing this burden, to Washington Headquarters Services, Directorate for information Operations and Reports, 1215 Jefferson Davis Highway, Suite 1204, Arlington, VA 22202-4302, and to the Office of Management and Budget, Paperwork Reduction Project (0704-0188,) Washington, DC 20503.

1. AGENCY USE ONLY (Leave Blank)	2. REPORT DATE 1999	3. REPORT TYPE AND DATES COVERED Interim 01 May 1998 to 31 Dec 1998

4. TITLE AND SUBTITLE
Interim Progress Report on Wide-Band Optical True-Time Delay and Adaptive Beamforming

5. FUNDING NUMBERS
G DAAG55-98-1-0244

6. AUTHOR(S)
Wm. Randall Babbitt

7. PERFORMING ORGANIZATION NAME(S) AND ADDRESS(ES)
Physics Department, EPS 264
Montana State Univeristy
Bozeman, MT 59717-3840

8. PERFORMING ORGANIZATION REPORT NUMBER
97-841

9. SPONSORING / MONITORING AGENCY NAME(S) AND ADDRESS(ES)
U. S. Army Research Office
P.O. Box 12211
Research Triangle Park, NC 27709-2211

10. SPONSORING / MONITORING AGENCY REPORT NUMBER
P-37769-PH-DPS

11. SUPPLEMENTARY NOTES
The views, opinions and/or findings contained in this report are those of the author(s) and should not be construed as an official Department of the Army position, policy or decision, unless so designated by other documentation.

12 a. DISTRIBUTION / AVAILABILITY STATEMENT
Approved for public release; distribution unlimited.

12 b. DISTRIBUTION CODE

13. ABSTRACT (Maximum 200 words)

The focus of the research under this ARO DEPSCoR grant is to explore and develop the inherent capability optical coherent transient technology to impose true-time-delays of up to several microseconds on signals with wide bandwidths far in excess of a gigahertz on optical waveforms. Coherent transient technolgoy has the advantages that the delays are controllably programmable, that over 10,000 delays can be programmed in a cubic centimeter of material, and that phase and amplitude sensitive processing and delay can be performed simultaneously. The research effort explores issues of implementing an optical coherent transient technology in the multi-gigihertz regime and develops adaptive beamforming system architectures that utilize optical coherent transient technology. Progress includes development of chirped lasers for material programming, initial demonstrations of continuous programming,

14. SUBJECT TERMS
Optical Coherent Transients, Spatial-Spectral Holography, Spectral Holeburning
True-Time Delay, Adaptive Beamforming, Phased Array Radar
Optical Correlation, Optical processing

15. NUMBER OF PAGES
11

16. PRICE CODE

17. SECURITY CLASSIFICATION OR REPORT	18. SECURITY CLASSIFICATION ON THIS PAGE	19. SECURITY CLASSIFICATION OF ABSTRACT	20. LIMITATION OF ABSTRACT
UNCLASSIFIED	UNCLASSIFIED	UNCLASSIFIED	UL

REPORT DOCUMENTATION PAGE (SF298)
(Continuation Sheet)

Objectives of the Proposal

The objective of the research effort is to demonstrate an optical coherent transient based adaptive beamforming architecture capable of operating on signals with bandwidth well in excess of a gigahertz. This work will be done by first modelling and analyzing our system architecture while at the same time pushing coherent transient true-time-delay technology from its current demonstration bandwidth of several megahertz to the required bandwidth of several gigahertz. Implementation of the refined architecture will first be done at low bandwidths, utilizing our expertise in and existing infrastructure for development of optical adaptive beamforming system. Relying on the lessons learned from these efforts, demonstrations of multi-gigahertz bandwidth adaptive beamforming will be carried out.

List of Manuscripts

Manuscripts for journals and conference presentation are currently in preparation, but none were submitted as of 12/31/98.

Scientific Personnel

At Montana State Unversity, the personnel working on this project up to 12/31/98 were a post-doctoral associates Kristian Merkel and Prof. Wm. Randall Babbitt, whose salary is covered under cost-sharing. Though no graduate students were available to join the effort in 1998, a student is lined up to work on the project full-time starting in 1999. The work on the chirped laser was done in collaboration with Prof. John Carlsten, also of the MSU Physics Department. At the Univeristy of Colorado, Prof. Kelvin Wagner and his graduate student Ken Anderson worked on developing and simulating adaptive beamforming architectures.

Report of Inventions

There were no inventions to report as of 12/31/98.

Scientific Progress and Accomplishments

Year one efforts at MSU have been geared towards extending our ability to do optical coherent transient true-time-delay regeneration (CTDR) in the multi-GHz bandwidth regime. To this end, a substantial work has been done on the development of optical sources that can provide multi-GHz signals. This laser work has been significant since we have determined that programming a CTDR unit is best achieved with frequency chirped pulses. Therefore, the optical source development has been geared towards an external cavity diode laser that can chirp over multi-GHz bandwidths on a microsecond time scale. More details of this development are reported below.

There are several issues that we have been examining as they apply to multi-GHz CTDR operation. These efforts are still in progress, and for the most part, these efforts have focussed on the use of frequency chirped programming pulses. A significant effort was geared towards the ability to achieve simultaneous processing and variable time delay, as is achieved as well with frequency chirped pulses. This represents a large step in the

right direction for adaptive array design. Other issues relating to delay resolution, bandwidth limitations, saturation effects, spatial multiplexing of delays, serial programming and parallel access of delays, frequency division multiplexed delays are being examined by simulation and analytical methods, in preparation for the experimental extension to the multi-GHz regime. A recent demonstration of the continuously programmed continuous processor (CPCP) at low bandwidths has served as a guide for the experimental design of the same concept at multi-GHz bandwidths. This experiment is the first action that will take place upon completion of the chirped laser.

In the first year of the University of Colorado DEPSCOR funding, there has been extensive investigation into the implementation of an adaptive beam former (ABF) using optical coherent transients (OCT's). We have worked through the theory to show the response to be consistent with what is required by the Least Mean Squared (LMS) algorithm and a conference paper is in preparation with the results. In addition, we have built computer simulations of the system that allows us to investigate noise effects and will allow us to investigate alternative algorithms for performing beamforming within an OCT material. Our work on more sophisticated algorithms for implementation in OCT have been delayed to the second year. To enable us with the capability to do experimental investigation into coherent transients, we are in the process of building a state of the art laboratory capable of doing high bandwidth experiments. This presently has been geared towards the study and use of techniques for stabilizing laser diodes, since highly stable lasers are needed for optimum performance of optical coherent transient experiments.

Chirped laser development (MSU)

Scaling our experiments to multi-GHz bandwidths requires a wide-bandwidth source. We have determined that the use of frequency chirped pulses for true time delay programming is optimal for our experiments. Thus, a majority of our recent effort has focussed on the development of an external cavity diode laser (ECDL) to meet the needs for a wide-bandwidth frequency chirped laser source for demonstration of wide-bandwidth optical coherent transient true-time delay. The progress of this laser development is reported here. Further development of the chirped laser will be carried out under Spectrum Lab funding, with the resultant advancements available for use under the ARO grant to carry out our multi-gigahertz demonstrations.

An EDCL in a Littrow configuration with an inter-cavity electro-optic (EO) crystal is the basis of the design for the frequency chirped laser source. The Littrow configuration was chosen because of the shorter external cavity lengths as compared to the Littman-Metcalf configuration and hence larger external cavity mode spacing. This is important because the external cavity mode spacing sets an upper limit on the frequency chirp. The disadvantages of the Littrow configuration as compared to Littman Metcalf configuration include less dispersion of the feedback and changes in the pointing of the output beam as a function of tuning.

The optical feedback from the external cavity forces the diode to operate at a specific frequency. This frequency is determined by the resonance condition of the external cavity, which requires that an integer number of half wavelengths fits into the optical path length of the external cavity. By changing the optical path length of the external cavity, the resonance condition changes and hence the frequency of the laser changes.

An inter-cavity EO crystal is used to change the optical path length of the external cavity and can therefore be used to tune an ECDL. This is accomplished by applying a voltage across the EO crystal that has the effect of changing the extraordinary index of refraction. The change in the frequency of the laser, $d\omega$, is proportional to the applied voltage and is given by the expression

$$d\omega = \frac{\omega l_{cry} n_e^3 r_{33} V}{2 l_{cav} d} \qquad (1)$$

where ω is the laser frequency, l_{cry}l is the crystal length, n_e is the extraordinary index of refraction, r_{33} is the electrooptic coefficient, l_{cav} is the external cavity length, and d is the width of the crystal. A 5x5x10mm lithium niobate crystal was chosen because it has the largest $n_e^3 r_{33}$ product for available EO crystals and will thus give the largest chirp for a given voltage. Figure 1 is an assembly drawing for the chirped laser that has been built, and Figure 2 is a photo of the actual chirped laser.

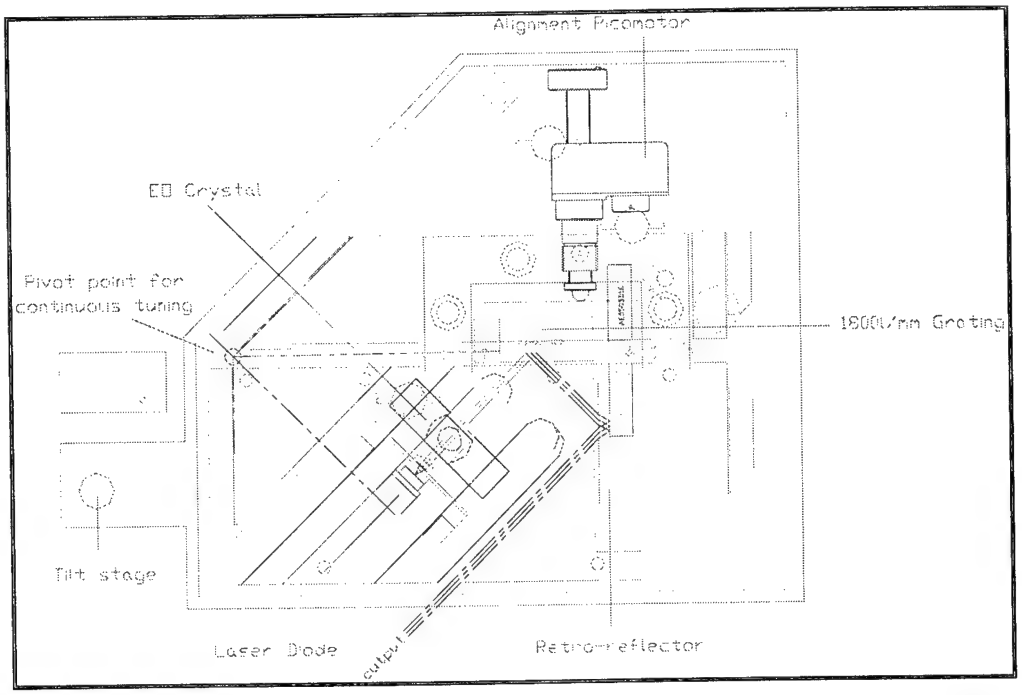

Figure 1. Top view assembly drawing for the chirped laser with a nominal wavelength of 795nm.

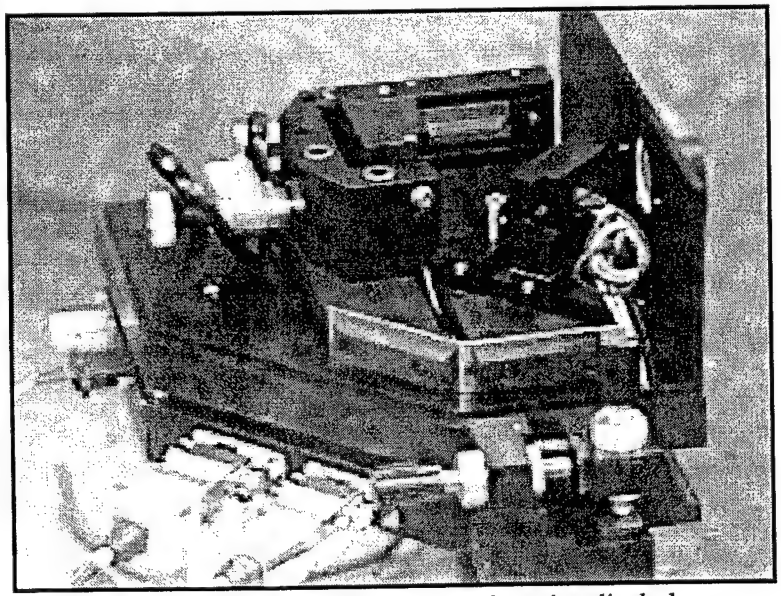

Figure 2. A picture of the external cavity diode laser.

The laser diode used in this chirped ECDL is AR coated to prevent competition between external cavity modes and laser facet modes. The AR coating has a measured reflectivity of R<1x10-3. The light from the laser is

collimated using a 4.5mm lens with a 0.55 numerical aperture. This light then travels through the lithium niobate crystal, allowing for the rapid chirp. The light is next incident on an 1800/mm grating and the 1st order reflection is sent back to the diode laser as the optical feedback. A picomotor allows for precise tilting of the grating to allow an easy way to direct the feedback to the diode laser. The 0th order reflection from the grating is incident on a right angle prism. The right angle prism and grating make a corner cube for the output light which minimizes the beam pointing problems associated with ECDL's in the Littrow configuration. The laser pivot point was chosen to allow for continuous tuning [M. de Labachelerie and G. Passedat, "Mode-hop suppression of Littrow grating-tuned lasers", App. Opt., Vol. 34 No. 3, 269-274 (1993)]. Tuning the wavelength of the laser is accomplished mechanically by rotating the grating about the pivot point relative to the diode laser. This is accomplished by the use of a 3/16 inch diameter 100 pitch set screw (accessible when the laser is enclosed in its box) and by a piezoelectric transducer (PZT) stack. The setscrew allows for mechanical tuning while the PZT stack allows for electrical tuning.

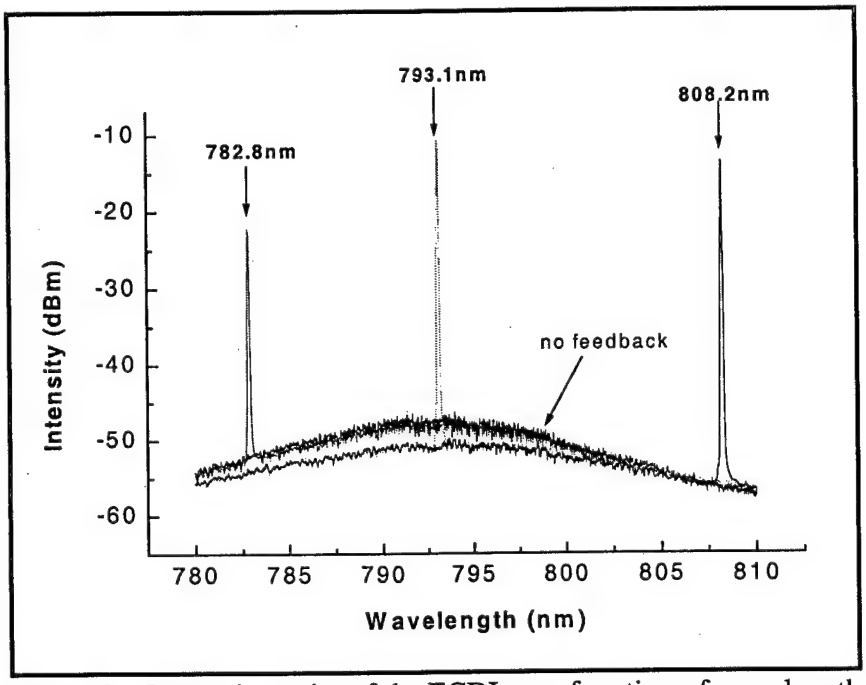

Figure 3. Output intensity of the ECDL as a function of wavelength

The ECDL is temperature controlled using 2 1x2 inch thermal electric coolers. The laser is sealed in an enclosed box with an output window AR coated at 795nm with a 3-degree wedge. The electrical connections are run through channels in the bottom of the tilt stage and connect to the outside world via 9-pin D connectors and a high voltage BNC. This was done to ensure vibrations are not transmitted via wires to the ECDL. The laser was designed for use with or without an EO crystal, to allow for maximum flexibility. The laser diode can slide in a dovetail grove and be locked down. This allows the user to set the laser position so that the pivot point will allow for continuous tuning with and without the EO crystal.

Current work involves the measurement of the ECDL laser performance without the intercavity EO crystal. These measurements will set the base performance of the laser. Figure 3 is a plot of the output intensity of the ECDL as a function of wavelength. A tuning range of 28nm is seen from this plot. Also, the wavelength of the ECDL can be tuned to 793nm that is the desired wavelength for the coherent transient experiments. Figure 4 shows a plot of the intensity as a function of wavelength with the laser operating at 793nm. A side mode suppression ration of 40nm for the ECDL is seen from this plot. Finally, Figure 5 is a plot of the output power

of the ECDL as a function of drive current without feedback and with feedback. This diode is not operating properly and a new AR coated diode is in transit as a replacement.

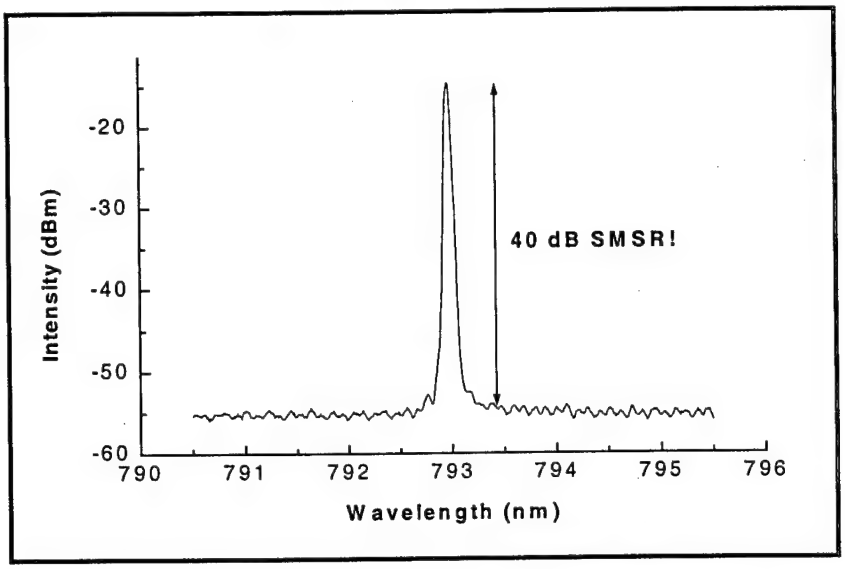

Figure 4. The side mode suppression ratio of 40 dB was measured at 793nm for the ECDL

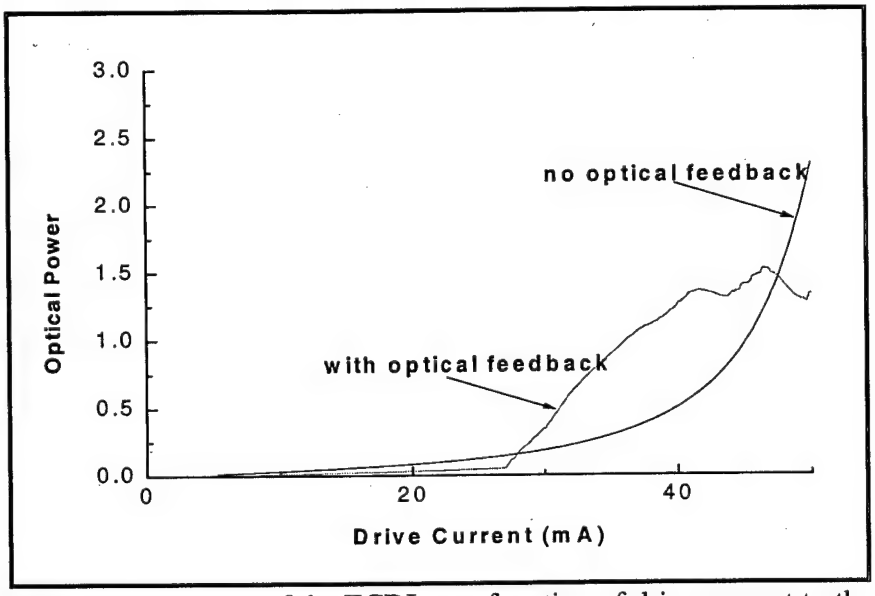

Figure 5 The output power of the ECDL as a function of drive current to the diode.

Investigation of adaptive beam forming using optical coherent transients (CU)

In year one, we investigated the implementation of adaptive beam forming using optical coherent transients (OCT) and proposed an architecture that utilizes the capabilities of the OCT as the central component of a true-time-delay adaptive beamforming algorithm. This algorithm is used to dynamically steer the gain of large RF phased array antenna towards a signal of interest while simultaneously recognizing unwanted interference signals and minimizing their effects.

In this architecture, shown in figure 6, a RF wavefront is detected with a phased array antenna where each antenna element is the driving signal for an electro-optic modulator that puts the incident RF signal onto an optical carrier. The optical signals are then carried by fiber to a central location and then are simultaneously

imaged in free space through a Rochon prism onto the OCT material which is contained in a cryostat. The Rochon prism splits each signal vertically and introduces it into the OCT material at a slight angle in the direction of Bragg degeneracy into the OCT medium. Interference with the feedback reference beam $f(t) = d(t) - o(t)$ yields OCT output signals from all the simultaneous correlations (i.e. for all j) that will co-propagate in the same and be coherently summed.

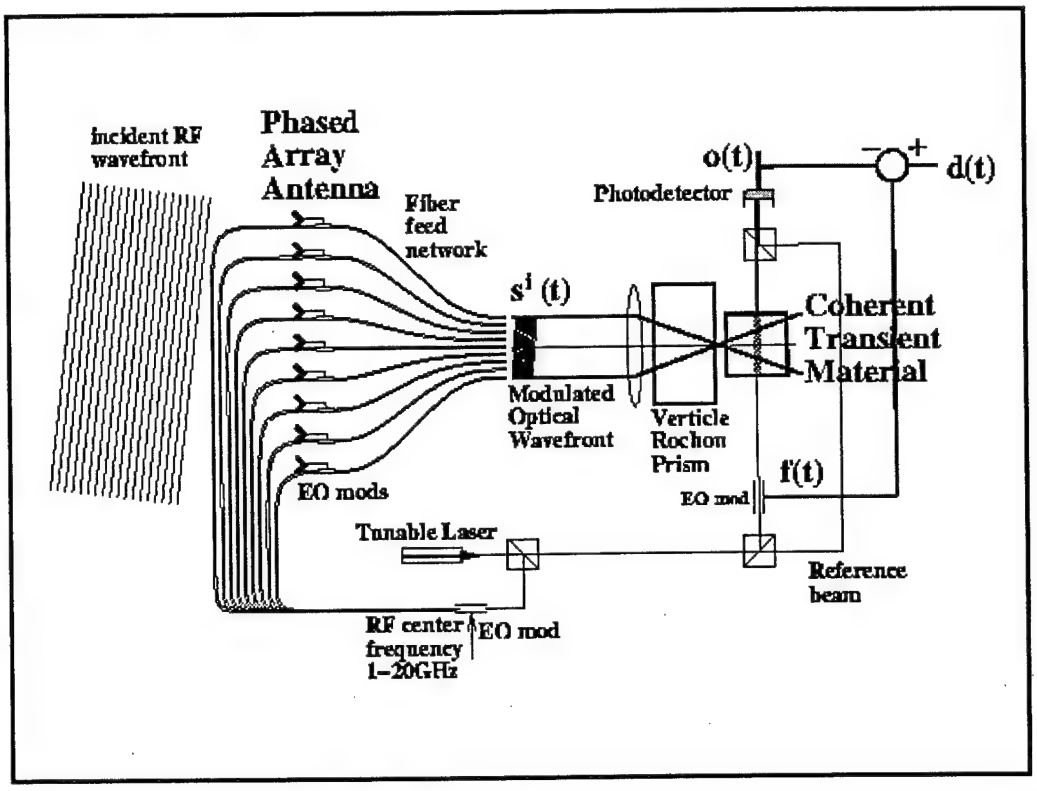

Figure 6 Optical coherent transient adaptive beamforming system that nulls jammers through the TTD correlation-cancellation loop.

Our approach uses the intrinsic delay processing capabilities of OCT materials to avoid the use of any time delay lines (TDLs), as required in other time-delay-and-sum adaptive beamformers. The similarity between OCT and the time-delay-and-sum ABF algorithm:

$$o(t) = \sum_{j=0}^{M-1} \sum_{i=1}^{N} s_i(t - j\tau) \int_{-\infty}^{t} s_i^*(t_1 - j\tau)\big(d(t_1) - o(t_1)\big) dt_1 \qquad (2)$$

becomes apparent if we examine the generalized OCT propagating along $\vec{k}_4 = \vec{k}_3 + \vec{k}_2 - \vec{k}_1$ direction which has an output

$$o(t) = A \int_{-\infty}^{t} dt_3 E_3(t_3, \vec{r}) \int_{-\infty}^{t_3} E_2(t_2, \vec{r}) E_1^*(t_3 + t_3 - t, \vec{r}) e^{\frac{-2(t-t_3)}{T_2} \frac{(t_3-t_2)}{T_1}} dt_2 \qquad (3)$$

where T_1 and T_2 are the longitudinal and transverse relaxation times, acting as windowing functions on the integration functions. Making the following substitutions into Equation **Error! Reference source not found.**:

$$E_1(t_1, \vec{r}) = \sum_{j=1}^{N} s_j(t) e^{-i\vec{k}_j \cdot \vec{r}} (1 + e^{-i\vec{k}_y \cdot \vec{y}})$$

$$E_2(t_2, \vec{r}) = f(t_2) e^{-i\vec{k}_f \cdot \vec{r}} \qquad (4)$$

$$E_1(t_1,\vec{r}) = \sum_{j'=1}^{N} s_{j'}(t-T)e^{-i\vec{k}_{j'}\cdot\vec{r}}(1+e^{-i\vec{k}_y\cdot\vec{y}})$$

in which $E_1(t_1,\vec{r})$ represents the array of write signals, $E_2(t_2,\vec{r})$ represents the feedback signal, and $E_3(t_3,\vec{r})$ represents the next waveform arriving on the array one pulse repetition interval T later. The Rochon prism produces the beam split in y, $(1+e^{-i\vec{k}_y\cdot\vec{y}})$, which produces a Bragg degenerate diffraction when $\vec{k}_y\cdot(\vec{k}_j-\vec{k}_j)=0$. Bragg matching enforces *j=j'*. The echoed output is spatial filtered to isolate the desired output waveform and interferometrically detected giving

$$o(t) = A\sum_{j=1}^{N}\int_0^{\infty} d\tau s_j(t-T-\tau)\int_{-\infty}^{t-\tau} dt_2 f(t_2)S_j^*(t_2-\tau)e^{-i(\vec{k}_f+\vec{k}_y)\cdot\vec{r}}e^{\frac{-2(\tau+T)}{T_2}\frac{(t-t_2-\tau-T)}{T_1}}dt_2 \qquad (5)$$

This shows that the OCT output is in the form of the desired spatio-temporal adaptive filter except for the limits of integration. This difference can be compensated by adjusting T_1 and T_2 to effectively vary the integration window. Utilizing a subsequent RF pulse as readout signal 3 produces the appropriate correlation cancellation loop output. Thus, OCT can perform all the necessary TTD adaptive processing for an entire array in parallel without any TDLs.

In addition, to address the causality issues associated with OCT's, it has been determined that a proper delay be implemented in the feedback loop such that for repetitive signals, repetition N will be sufficiently delayed with respect to repetition N-1 that causality will be not be violated for the response signal output.

Computer simulations (CU)

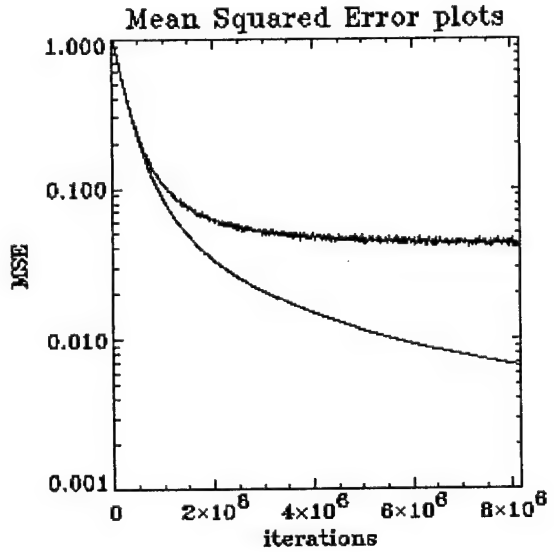

Figure 7 The learning curve during beamforming when the noise (gaussian white, mean zero) is 10 dB above the signal power (upper trace) and 60 dB below signal power (lower trace). The effect of noise is monotonic: the higher the noise the higher the mean squared error, at all times for a given convergence rate.

We have worked extensively to build a set of computer simulation tools that will allow us to analyze phased array beamforming algorithms under varying conditions. One of the key concerns of implementing a practical system of ABF is performance in the presence of noise. The results of a simulation that was performed to quantify the effects of noise is shown in Figure 7.

Experimental setup, including frequency stabilized laser diodes (CU)

Additional work accomplished includes building up the lab facilities in order to perform OCT experiments. The first step of this included studying and becoming familiar with techniques for stabilizing laser diodes since highly stable lasers are needed for optimum performance of OCT experiments. Once this was accomplished, we designed and built two frequency stabilized semiconductor lasers, each of which has frequency stability of less than 50KHz over 100us time intervals. Figure 8 shows the variation of laser linewidth over a 80 millisecond time interval. Due to thermal drifts in the stabilization system, the laser frequency drifts over 23MHz; however, the linewidth over a 40 microsecond interval is less than 48kHz. This result is significant since coherent transient experiments are effected more by the short term linewidth (10's of microseconds) than about the long term linewidth (>100 microseconds). This is due to the fact that the coherence time of the resonant atoms is on the order of 10's of microseconds. A linewidth much narrower than this wouldn't contribute significantly to the processing capabilities of the system, whereas a much larger linewidth would significantly reduce the potential time-bandwidth product of the system.

One laser was built using optical feedback from a custom designed thermally compensated confocal Fabry-Perot cavity. The second laser was built using optical feedback from an external diffraction grating in the Littman configuration. Once we had implemented these lasers, it was necessary to test their performance which necessitated measurement instruments with far more sensitivity that that available commercially. We thus investigated and became familiar with techniques for measuring highly stable lasers. The first measurement device we build included a self-heterodyning linewidth measuring interferometer to measure laser stability on the order of sub-100Khz. The second device built was a cross-heterodyning linewidth measuring interferometer to measure relative stability between two lasers.

The next step in setting up an OCT laboratory included the specification and purchase of a large number of high performance pieces of equipment including a high speed oscilloscope, spectrum analyzer, arbitrary waveform generators, acousto-optic devices, electro-optic devices, cryostats, and near infrared optics. Once the equipment was obtained, we began building the laboratory setups necessary for performing OCT experiments. Currently, the lab is capable of running low bandwidth photon echo experiments (40MHz) in co-linear or crossed beam configurations.

New Focus and External Grating Mixing Experiment I

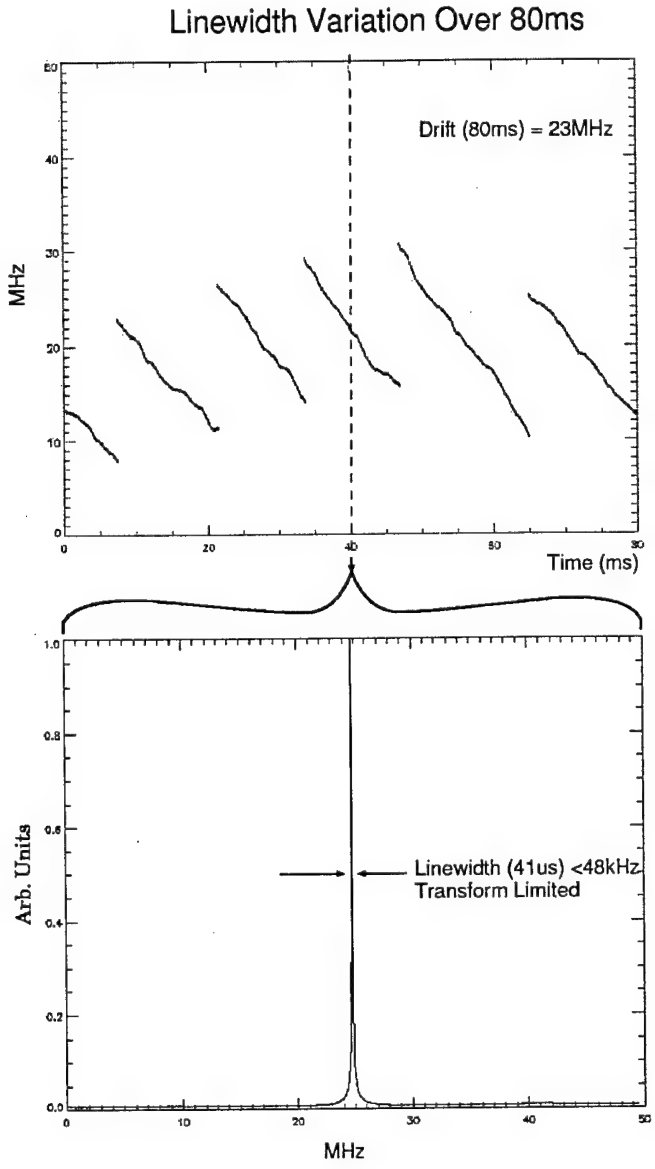

Figure 8 a) Frequency drift of stabilized laser as a function of time. b) Cross section of the laser linewidth showing the linewidth over a 41 microsecond interval.

Technology Transfer

The continued development of the chirped laser at MSU has been transitioned to Spectrum Lab, the Spectral

Information Technology Laboratory at MSU. Though development is now funded by Spectrum Lab, we will have full access to the resultant chirped laser technology to use in our demonstrations of true-time-delay processing under the current ARO grant.

Appendix 2

Robert D. Peters " Programming high bandwidth true-time delays in an optical coherent transient material," graduate research report, Department of Physics, Montana State University (2001)

PROGRAMMING HIGH BANDWIDTH TRUE TIME DELAYS IN AN OPTICAL COHERENT TRANSIENT MATERIAL

by

Robert Donald Peters

Physics 570

MONTANA STATE UNIVERSITY
Bozeman, Montana

August 2001

© COPYRIGHT

by

Robert Donald Peters

2001

All Rights Reserved

ABSTRACT

An experimental examination of creating a true time delay device from an optical coherent transient material is presented. A frequency stabilization system is used to allow for accumulation of several pulse pairs. High bandwidth programming is achieved using a compact frequency chirped external cavity diode laser. The chirped system has the advantage of spreading the programming power out over time, thus allowing for diode laser to take the place of high power Ti:Sapphire systems. A novel technique is used to program a grating from a single frequency chirped pulse, thus lowering the stability requirements.

TABLE OF CONTENTS

1. CHIRPED LASER PROGRAMMED TRUE TIME DELAY 1
   Optical Coherent Transients 4
   Accumulation 10

2. FREQUENCY STABILIZATION 13
   Stability Measurements 17
   Operation of the Locking System 20

3. FREQUENCY CHIRPED LASER 23
   Characterization 27
   Operation 33

4. EXPERIMENTAL CHIRPED LASER PROGRAMMED TRUE TIME DELAY 35
   Single Shot Results 39
   Accumulated Results 45

5. SUMMARY AND CONCLUSIONS 48

6. ACKNOWLEDGEMENTS 50

7. REFERENCES 51

CHIRPED LASER PROGRAMMED TRUE TIME DELAY

The ability to set an arbitrary time delay on a signal is a necessary part of phased array radar applications. In a phased array radar, a radio frequency (RF) signal is generated and sent to a large number of antenna elements. The RF signal sent to each element must be delayed a specified amount in order to create a wavefront that propagates in a particular direction. The time delay can be done electronically with devices such as silicon delays or phase shifters.

In a silicon delay, the signal is sent through one of several paths etched on a chip with different lengths. The effect is similar to adding or removing lengths of cable, and the delay is set by the distance traveled divided by the speed of the signal through the material. This system has a very flat frequency response, however it has some major drawbacks. These devices typically have maximum delays on the order of a few hundred nanoseconds, and can only be programmed in discreet steps.

Phase shifters offer continuous arbitrary delays over their control range, however they suffer from frequency dependent response. As the carrier is modulated, the time delay for each element can change. This results in a condition called beam squint, where the beam size and direction is scaled with modulation. As modulation bandwidth increases, this becomes much more of a problem.

A more desirable solution would be a device that can accept an arbitrary time delay, a large range of delay times, high resolution, and no frequency dependance of the time delay. One possible solution is to use the properties of optical coherent transients (OCT) to produce a true time delay device. It has been demonstrated at low bandwidth that an OCT device can be used for a TTD where the delay can be programmed up to a

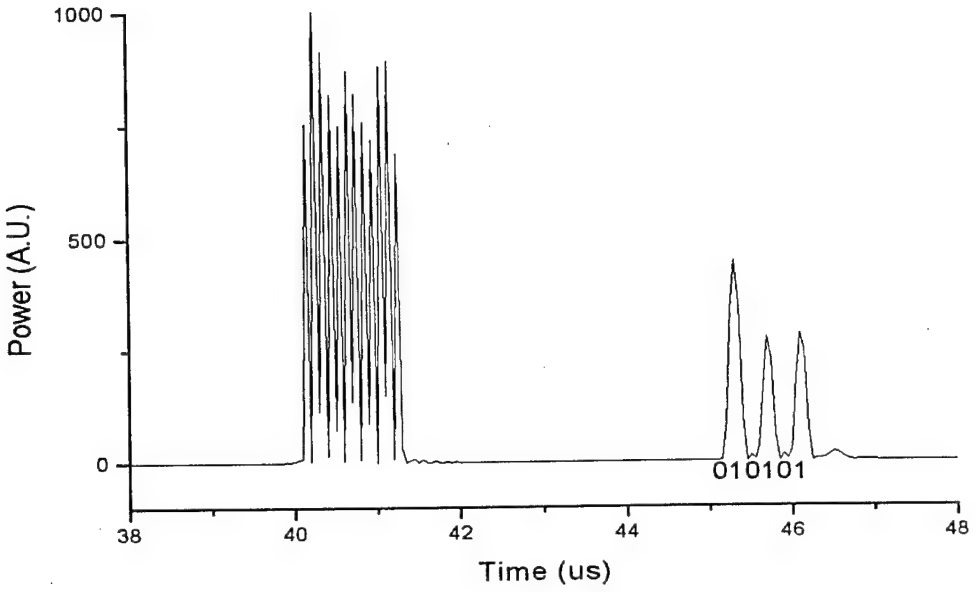

Figure 1: Simulation of delayed data using optical Bloch equations. The data sequence 010101 is delayed 5 us from the input at 40 us. The input data shown at 40 us is distorted due to the simulation.

few microseconds with sub hundred picosecond resolution[1]. The bandwidth of the delayed signal is limited by the bandwidth of the programming pulses and the inhomogenous linewidth of the material.

A simple example of a true-time delay can be made with brief square pulses. In this example a pair of pulses is first sent into the OCT material to program it. The pulses are separated by an arbitrary time τ_{21} limited by the homogeneous dephasing time of the material, T_2, such that $\tau_{21} << T_2$. After the material is programmed, a data pulse may be sent through the material. The output from the material will be delayed from the data pulse by the time τ_{21} programmed from the first pulse pair. The maximum bandwidth is set by $1/t_p$ where t_p is the pulse time. The output can be predicted from the optical Bloch equations for thin medium. Figure 1 shows the results of a simulation delaying the data

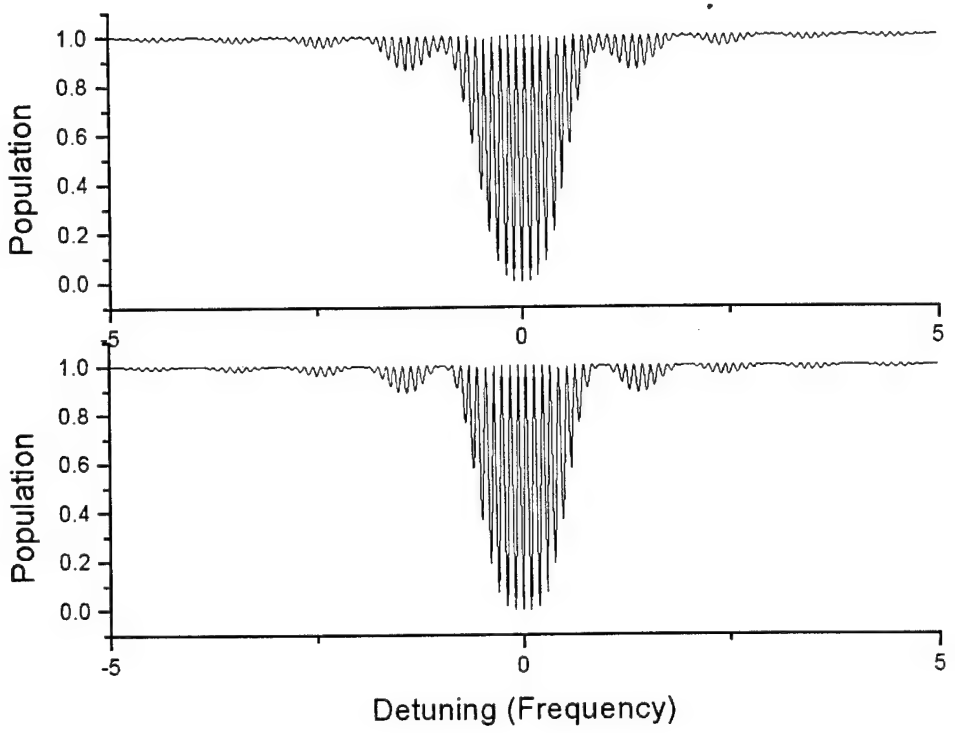

Figure 2: Ground state population after excitation by two chirp pulses (top) and two brief pulses (bottom). The populations run from 0 (ground state) to 1 (excited state) with the detuning in units of frequency.

sequence 010101. The programming was done by two 100 ns pulses at time 5 μs and 10 μs. The data sequence was input as an amplitude modulated signal of 200 ns pulses starting at 40 μs. The expected output should then be observed at 45 μs as shown. Although this provides the desired results, it is difficult to produce high bandwidth pulses that can program the material. It is also difficult to control the delay in a variable way, as it must be set either through a optical path delay, or through setting an electronic delay to trigger the optical pulses.

The OCT material stores the power spectrum of the programming pulses in its population. The two pulses interfere with each other within the population of the material

to create a spectral grating. For brief pulses, the power spectrum that is stored is the Fourier transform of the pulses in time to frequency space. For chirped pulses, the Fourier transform is more complicated, however, the power spectrum is very flat. The interference of the power spectrum stored from two frequency chirped pulses is very similar to that of the interference created by two brief pulses. Thus, we may use two frequency chirped pulses to achieve the same effect as brief pulses. Figure 2 shows a comparison of the atomic population for two frequency chirped pulses and two brief pulses. The ground state population is shown after excitation from two chirped pulses (top) and two brief pulses (bottom). The structure recorded by the medium is the virtually identical for both sets of programming pulses, and it is this structure that gives rise to the delay.

An advantage of chirped pulses is that the power required is much less since it is spread out over time. Another is that the delay time τ_{21} can be changed by shifting the starting frequency of the chirps up or down. This is because the time difference depends on the time between the same instantaneous frequency of the chirp. If the two chirped pulses have a difference between their starting frequencies of $\delta\nu$, and they are separated by a time τ_s, then the time delay programmed is given by[1]

$$\tau_{21}=\tau_s+\delta\nu\left(\frac{\tau_{ch}}{\beta_{ch}}\right) \tag{1}$$

where τ_{ch}/β_{ch} is the inverse chirp rate. Here we still must obey $\tau_{21}<<T_2$.

OPTICAL COHERENT TRANSIENTS

For this work, the inhomogeneously broadened material used is Tm^{3+}:YAG. The Tm^{3+} ion has a very narrow transition from $^3H_4 \rightarrow {}^3H_6$ at 793 nm. This transition is shifted

in frequency due to each ion's local environment. When cooled to under 5K, these shifted transitions do not suffer from phonon interaction. The result is that if a narrow band laser sits on one of these shifted transitions, all the ions get moved into the excited state, and no more absorption can take place. If the absorption profile is then probed, a hole will be apparent at the frequency that had been saturated. This property can be used to program a spectral grating into the material. However, it would be impractical to write a grating by having a narrow band laser sit at each place a hole is desired; therefore, a better way must be used.

The process used is analogous to the way a spatial grating is created in a holographic material. In holography, two beams are incident on the material with an angle between each other. The material stores the intensity of each beam along with an interference term. The interference term leads to a spatial grating that a recall beam can scatter off to produce the information recorded by the first two beams.

Similarly, if two pulses, $E_1(t)$ and $E_2(t)$ separated in time by τ_{21}, are applied to the material it will store the spectral information, $E_1(\omega) \bullet E_2(\omega)e^{-i\omega\tau_{21}}$ of the pulses in the ground and excited state population by linear absorption. When the combined power spectrums of these pulses are stored by the material, an interference term will be present. It is this interference term that leads to the spectral grating stored in the materials population. If a third pulse is then applied to the material, $E_3(t)$, then it will interact with the spectral grating stored in the material to produce a fourth pulse whose signal is given by

$$E_s(t) \propto \int_{-\infty}^{\infty} d\omega E_1^*(\omega) E_2(\omega) E_3(\omega) g(\omega) e^{i\omega t} e^{-i\omega\tau_{21}} \qquad (2)$$

where g(ω)is the absorption profile of the material being used. This equation is valid assuming the input pulses are acting within the linear regime, i.e. none of the input pulses saturate the absorbers at any frequency. We further simplify the equation since the data bandwidth is much narrower than the bandwidth of the inhomogenous medium, we let g(ω)=1.

We can now predict the output signal for temporally complex inputs. First, we will rewrite equation 2 in the time domain to better understand when the output will occur.

$$E_s(t) \propto \int_{-\infty}^{\infty} d\tau_1 E_1^*(\tau_1) \int_{-\infty}^{\infty} d\tau_2 E_2(\tau_2) E_3(\tau_1 + t - \tau_2) \tag{3}$$

We can again use the example previously outlined where we apply two identical brief pulses for pulse 1 and 2, followed by a temporally complex pulse 3. From the equation above, we see that the output should have the same temporal structure as pulse 3 and will occur at a time $t=t_3+\tau_{21}$. We can also put data on pulse 1, and brief pulses on pulses 2 and 3 then the output will be a time reversed representation of pulse 1. Or, we can make the third pulse the same data sequence as the first and obtain a correlation peak. Thus, this material has the potential of doing true time delay as well as optically processing the signal sent through it.

Another condition is that phase matching must be satisfied. For a four wave mixing process such as this, the condition is $\vec{k}_s=\vec{k}_3+\vec{k}_2-\vec{k}_1$ where k_j is the wavevector of the j^{th} pulse, and k_s is the wavevector for the output signal. For example in the chirped experiment, all the pulses are collinear, $\vec{k3}=\vec{k2}=\vec{k1}$. Under this condition, the signal follows the same wavevector as the input pulses. However, if the pulses were separated,

then we are in the realm of spectral-spatial holography, where the output can be spatially isolated from the inputs traveling through the crystal allowing for continuous programming without interfering with the output.

While this gives us a feel for how the system will respond, a more accurate model is given by the optical Bloch equations. By integrating the optical Bloch equations we can accurately predict the response of a thin medium with any variety of inputs. The Bloch equations can accurately model a two level atom where the Bloch vector is used to represent the dipole moment and inversion for an ensemble of atoms[2].

The transition used in Tm^{3+}:YAG is a three level system where the laser interaction occurs between $|1\rangle$ and $|2\rangle$. There is an intermediate state $|3\rangle$ where population from $|2\rangle$ can decay to and eventually decay to $|1\rangle$. The decay from $|3\rangle$ is on the order of several milliseconds, and creates a bottleneck for the population returning to the ground state. If we ignore population decay, then we can use a 2 level system as a model. We are left with a system $|\Psi(t)\rangle=c_1(t)|1\rangle+c_2(t)|2\rangle$.

The Bloch equation can be derived for this system from Schrodinger's equation of motion. See reference 2 for a complete derivation. The Bloch equation is given in terms of r1, r2, and r3 where r1 and r2 represent the in phase and out of phase components of the Bloch vector, and r3 represents the population. The Bloch equations are then written as equations 4-6 where $\Omega(t)$ is the Rabi frequency. Physically, the Rabi frequency is the

$$\frac{\partial r_1}{\partial t} = -(w_0 - w) r_2 \tag{4}$$

$$\frac{\partial r_2}{\partial t} = (w_0 - w) + \Omega(t) r_3 \tag{5}$$

$$\frac{\partial r_3}{\partial t} = -\Omega(t) r_2 \tag{6}$$

rate the Bloch vector is driven through the r3 axis for a given field amplitude. For example, consider a system starting entirely in the ground state such that r3=-1. We then apply a field with sufficient amplitude to drive the Rabi frequency through a π rotation then the population will wind up in the excited state. We then can describe our pulses in terms of their pulse area $A = \int \Omega(t) dt$ such that to directly determine the amount of inversion for a given pulse.

These equations are typically solved in our group utilizing a computer program developed by W. R. Babbitt. This program can solve the equations for a variety of inputs to accurately predict the outputs from an experimental setup. The Bloch equations do not predict the results from the pulses propagating through the material, therefore this program assumes an optically thin medium. Figure 3 shows an example of the output from this program. Here a pulse with area pi/2 is applied at time 5 to 5.5, and a pulse with area pi is applied from 15 to 15.5. The echo is then calculated to appear at time 25. The applied pulses are square pulses, however since the program only shows the polarization after the last pulse, the first two pulses are shown distorted. Since we only are interested in what happens after the last pulse is applied, this is not a problem.

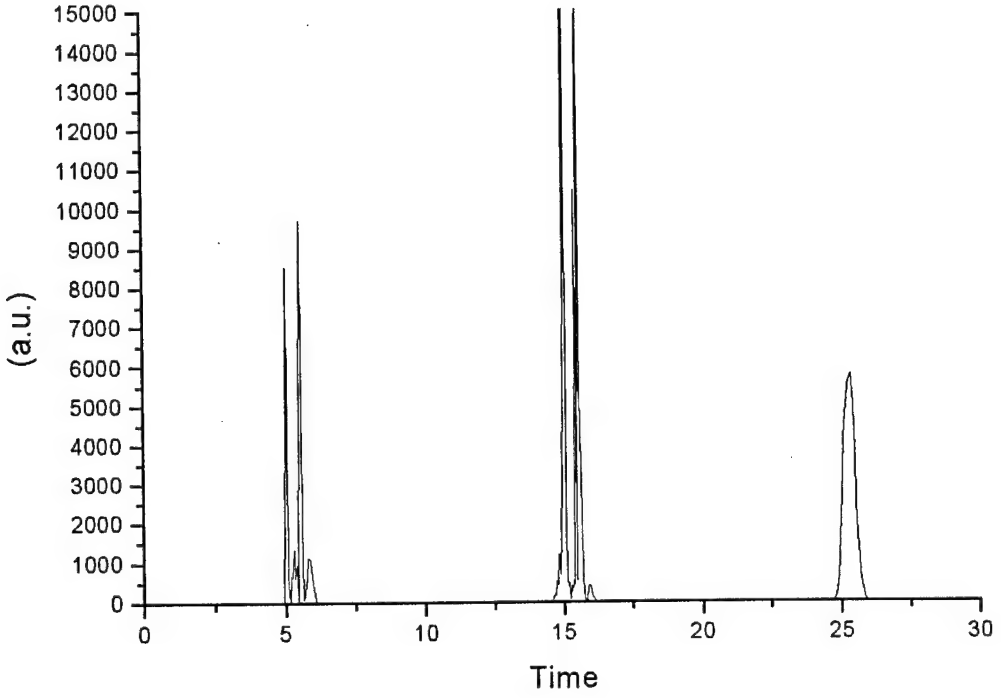

Figure 3: Example of the output of the Bloch simulation program for a two pulse echo. Pulse 1 is from 5 to 5.5 with a pulse area of pi/2, and pulse 2 is from 15 to 15.5 with a pulse area of pi. The echo is observed at 25.

In summary, the purpose for doing these experiments is to investigate potential for developing an optical true time delay in Tm:YAG programed by a frequency chirped pulse. A qualitative description of the optical coherent transient process has also been presented to physically understand the process by which this will be accomplished. This process relies on a material with an inhomogeneously broadened transition within which a spectral grating can be written. In the linear case, this process can be thought of as a pulse scattering off a spectral grating in a way analogous to spatial holography. Finally, for a more accurate prediction of the experimental results, a computer program which integrates the optical Bloch equations can be used.

Accumulation

Accumulation of a grating involves the repeated application of low power programming pulses to the medium. This allows a strong grating to be developed in the material with relatively weak programming pulses. The grating may also be maintained to survive long after population decay would have destroyed a single shot grating. This allows us to use non-persistent materials for continuous processing. Non-persistent material is generally more desirable than persistent materials since they can be easily reprogrammed. While persistent materials can store a grating for long periods of time for repeated access they typically must be heated in order to reprogram the grating. For true time delay, we must be able to change the timing for applications such as phased array antenna control.

The basic setup for accumulation is the same as for singe shot with some added constraints. First, while the process can be done collinear, this is generally not useful since the output follows the same path as the inputs. Generally, the programming and data pulses are sent through on spatially distinct paths which follow the phase matching condition above. This results in the output being spatially separated from all inputs.

Frequency stability is also a very important consideration for accumulation. If two brief pulses are generated by a continuous wave laser with an acousto optic modulator, these pulses will store a spectral grating[3], $G(\omega)=E_1^*(\omega)E_2(\omega)e^{i(\omega\tau_{21}+\phi_{21})}$ + c.c. where ϕ_{21} is the phase difference between the pulses. Now if the laser frequency fluctuates due to short term instability, then the phase difference between the pulses will be different from the previous pulse pair. If we take the first pulse pair as our reference

written at the laser frequency ω_0 then shift the lasers frequency by an amount $\delta\omega_0$ for the next set of programming pulses, the phase difference between the next programming pulses will $\delta\omega_0 * \tau_{21}$. If this is roughly π different from the previous pair, then the grating could be partially destroyed. Thus we must constrain the phase difference between any two pulse pairs to be much less than π. This constrains the frequency fluctuations of the laser to $\delta\omega_0 \ll \pi/(\tau_{21}+\delta\tau_1+\delta\tau_2)$ where t_{21} is the time difference between the pulses, and $\delta\tau_n$ is the duration of the nth pulse. This applies for all pulse pairs applied within the grating lifetime of the material. Frequency difference between pulses outside the grating lifetime of the material do not affect the accumulation. If we take for example a pair of 50 ns long programming pulses with a desired delay of 1 μs, then the above equation requires that the frequency stability of the laser be much less than 0.5 MHz over the grating lifetime. For solids, the grating lifetime is on the order of milliseconds. Thus, for this example, a laser with stability on the order of a hundred kilohertz or better for a few milliseconds would be desirable. This is easily attainable by using frequency stabilization techniques such as the one outlined in the following chapter.

The repetition rate for the programming pulses is also restricted by the material. If the programming pulses are repeated too fast, then coherent interference between pulse pairs can cause a loss in the grating efficiency. This occurs when the successive pulse pairs are sent in within the homogeneous dephasing time, T_2, for the material. To minimize this effect, we set the repetition rate[3], $\tau_r \geq 2T_2$. However, if we want to do continuous processing, then we also want a grating that can be held at steady state. Therefore, we must have the repetition rate fast enough to prevent the grating from fluctuating too much in between programming pulses. To accomplish this, we must have

the repetition rate much less than the grating lifetime. With the previous condition, the most desirable repetition rate is near $2T_2$.

These conditions allow us to determine the proper setup for accumulation of a spectral grating. This allows us to create a spectral grating that can be maintained over a time much longer than the grating lifetime. We may also use this grating continuously with the proper choice of input beam paths. The grating may be easily reprogrammed by simply waiting until the previous grating has decayed away and writing a new one with the desired programming.

FREQUENCY STABILIZATION

To provide the frequency stability needed to accumulate a spectral grating with brief pulses carved from a CW laser source, it is necessary to lock the laser to a stable frequency reference. Such a system was developed to provide a method to measure the frequency shift, and then externally counteract that shift with an acousto-optic modulator. The technique used here is that of Pound-Drever-Hall[4] which makes use of FM spectroscopy[5] with the addition of regenerative spectral hole burning as a narrow frequency reference.[6,7] Previous work describes the external stabilization of amplitude[8] as well as frequency and phase of a ring laser.[9] For our purposes, it has so far been sufficient to reduce the multiple stabilization loops to just one stabilization element, an acousto -optic modulator (AOM), for correcting the frequency. Because our applications typically require more optical power than available with external cavity diode lasers, we have adapted the previous method[6] for use with a Ti:S ring laser to produce nominally 1 W of stabilized output.

For this application, a transient spectral hole in Tm:YAG was chosen as the frequency reference, however other forms of frequency references could have been used with this system. The most common is to use a high finesse Fabry-Perot cavity. This can be constructed to provide a narrow band filter at the desired frequency. While this works well for many applications, it has the disadvantage of being unstable with respect to vibration and temperature. In a Fabry-Perot cavity, the reference frequency is set by the spacing of the mirrors in the cavity. Vibrations can cause rapid changes in the frequency reference, which will be translated by the locking system into frequency instability on the output. Temperature changes can cause the mirrors to change more slowly, altering the

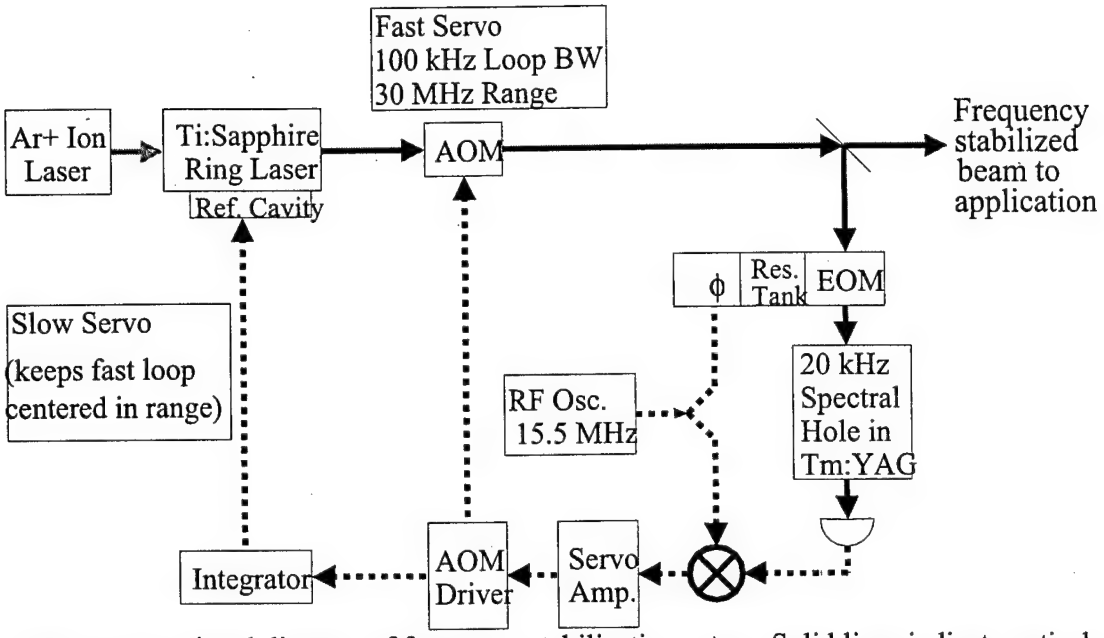

Figure 4: Functional diagram of frequency stabilization setup. Solid lines indicate optical beam paths, while dashed lines indicate electronic connections.

operating frequency. Thus such a system has to be very well isolated both mechanically and thermally. A spectral hole is fairly insensitive to temperature fluctuations so long as it remains below the zero phonon line and acoustic vibrations, so long as the beam stays within the region where the hole is burned. The hole may be placed in frequency anywhere within the inhomogenous line width of the material which leads to much easier frequency selection. The hole width is determined by the homogenous line width of the material, which can be very small. Finally, the OCT crystal could be mounted in the same cryostat as the crystal being used for the accumulation experiment, or different parts of the same crystal may be used for both, thus simplifying the overall experimental setup.

The process is started when the laser is turned on and begins to burn a hole. At first, the hole is very broad and shallow. However, over time, the hole will become

narrow as it restricts the lasers frequency variations. As the hole becomes more narrow and deeper, the locking system can further restrict the frequency variations. This leads to frequency reference that is very narrow and continuously regenerated by the locking system.

Figure 4 shows a functional diagram of the stabilization setup. For the actual experimental setup, the output from the Ti:Sapphire was sent through the AOM twice. This double-pass configuration gives twice the tuning range for the same input. We use the $^3H_6$-$^3H_4$ transition in Tm^{3+}:YAG at approximately 793.2 nm, which is the same transition often used when studying coherent transient applications. Fast frequency jitter is compensated by utilizing the frequency shift of an AOM. The fast corrections are completely external to the laser and have a 30 MHz range of tuning. The output of an argon ion pumped Coherent 899 ring Ti:S laser is first sent through the AOM in a double pass configuration. The output of the AOM is then passed through an electro-optic modulator (EOM) to add sidebands to the laser fundamental at 15.5 MHz. This beam is passed unfocused with a spot size of 2 mm and a power of 70 μW to a 7 mm long 0.1% Tm^{3+}:YAG crystal held in a continuous flow cryostat containing liquid He at 4.5K. The output is detected on a New Focus AC coupled fast photo detector and the electronic signal is mixed with the original 15.5 MHz RF signal. Phase is adjusted before the EOM to allow for the difference in path lengths optically and electronically before the mixer. The mixer output is the error signal needed to provide corrections to the frequency of the laser. It is amplified by a servo amplifier with a response function matched to that of the homogenous hole width. The servo amplifier drives the AOM driver to adjust the frequency of the laser.

Over time, the laser can drift out of the range able to be compensated by the AOM. Therefore, we provide feedback to the laser to keep it within the range of the AOM. The output of the servo amplifier is split and sent to the AOM driver and also into an integrator. The reference cavity circuitry of the Coherent 899 is modified to add a slowly varying corrective voltage offset to the fringe seen by the reference cavity photo detector; this slower servo loop keeps the fast, but limited-range AOM loop centered in its range. The laser then compensates for long-term drift internally allowing for continuous locking periods of tens of minutes or more, so long as the cumulative long-term drift is less than the halfwidth of the reference cavity fringe (≤ 100 MHz). This drift limitation is because we are only adjusting the voltage detected by the photodiode on the reference cavity and not adjusting the rotating Brewster plate within the reference cavity as is normally done when the laser is scanned. The rotating Brewster plate within the 899's reference cavity is what gives it the ability to scan several gigahertz continuously while locked. While this could have been used it would have been more complicated since the range of tuning is set by the front of the 899's control box, and the servo gain would need to be drastically adjusted for every setting. An additional monitoring circuit automatically resets the slow control should it exceed the laser drift outside the range able to be compensated by the slow control. This is accomplished by monitoring the transmitted power through the crystal. If the transmitted power drops below a set threshold, the slow control will shut off to allow the laser to regain lock.

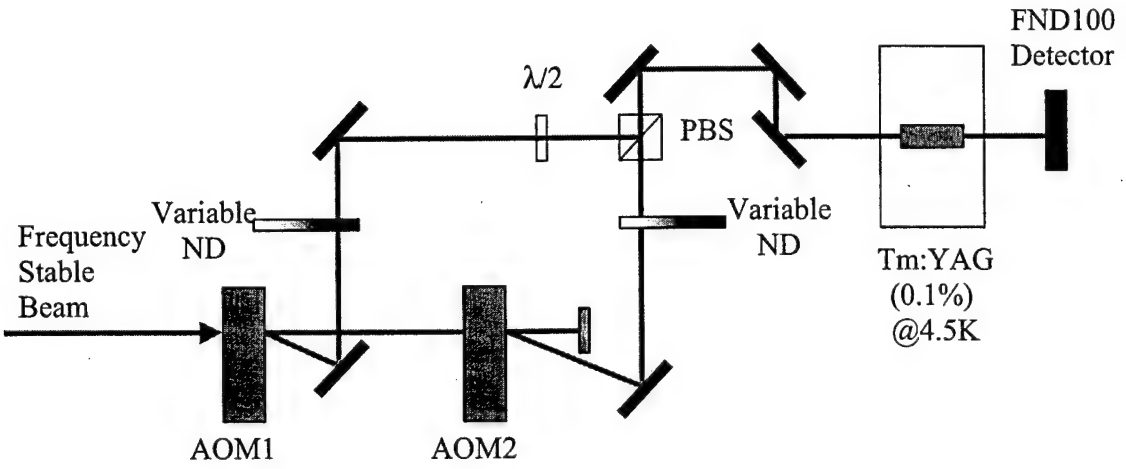

Figure 5: Setup used to measure laser stability. The first acousto optic modulator (AOM) 1 is used to burn a spectral hole, while AOM 2 is used to scan the hole. Both beams can be independently attenuated with the variable neutral density (ND) filters and are combined with a polarizing beam splitter (PBS).

Stability Measurements

Stability measurements were done in a separate 15 mm long 0.1% Tm^{3+}:YAG crystal in the same cryostat. Figure 5 shows the setup used for measuring stability performance. The stabilized output is sent through an AOM1 to make a 1 ms pulse with a single frequency offset of 125 MHz driven by a local oscillator controlled by a series of RF switches. After a delay τ, AOM2 is used to generate a 5 ms pulse with a linear frequency ramp of 5 MHz centered about 125 MHz driven by the tracking generator output of a HP spectrum analyzer. Timing was controlled by a Stanford Research Systems digital delay generator, which triggered the shot, and set pulse widths and spacing. The output is captured with a digitizing oscilloscope and FND100 photo detector. The resulting output is displayed in Figure 6. The captured output is fit with a Lorentzian to find the center of the hole in time (arrival time). If the laser has changed its frequency between when the hole was burned in the material and the probe scan, then the center of

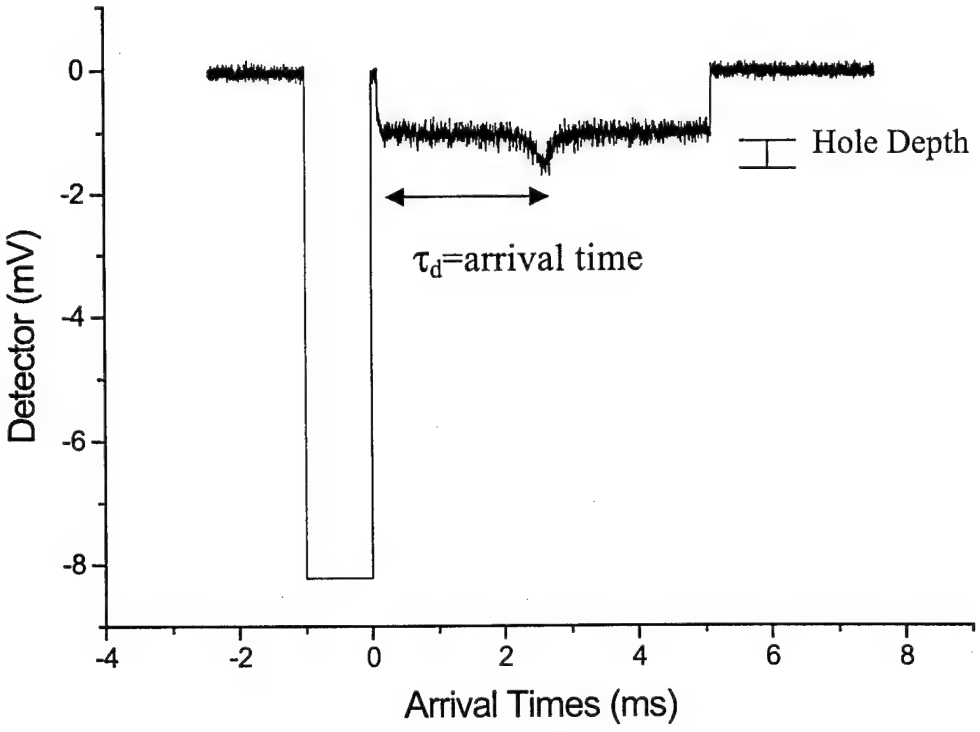

Figure 6: Single shot capture with expected arrival time of 2.6 ms.

the hole will not be at the expected time, but will be shifted in time by an amount proportional to the frequency shift. For the scan given, 125 MHz = 2.6 ms, and the time to frequency conversion is 1 kHz/μs. Several random samples are analyzed this way to find the standard deviation in the arrival times. Figure 7 shows how with a τ_d of 2.6 ms, we measured a deviation of 5.6 kHz. The measurement is limited by the ability to determine the center of the hole. The average error in the fit for this graph is 2.3 kHz. As τ is increased, the hole depth decreases, thus the error in determining the hole center increases. Short-term measurements of 640 μs showed a stability of better than 13 kHz.[3] This can be compared to a measured jitter of 420 kHz at 640 μs, and over 2 MHz at 2.6 ms when the laser is locked only to its internal reference cavity.

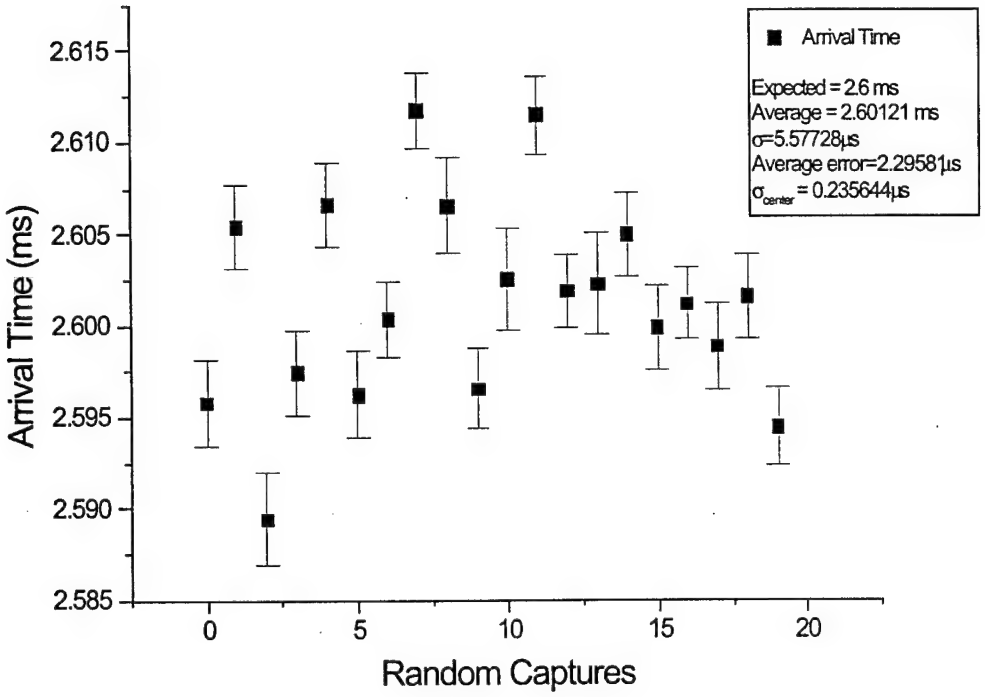

Figure 7: Random captures with an expected arrival time of 2.6 ms.

The effects of the locking system can also be easily seen when doing measurements. When the locking system is turned off, because of uncorrected jitter which alters the starting sweep frequency, the spectral hole is randomly delayed anywhere within the displayed entire scan range window. If we average several single shots, as in Figure 8, we see that when the laser is locked only to the internal reference cavity, the accumulated average of all hole positions is shallow and wide. However, when the external locking system is activated, the hole always appears in the same location and is burned much deeper and narrower.

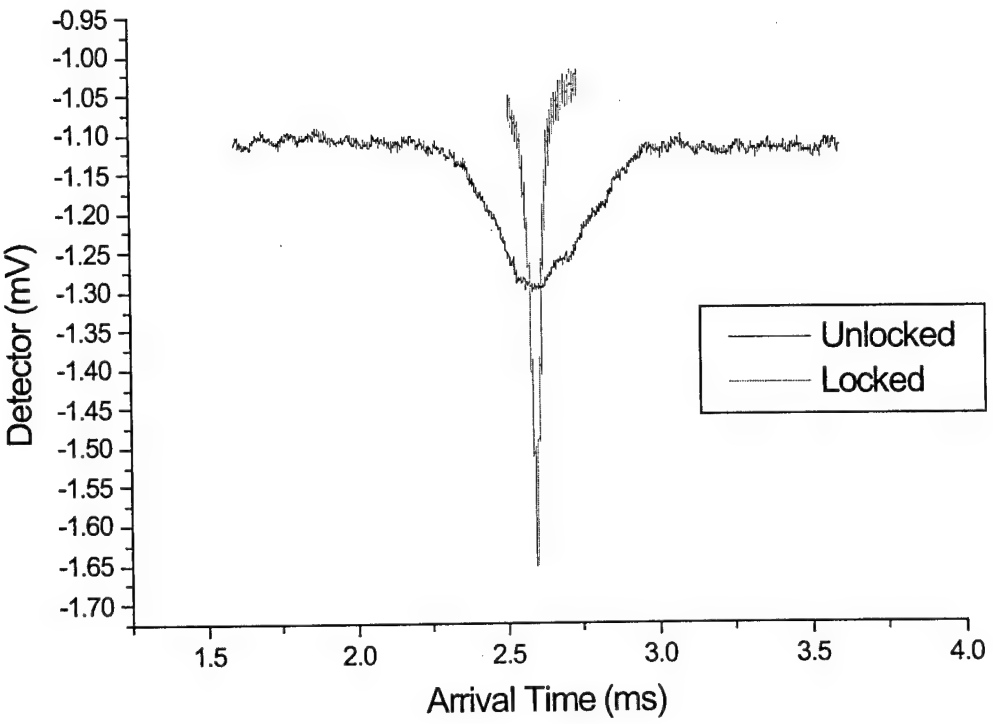

Figure 8: Comparison of measured hole when laser is locked to the spectral hole, and when only stabilized by its internal cavity.

This system has also been used to investigate the effects of continuous programming to accumulate a grating.[10] For the demonstrations done in reference 10 several pulse pairs were applied to the material to build up a spectral grating over time. This programmed grating was then used as a true-time delay with a bandwidth limited by the 125 MHz AOM's used to carve the pulses out of the CW beam. This serves as a successful demonstration of the use of the stabilization system outlined here.

Operation of the Locking System

Operation of this system is fairly straight forward. The beam alignment must be checked before anything can be done with the system. This must be done with both the

fast and slow servo's turned off. The most critical part is the beam must be straight through the electro optic modulator (EOM). Any misalignment can result in amplitude modulation noise, which will reduce the overall frequency stability. With the EOM aligned, the beam may be sent through the Tm:YAG crystal held at approximately 4.5 K. The transmission is then aligned to the New Focus fast phototdetector. The output of the AC coupled (fast) port on the New Focus detector is sent to the mixer and RF spectrum analyzer. The DC coupled (slow) port is sent to an oscilloscope.

The laser may now be set to sweep the maximum amount (19 GHz) with the scan sent to the X channel of the oscilloscope and DC coupled output of the New Focus detector sent to the Y. The laser may now be tuned to find the center of the transition in Tm:YAG. This is apparent by a dip in the transmission where the laser is being absorbed by the crystal. The laser should be tuned to approximately the center of the transition.

The fast servo may be turned on with both integrators. The gain must be adjusted to obtain a smooth profile on the RF spectrum analyzer centered around 15.5 MHz. Too low gain can be observed by the laser rapidly going in and out of lock. Too high of gain can be observed by higher frequency peaks starting to gain power. The higher order peaks are the result of the laser locking and being over driven by the servo amplifier. The DC output may also be monitored, however this is not a good indication of locking performance.

The slow servo may now be turned on, and the output of the DC coupled port from the New Focus detector put into the transmission in port. This allows the slow servo to reset itself if it exceeds the locking range. Gain on the transmission must be set so the circuit turns on when the fast servo is locked, and off when no locking is present.

Gain on the slow servo amplifier is set in a similar way to the fast servo amplifier.

Once all this is set, the system should be operating at maximum locking stability. The laser should remain locked for many minutes, resetting occasionally. It is a good idea to monitor the voltage output of the slow servo with a volt meter to know when it is getting close to its maximum range. Ideally, it should stay around zero Volts, but laser drift will be evident by a trend towards positive or negative voltages. If this range gets too far, it may be good to manually reset the locking system. This is most easily done by momentarily blocking the locking beam with a card.

To summarize, an external frequency stabilization system for has been presented and successfully tested. This system has been used to allow the accumulation of a spectral grating where it would not have been possible with the laser alone. Since this system does all fast frequency corrections externally, it could be easily adapted to any laser system without modifying the laser. The system could also be adapted to most inhomogeneously broadened materials. Finally, with the current technology in fiber based frequency shifters and phase modulators, the system could be built into a fiber coupled package that could be made very small and portable.

FREQUENCY CHIRPED LASER

For true time delay programming in optical coherent transient materials, chirped pulses may be substituted for brief pules. The principle advantages to using chirped pulses is that it spreads the power required to program a given bandwidth over the duration of the chirp, and the timing can be changed by shifting the start frequency of the two chirps with respect to each other. Thus, the total pulse power required can be much less than that of a comparable brief pulse and a simple means of choosing the time delay can be created. While acousto-optic modulators are capable of creating frequency chirps from a frequency stable CW laser, the bandwidth of the acousto-optic modulators available was relatively low. The bandwidth of the signal that can be delayed must be less than the bandwidth of the chirp to prevent distortion of the delayed signal by spectral filtering. Also, the chirp must be programmed such that homogenous dephasing in the material does not interfere with the spectral grating being programmed. Thus, a laser capable of spanning a large frequency range in a short period is desirable. Such a laser was designed by Kevin Repasky based on work done at the University of Oregon[6], and built by Joe Fischer and myself.

There are many ways that a external cavity diode laser can be tuned. The most common methods are by adjusting the current and temperature for small tuning, and mechanical tuning of the grating feedback with a screw and piezo electric stack. The fastest method of these is adjusting the current. However, tuning with diode current over a large range results in drastic changes to the laser output power. For chirp programming, we desire a flat power spectrum, thus this is not desirable. The mechanical tuning with the piezo electric stack is the next fastest, and while it can tune the laser over much larger

ranges, its response is on the order of kHz. Temperature tuning is very slow with responses on the order of seconds. These methods do not satisfy the requirement of programming within the homogenous dephasing time. Thus, the method chosen includes an intra-cavity electro optic crystal. This method has a range limited by the free spectral range of the cavity, and the response is on the order of MHz.

An external cavity diode laser in the Littrow configuration was chosen to minimize the cavity length and thus maximize the free spectral range of the laser[11]. With the free spectral range maximized, we obtain single longitudinal mode output, and achieve the most tuning range without mode-hop. In this design, a diode laser with an anti-reflection coating on the first surface is directed at a grating. The first order of the grating is reflected back to the diode, while the 0^{th} order is used as the output of the laser. As the grating is rotated, the frequency of the laser is selected.

The frequency of the laser also changes as the optical path length of the cavity is changed. Any integer number of half wavelengths will be resonant with the cavity. Therefore, the optical path length is given by $m\lambda/2 = n\,l$ where m is an integer, λ is the wavelength, n is the index of refraction and l is the distance the beam travels with index of refraction n. If multiple mediums is present, the n*l from each segment is added.

In between the diode and grating, a lithium niobate crystal was placed in the beam path (Figure 9). The crystal was oriented to take advantage of the r_{33}=30.9 X 10^{-12} m/V electro-optic coefficient, with electrodes plated on either side of the crystal to which high voltages could be applied. The extraordinary refractive index for this crystal is n_e=2.2. The crystal length was l=10mm, and the electrode spacing was z=2.5mm. As the voltage is changed on the crystal, the index of refraction changes for the polarization of the diode,

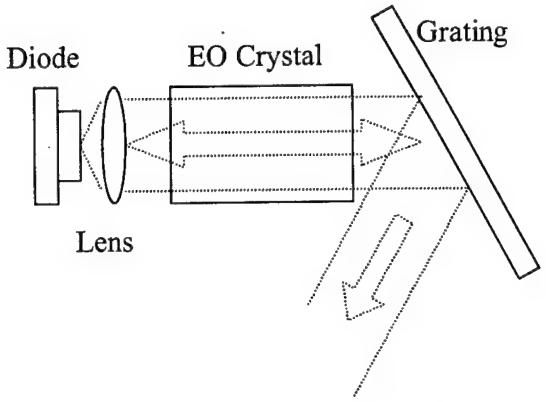

Figure 9: Essential parts of a Littrow configuration chirped external cavity diode laser. The dashed line indicates the beam path, while the double arrow indicates feedback from the first order of the grating. The intra-cavity electro-optic crystal is used for rapid frequency tuning.

changing the optical path length is changed and thus changing the frequency of the laser. This path length change can be found by[11] $dL = \lambda V/(2V_\pi)$ where L is the cavity length and where the half-wave voltage is given by[11] $V_\pi=\lambda z/(r_{33} n_e^3 l)$ which is approximately 600 V for this crystal at 793 nm. Here z is the electrode spacing and l is the crystal length.

A disadvantage to using the Littrow configuration is that the output beam changes angle when the grating is tuned to select a desired frequency. This makes beam alignment very difficult, especially when coupling into a fiber. To compensate for this behavior, a roof prism is placed at 90 degrees to the grating, thus forming a corner cube. The result is that angular shifts are changes to linear shifts, making alignment much easier.

Figure 10 shows the completed laser assembly. The laser and crystal were mounted on an aluminum base which was thermoelectrically temperature controlled. The grating and roof prism assembly were mounted on a separate aluminum plate. This plate was hinged on a piece of phosphor bronze in a pivot point calculated to change the length of the cavity while simultaneously changing the incident angle of the laser on the

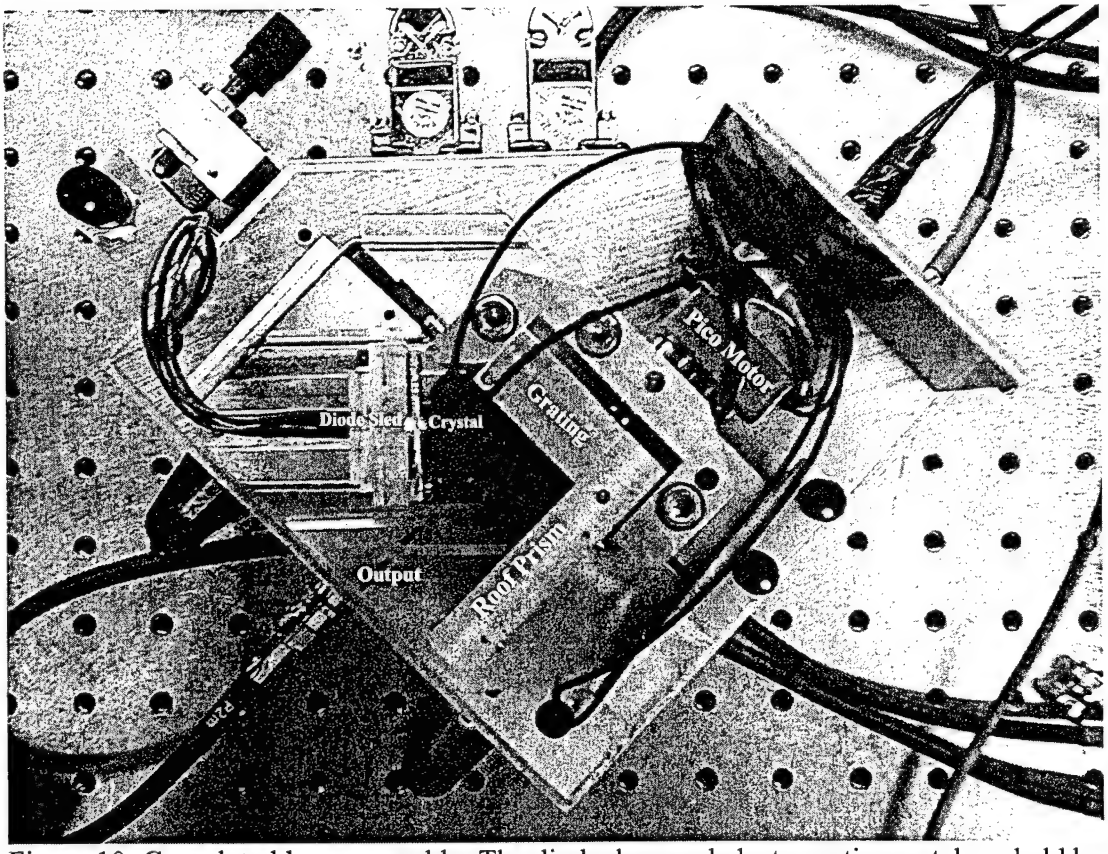

Figure 10: Completed laser assembly. The diode, lens and electro optic crystal are held by the diode sled. The pico motor is used for fine adjustments of the grating to maximize feedback. The adjustment screws are used to maintain the proper feedback through course tuning. During operation, the entire assembly is housed by an aluminum box (not shown) to minimize temperature changes.

grating[12]. Course frequency tuning was accomplished by a 100-pitch screw that could push against the base plate for the grating. Finer tuning was done by a PZT stack mounted in the grating base plate to push against the course tuning screw. The laser was mounted on a tip-tilt plate and enclosed to minimize temperature changes.

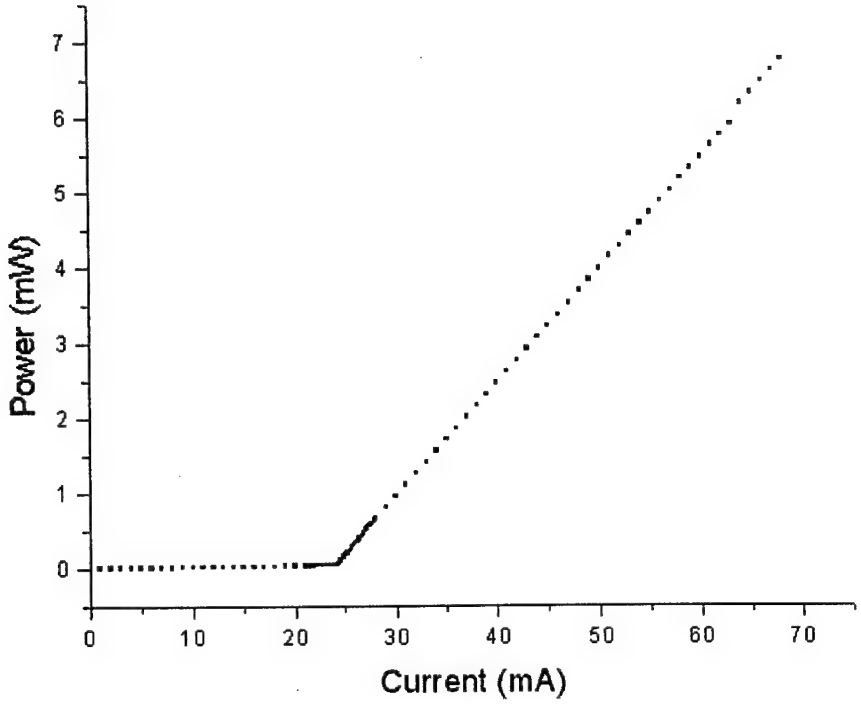

Figure 11: Power vs. Current curve for diode with feedback.

Characterization

One of the first tests done on the laser was the generation of a power vs. current (PI) curve. Figure 11 shows the plot of measured power for several different current settings. Power was measured directly on a New Focus 810 power meter. This graph shows that the laser threshold is at ~25 mA, and the laser is capable of producing a maximum of 6-7 mW. While this may be enough power to do accumulation, it will need to be amplified for single shot experiments.

The lasers response to voltage on the PZT stack and crystal were both characterized prior to using the laser for experiments. To characterize the PZT, the

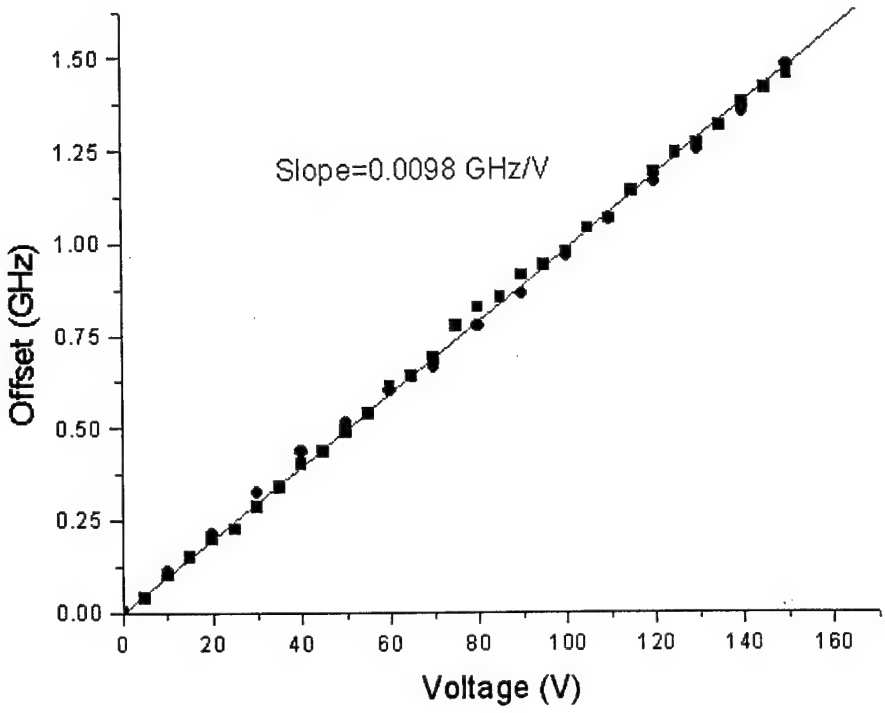

Figure 12: DC response of the electro-optic tuning with voltage. Here a DC voltage is applied to the crystal, and the frequency read directly on a Wavemeter.

voltage was stepped from 0 to 149 V dc in one Volt increments. At each step, the frequency was measured on a Burleigh Wavemeter. There did seem to be some problem with the PZT tuning, as it was very unpredictable. A linear increase in PZT voltage resulted in very strange sawtooth like frequency shifts. The behavior was similar to mode-hopping, however on a much smaller scale. The graphs were not repeatable, and the frequency shifts move on every run. The problem did not appear to be due to the PZT stack, as another stack was tried with the same result. I decided to not peruse the problem since the frequency would stay wherever it was set, and I could get between 5 and 10 GHz of tuning, although the path was not predictable. I think the problem lies in the

crystal used in this laser, which was significantly longer than the one it was designed for. This can be checked when the crystal the laser was designed for is put in place and the laser is realigned.

To determine the response on the crystal was more complicated. The DC response was measured in a similar way to the PZT stack. A voltage was applied to the crystal and stepped from 0 to 150 V dc in 1 Volt increments. The frequency was measured on a Burleigh Wavemeter, and then the data was plotted and a linear fit applied. Figure 12 shows a plot of the frequency shift for a given DC voltage applied across the crystal. The slope of the linear fit gives us the tuning response for the crystal R_{∞}=9.8 MHz/V.

Unfortunately, the time response of the Wavemeter is about 1 Hz, which is far to slow to verify the laser frequency can be changed on the order of a microsecond. To verify this response of the lasers electro-optic tuning at high speeds, a method utilizing the deviation from the Lorentzian line shape transmission of a flat plate Fabry-Perot cavity was used[13]. In this method, the Lorentzian line shape is measured with and without modification from the frequency chirp of the laser. The non-modified Lorentzian is then shifted in time and then we look for the intersection of the two Lorentzians. By equating the phase of the shifted and non-shifted Lorentzian, the intersection can be found and related to the magnitude of the chirp. With the laser frequency ν_0 much greater than the change in frequency caused by the EO crystal $\Delta\nu$ and the scan length of the Fabry-Perot cavity $\Delta L(t)$ is much less than the total length of the cavity L_0, then the frequency as a function of time is found by[18] $\nu(t)=FSR\ (t_s/t_{FSR})$ where t_s is the time shift of the Lorentzian and t_{FSR} is the time it takes to scan one free spectral range. This relationship holds true

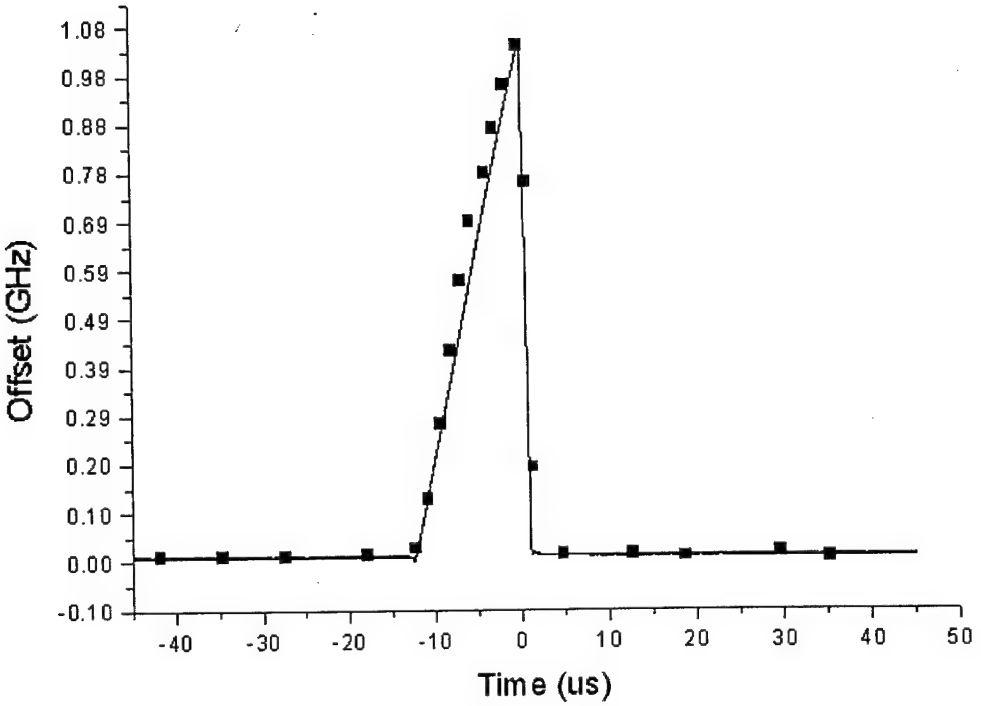

Figure 13: A 1 GHz chirp in 12 us. The solid line is the voltage input to the crystal and the points are the measured frequency.

only for linear ramps.

For these measurements, the free spectral range of the Fabry-Perot cavity is 22.4 GHz and scanned one free spectral range in 33 ms at 793 nm. The cavity transmission was detected on a New Focus 2001 detector and captured on a digital storage oscilloscope. The electro-optic crystal in the laser was driven by a ConOptics high voltage amplifier with a gain of G_{HV}=200 V/V, and the ramp was generated by a HP function generator. The expected output from the laser is given by $\Delta\nu(t)=V(t)G_{HV}R_{eo}$ where V(t) is the ramp applied from the HP function generator. This gives the solid line shown in figure 13. To compute the frequency, the non-modified Lorentzian is

graphically shifted in time from the modified Lorentzian. For example, for a shift of 0.1 ms corresponds to a frequency shift of 67 MHz. When the shifted Lorentzian intersects the non-shifted Lorentzian, this corresponds to a frequency shift of 67 MHz. This time can then be plotted against the input to see how well the laser frequency tracks the input. From figure 13, we can see that the laser frequency follows the input very well. There is a slight deviation from the expected output, however this is probably due to power fluctuation of the laser during the chirp. When the laser uses electro-optic tuning to change the frequency, the feedback from the grating remains the same. Therefore, the feedback from the grating may be less during part of the chirp. This results in a change in the power extracted from the diode, and thus a difference in the output power.

The next generation of chirped lasers is currently being designed. These designs could dramatically increase the tuning range of the laser while lowering the voltage requirements. The overall size of the laser could also be decreased substantially.

To increase the output power of the chirped laser, it was injection locked[14,15] to a high power slave diode laser. Injection locking is a technique where the output from a low power diode laser is fed into a higher power free running diode laser with a similar gain profile. The result is that the high power free running laser emits a beam with the same spectral characteristics as the low power diode laser, with more optical power. Injection locking was used to increase the power from the chirped external cavity diode laser. The injection locking system designed by R. Reibel and Z. Cole was used for this laser. In this setup, the free running diode laser's front facet was anti-reflection coated for R=1.0E-3 and the power from the master just before the slave was on the order of ~200 μw. The master chirped laser is coupled into a single mode polarization preserving fiber

to access the injection locking setup. This is done due to the critical alignment needed to inject the master into the slave laser. By fiber coupling the master into the slave setup, the master laser can be easily changed without affecting the beam alignment into the slave. While injection locking systems may be used to modulate a master lasers signal, in this application it was only used for amplification.

Using injection locking for amplification offers advantages over more traditional means of diode amplification. Doped fiber amplifiers are not always available at the wavelength required, such as with 793 nm. There may also be a problem with amplified spontaneous emission when the master signal is not present. However, with injection locking, the same types of diodes used in the master can be used as the slave. In addition, when the master signal is turned off, the slave laser quickly changes its frequency away from the operating frequency of the master. The shift can be on the order of nanometers away from the desired operating frequency. Since the slave continues to lase even without the master, the background remains low. Since it lases far away from the desired operating wavelength, leakage is not a problem.

To summarize, a laser system was created to produce high bandwidth frequency chirped pulses. The system included a custom built external cavity diode laser to produce the desired frequency characteristics which was amplified by an injection locking system to increase the output power of the master without affecting the frequency characteristics. Future work on the chirped laser should produce even higher bandwidths than that achieved here. In addition, the power requirements of the experiment may not require the use of injection locking, further simplifying the laser system.

Operation

The laser and all electronics must be given time to warm up and stabilize before any adjustments are done. For this system at least an hour is needed. After that, the laser must be tuned to approximately the correct wavelength using the course tuning screw. This is a very course adjustment, and should not need to be done unless the cavity configuration has been changed. The output of the chirped laser should be checked on the optical spectrum analyzer to verify single mode operation and good side-mode suppressing. If any adjustments are needed, they should be done using only the pico-motor.

Once single mode operation has been verified, mode-hop free operation should be checked with the Fabry-Perot spectrum analyzer. This should be done with a chirp frequency on the order of a few Hertz, and no more than two volts peak to peak should be applied to the high voltage amplifier input. If the laser mode hops during the frequency the bias control on the high voltage amplifier can be adjusted to make the sweep continuous.

After the chirped laser is performing adequately, it may be coupled into the injection locked laser. Start with the injection locked laser well below threshold and observe the output on the optical spectrum analyzer and Fabry-Perot spectrum analyzer. The output should be exactly what was seen before the injection locked laser. Adjust for the maximum input power and then ramp the current on the injection locked laser to its operating level. For this laser, a current of around 100 mA should be suitable. If the injection locked laser won't lock to the chirped laser between 100 and 110 mA, then the temperature controller for the injection locked laser probably needs to be adjusted to

bring the gain region close enough to the output from the chirped laser.

The output from the injection locked laser may now be sent through the Tm:YAG crystal. A photodetector measuring transmission through the crystal should be monitored for absorption. The PZT adjustment on the chirped laser can be used to bring the chirped laser to within the absorption bandwidth of the Tm:YAG crystal. If the chirped laser mode-hops over the transition, then the temperature of the chirped laser must be changed. This is a slow adjustment, and time must be given for the temperature to equalize before further adjustments are made. Once the temperature is set, it should not have to be changed from day to day unless the cavity configuration is changed.

EXPERIMENTAL CHIRP LASER PROGRAMMED TRUE TIME DELAY

As stated in chapter 1, a frequency chirped pulse may be used to program a true time delay in an OCT material. The goals of this experiment were to demonstrate a method for writing a spectral grating utilizing a frequency chirped laser, and that the spectral grating could be accumulated. For this experiment, the frequency chirps were formed from the external cavity diode laser described in the previous chapter. However, since this laser changes its cavity frequency instead of having an external device modify the frequency the normal method of using two pulses separated in time, it would be very difficult if not impossible to accumulate a spectral grating. As the laser changes its cavity to change the frequency, there is no way to return to the starting phase of the pulse without some external device. An external phase locking device was considered, however we found a method which made it unnecessary.

A novel technique is then used to create a time delay τ_{21} in the crystal. A single chirp from the injection locked chirped external cavity diode laser is passed through an acousto-optic modulator driven with two frequencies with an offset $\delta\nu$. This eliminates the time shift τ_s in the equation above. The delay time is then found by determining the time when the instantaneous frequency of the downshifted chirp overlaps with the start of the up-shifted chirp. This also eliminates the need for an external phase locking system for accumulation, as the phase between the chirps is set by the digital frequency synthesizer used to drive the AOM.

The experimental setup is outlined in figure 14. The output power of the chirped external cavity diode laser is at most three mW. In order to achieve the power needed to program a grating in Tm^{3+}:YAG, the output from the chirped external cavity diode laser

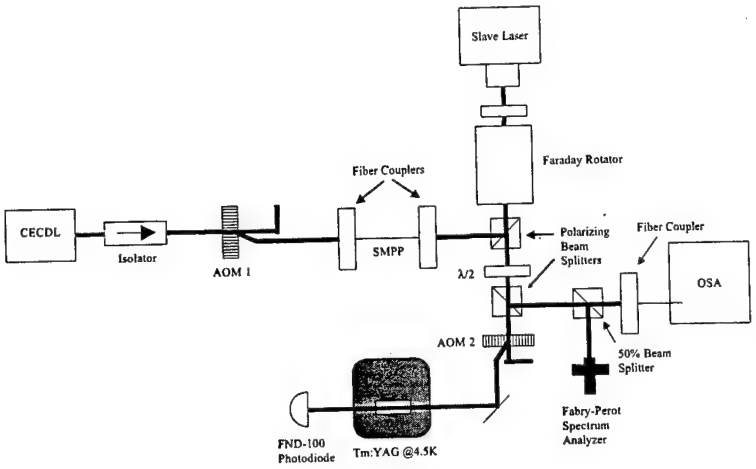

Figure 14: Representation of optical setup.

must be fed into a diode laser for injection locking. The output from the injection locked diode laser has the same frequency properties of the chirped external cavity diode laser and 50-60 mW of power.

The inhomogeneously broadened material used for these experiments was a Tm^{3+}:YAG crystal on the $^3H_4 - {}^3H_6$ transition at 793 nm with an absorption length, αL=1.4, held at a temperature of 4.7K in a continuous flow liquid helium cryostat. The beam was focused to a ~70 μm ($1/e^2$ diameter) spot in the crystal. The pulses were detected after the crystal on an FND100 photodiode and displayed on a 350MHz digital storage oscilloscope. The frequency chirp of the laser is set by a HP function generator operating in sawtooth mode. The output is sent through a Con Optics high voltage amplifier with a gain of 200 V/V. This generates the voltages required to drive the electro optic crystal within the cavity of the external cavity diode laser. The response of

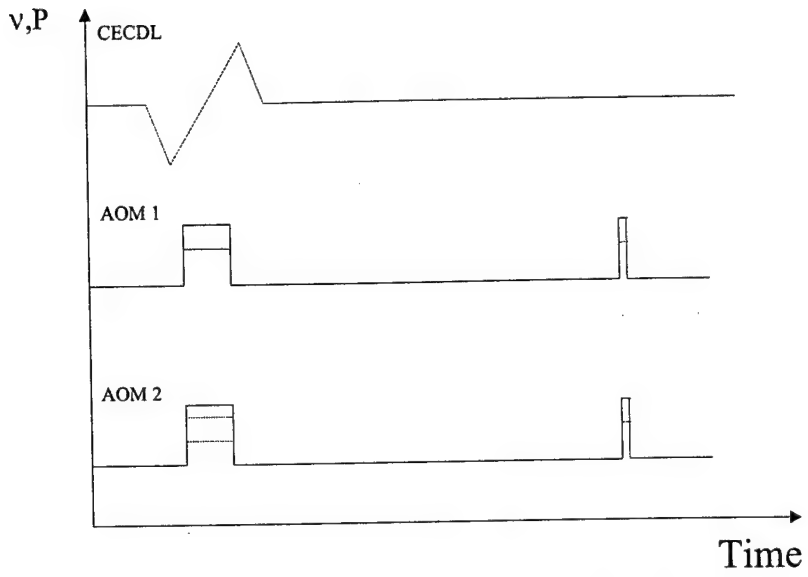

Figure 15: Schematic of the pulse inputs into the crystal. The delayed signal would appear after the last pulse.

the high voltage amplifier is better than 1 MHz.

An AOM after the chirped laser is used to provide better noise suppression for the experiment. The AOM is only opened during the up ramp of the frequency chirp, and at a time later for the data pulse. This AOM is controlled by a local oscillator with amplifier turned on and off by the video input. When open, the power is high enough to operate the injection locking system. When off, there is not enough power to be injection locked, and the free running diode laser jumps to its natural lasing wavelength. The injection locked laser is set so that its wavelength with no input is about 5 nm away from the transition in Tm:YAG.

The AOM after the injection locking system is used split the chirp by driving it with two offset frequency and at a single frequency for the data pulse. The beam was focused in the AOM to ~100 μm ($1/e^2$ diameter) spot size. The AOM is controlled by a

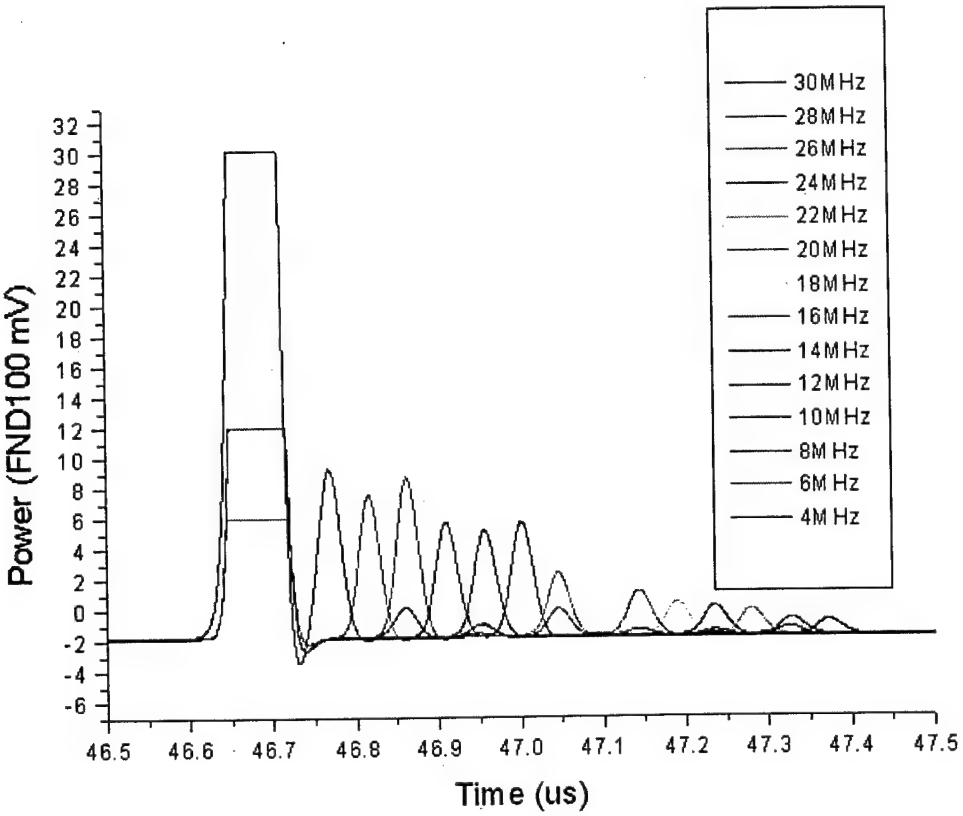

Figure 16: Several single captures at various offsets. The first pulse is the probe, followed by the delayed pulse.

Tektronix arbitrary waveform generator. The AOM has a bandwidth of approximately 35 MHz. The driving equation for the AOM was

$$P_{rf}=\cos(2\pi(125-\delta\nu)*10^{6}t)+\cos(2\pi(125+\delta\nu)*10^{6}t) \qquad (7)$$

where 125 MHz is the center frequency of the AOM, and $\delta\nu$ is the frequency offset. As this function ranges from 0 to 2, the amplitude on the ARB was set to ½ to allow for the full signal range to be set to the AOM. Figure 15 shows a schematic of the pulse sequence into the crystal.

All devices were triggered by separate channels on a Stanford Research Systems digital delay generator. This allowed the timing of each device to be adjusted to

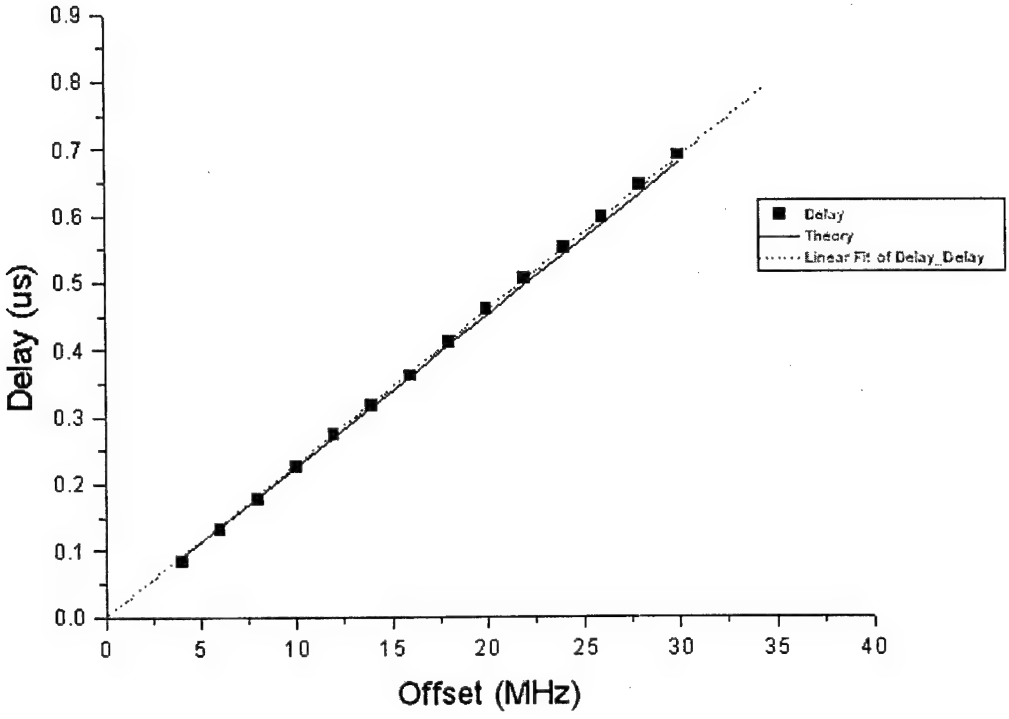

Figure 17: Plot of measured delay Vs programmed offset. The theory line is plotted based on the programmed offset and measured chirp rate. Also a linear fit is made through the 0,0 point.

compensate for the delay caused by the speed of sound in each AOM. The SRS delay generator is also set the repetition rate, which for all experiments was 10 Hz.

Single Shot Results

For the first experiment, the chirp rate was kept constant, the offset of the two frequencies into the acousto-optic modulator, $\delta\nu$,was changed to demonstrate how the time delay τ_{21} changes with offset. For this experiment, the chirp rate was 45 MHz/μs with a 10 μs long chirp pulse and the bit being delayed had a bandwidth of 30MHz with a

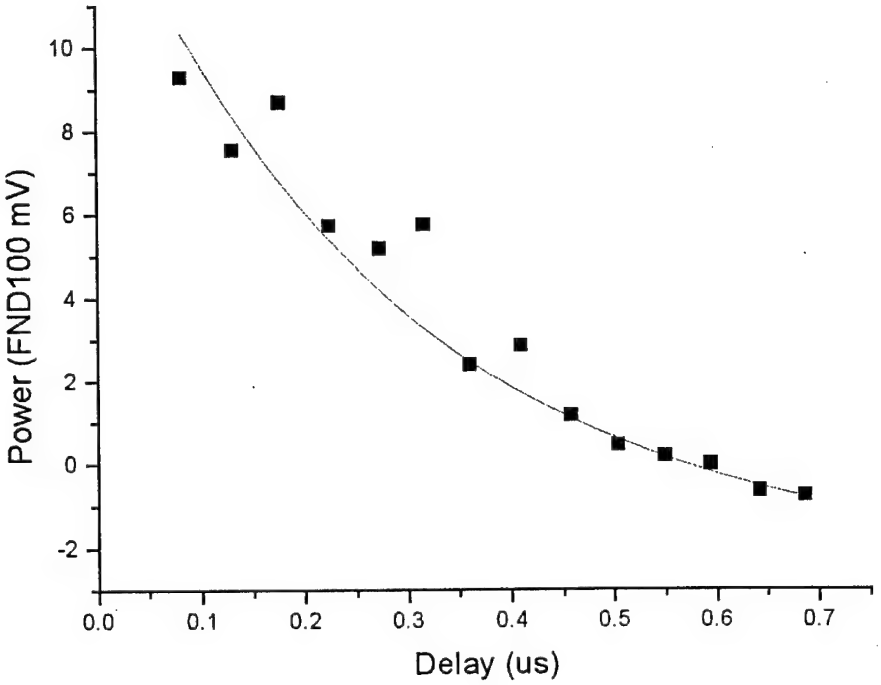

Figure 18: Plot of the data power Vs delay as the offset on the AOM is changed. The exponential fit predicts a T2 of 1.15 us, much less than the measured T2.

center frequency at the center of the chirp and a power of 40 mW. Figure 16 shows several single shot captures with the offset frequency $\delta\nu$ varied from 4 to 30 MHz. The delay between the input and output pulse is plotted on Figure 17. The theoretical line is calculated by inserting the appropriate offset and chirp rate into equation 1 above. From this graph, we can see good agreement between the programmed delay and actual delay.

The echo's power diminishes as the delay is pushed farther from the input data. This is expected and is normally a function of the homogenous dephasing time of the material and is given by the equation

$$I_{echo} \propto e^{\frac{-4\tau_{21}}{T_2}} \tag{8}$$

where τ_{21} is the delay and T_2 is the homogenous dephasing time. However, if we look at the rate of decay for the power, we notice it is much faster than is predicted from the homogenous dephasing time. Figure 18 shows a plot of the power of the delayed data pulse versus the delay programmed by the offset into the AOM. The exponential fit predicts a T_2 of 1.15 μs, much less than the measured T_2. We must then assume that the rapid decay is a result of something other than just homogenous dephasing. While some part may be contributed to spectral diffusion, it is probably not the main cause since this effect has been observed with a chirped pulse of 40 MHz and spectral diffusion should have much more of an effect at higher bandwidths than at the lower bandwidths. Another possibility may be beam diffraction within the AOM. If the beam is focused too tightly into the AOM, the two-tone input could make two separate beams instead of one beam with two frequencies. The result is that as the offset is increased, the beam separation will also increase. Thus the beams will no longer be collinear within the crystal, and the strength of the echo will depend on the phase matching of the beams. This can be checked sending the output of the AOM through a fiber before it gets to the crystal. Any angular separation between the beams should then be eliminated.

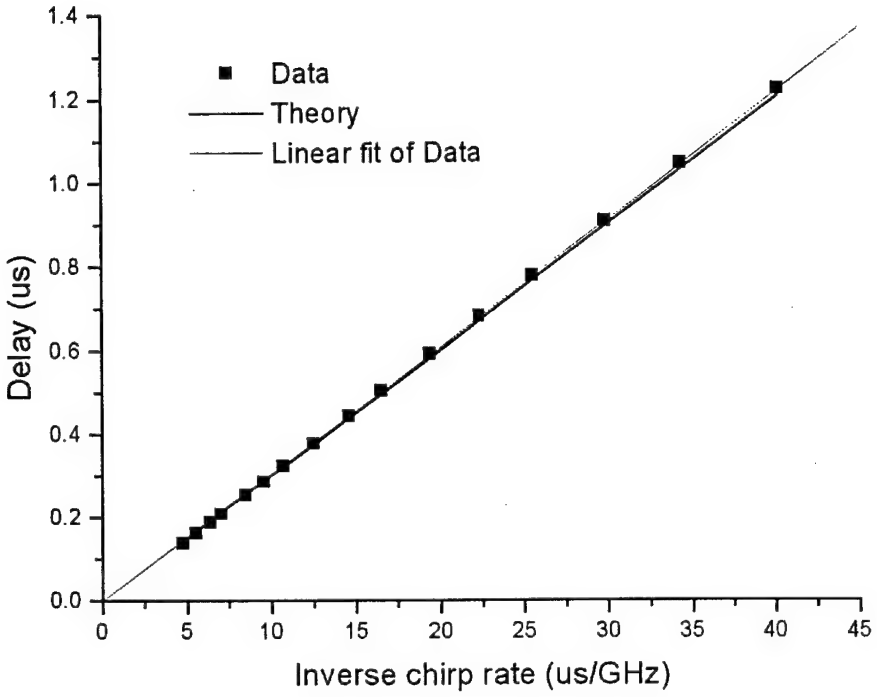

Figure 19: Delay plotted vs. chirp rate with AOM offset set constant at 30 MHz. This shows nice linearity and good prediction between theory and a linear fit of the data.

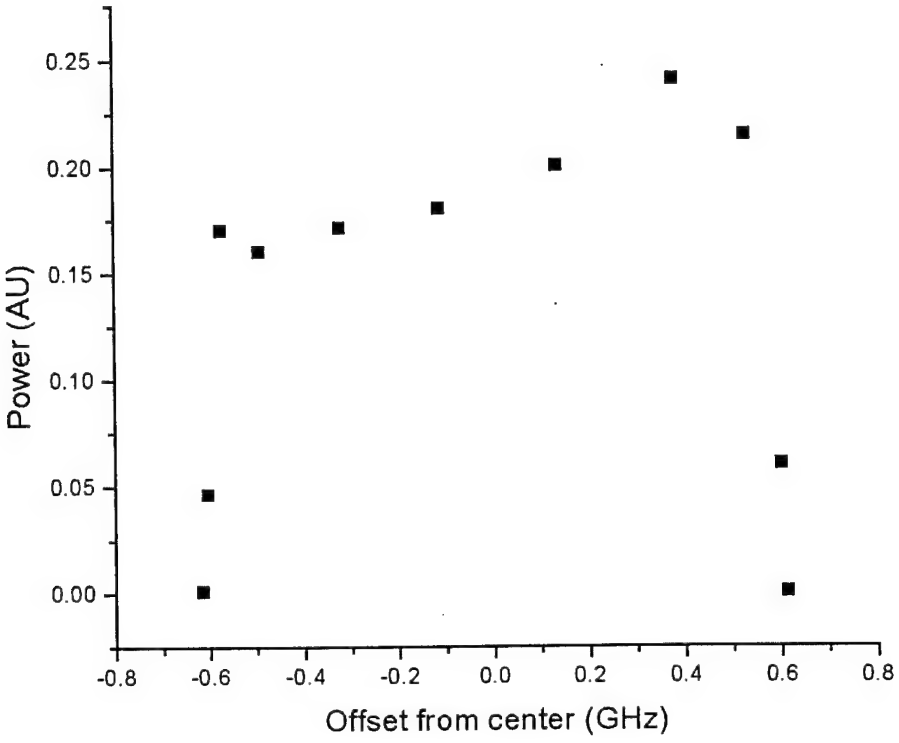

Figure 20: Power plotted versus offset from center of the programming chirp.

For the second experiment, $\delta\nu$ was kept constant at 30 MHz, and the chirp rate was varied by holding τ_{ch} constant and changing β_{ch}. The time between the middle of the brief pulse and the center of the echo was measured as τ_{21}. The results shown in Figure 19 show that the dependance of τ_{21} on bandwidth as described in equation 1 above. The chirp rate here was varied from 0.02 GHz/μs to 0.2 GHz/μs by changing the output peak to peak voltage into the high voltage amplifier and maintaining a constant chirp duration of 10 μs. While this does show good agreement between theory and measured delay, changing the chirp rate would probably not be used in a true time delay device. In a particle true time delay device, chirp rate would be held constant to accommodate the

bandwidth of the signal being delayed, and only offset would be changed.

The bandwidth of the data you can delay is limited by the amount of overlapping bandwidth of the chirp, given by β_{ch}-2$\delta\nu$. Although this setup could not generate a bit much shorter than 33 ns, corresponding to a bandwidth of 30 MHz, it was possible to change the center frequency of the data bit. Thus, we are reasonably sure that we are programming the full bandwidth even if we are not entirely utilizing it.

Figure 20 shows the results of changing the offset of the probe pulse through the bandwidth programmed by the chirp. The frequency chirp is over 1.27 GHz centered about 0 in 10 μs. The probe pulse is 30 MHz and is applied at several offsets within the bandwidth programmed. It is expected that the echo should rise rapidly once it is within the overlapping bandwidth, and have a constant amplitude while within the overlapping bandwidth. The figure does show some variation in echo power. These are probably due to the power response of the chirped laser into the injection locking setup. As the frequency chirps, the feedback to the diode varies slightly resulting in a change in the output power. Unfortunately this effect is unavoidable with this laser design, however future chirped laser designs may not have this flaw.

All these experiments have been with single shot programming and probing, however this is not useful for a true time delay device. With single shot programming in a non-persistent material such as Tm:YAG the data can only be delayed as long as the programmed grating is present. After the grating is programmed, the excited absorbers will decay back to the ground state. The useful time for the grating, T_1, is typically defined as the 1/e time for the exponential decay from the excited to ground state.[3]

Accumulated Results

A possible solution to this problem is to use continuous programming to accumulate a grating over time. In this method, the programming pulses are lowered in power and repeated over time. The repetition rate is set such that the time between programming pulses is long enough to minimize coherent beating effects between the programming sets.[10] The phase relationship between programming pulses must be maintained for all pulses that fall within T_1. Any phase changes longer than T_1 will not be remembered by the material.

With this method, the grating can be built up to steady state and maintained through long periods. If the programming pulses and probe pulses are input along spatially distinct directions, then the material may be programmed and probed continuously. The inputs must obey the phase matching condition $k_e=k_3+k_2-k_1$ where k_e is the direction of output, and k_1, k_2, k_3 are the first two programming pulses and the probe pulse directions respectively. This is the configuration that would likely be used in a true time delay device.

For the experimental demonstration of accumulation with high bandwidth two-tone chirped pulses, the input power of the chirp was reduced to $1/10^{th}$ that of the single shot experiments. The chirps were of 1 ms duration and covered ~500 MHz bandwidth. The programming pulses were sent in with a 30 μs delay between pairs. After N number of programming pairs had been sent into the material, a probe pulse was applied 30 μs after the last programming pulse. N was varied from 1 to 20, limited by the memory in the arbitrary waveform generator used. Figure 21 shows how the echo power grows after N number of programming pulses. The echo can be detected after 3 programming pulses,

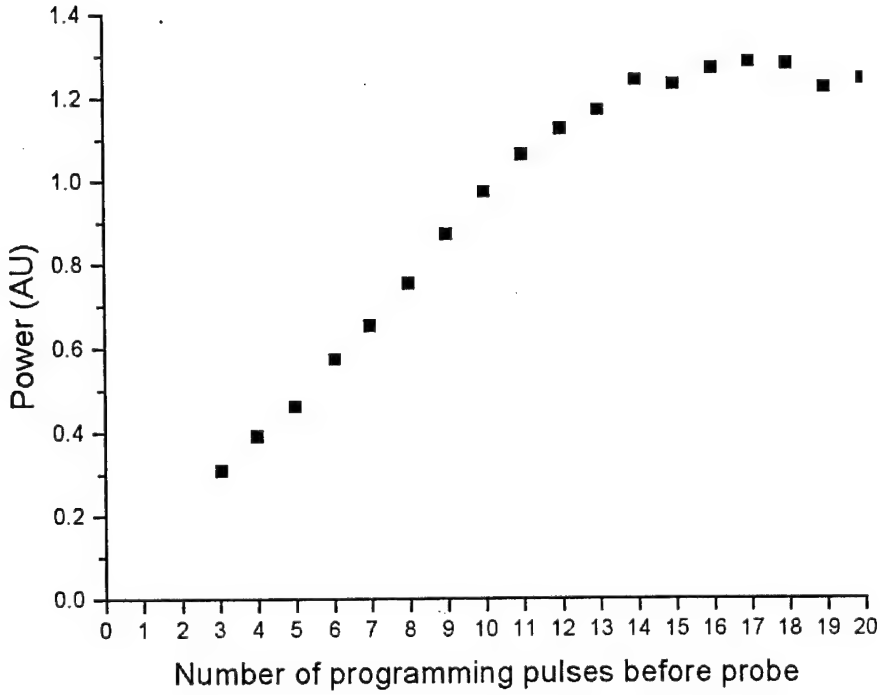

Figure 21: Plot of echo power probed after N number programming pulses.

and grows fairly linearly up to about 12 programming pulses. After N=12, the echo power can be seen flattening out as the steady state is reached. Due to memory limitation in the AWG, the extent of the steady state could not be probed with this setup, however this may be done in future experiments.

This does show that a true time delay can be programmed with pulse power of about 4 mW. This could eliminate the need for injection locking the chirped laser to increase it's output power, thus lowering the overall size and complexity of the device.

Further investigations with this system should include application of high bandwidth signals from a mode-locked Ti:Sapphire laser to investigate the full bandwidth programmed by the chirped laser. Bandwidth filtering should be seen as the pico-second

laser can produce bandwidth much higher than can be programmed with this current chirped laser. Thus, by comparing the pulse widths of the input and delayed output, the full usable bandwidth programmed could be measured. The inputs will also be moved from the current collinear configuration to an angled beam configuration. With this setup, the grating could be continuously programmed by the chirped laser, and continuously probed by the pico-second laser. This could also reduce any noise on the delayed output by spatially separating it from all other outputs. Future advances in chirped laser design should lead to higher bandwidth ranges and smaller laser footprints. Improvements to computer simulations to include propagation effects should help in understanding noise that may be coming from using a two-toned programming pulse.

In summary, this represents a first look into the ability to program a true time delay with a frequency chirped diode laser. The programmed delay shows good agreement between the expected and measured delay while varying chirp rate and AOM offset frequency. The ability to accumulate a spectral grating was also demonstrated. With further investigation, this could lead to a device capable of controlling a continuous multigigahertz signal to an element of a complex array antenna.

SUMMARY AND CONCLUSIONS

This research represents a preliminary look into high bandwidth true time delay devices. The work involved the construction of an external frequency stabilization system for a Ti:Sapphire ring laser to study the effects of accumulation. A high bandwidth frequency chirped external cavity diode laser was also constructed to program large bandwidth true time delays in Tm:YAG. The experiments performed with the chirped diode laser represent a first look into high bandwidth true time delays programmed with chirped pulses.

We have shown how a laser can be frequency stabilized externally by using a non-persistent spectral hole as a frequency reference. This frequency reference is desirable because it is narrow which provides very good response, and it is in the same frequency region of interest to study optical coherent transient effects in Tm:YAG. By doing the fast frequency correction externally, we could apply this system to virtually any commercial laser system without extensive modification.

We constructed an external cavity diode laser based on the Littrow configuration with an intra cavity electro optic crystal. This laser is capable of producing frequency chirps on the order of 2 GHz and a time response on the order of microseconds. The laser was then amplified by the use of an injection locked diode laser. This laser was then used to conduct experiments where high bandwidth gratings were programmed into an optical coherent transient material for use in true time delay. We studied the effects of changing the AOM offset and chirp rate on the delay.

The measured delay matched very well to the expected delay for a given set of input parameters. There were some strange effects that still need to be studied. The rapid

decay of the echo needs more investigation.

Finally, we demonstrated the ability to accumulate a spectral grating. This lowers the power required to the point where the chirped laser could run without the need for injection locking.

ACKNOWLEDGMENTS

We gratefully acknowledge support for this work by the U.S. Office of Naval Research and the University of Colorado under the Multidisciplinary University Research Initiative Program (grant N00014-97-1-1006) and by the U.S. Air Force Office of Scientific Research (grant F49620-98-1-0283) and by the Army Research Office Defense Experimental Program to Stimulate Competitive Research under grant DAAG55-98-1-0244 and by the Spectrum Lab of Montana State University.

The author also wishes to thank Randy Babbitt for giving me the opportunity to explore a very interesting area of photonics. I also would like to thank Randy Reibel and Zack Cole for the use of their injection locking system for the chirped laser experiments. Kevin Repasky for his expertise in laser development on the chirped laser and for the first work on the laser stabilization system. Pete Sellin for his expertise in locking to spectral holes. Kris Merkel for his help in accumulated gratings. Mingzhen Tian for her help with the chirped experiments. Joe Fisher and Norm Williams for their help in the machine shop during the construction of the chirped laser. Steve Kelly for his help in the electronics lab. And finally Shannon Jones for still wanting to marry me after all this.

1 K. D. Merkel, W. R. Babbitt, Opt. Lett. **23**, 528-530 (1998)

2 C. S. Cornish, Ph. D. thesis, University of Washington (2000)

3 K. D. Merkel, J. Zhao, K. S. Repasky, W. R. Babbitt, SPIE **3802**, 248 (1999)

4 R. W. P. Drever, J. L. Hall, F. V. Kowalski, J. Hough, G. M. Ford, A. J. Munley, and H. Ward, Appl. Phys. B **31**, 97 (1983); M. Zhu and J. L. Hall, J. Opt. Sci. Am. B **10**, 802 (1993)

5 G. C. Bjorklund, M. D. Levenson, W. Lenth, C. Ortiz, Appl. Phys. B **32**, 145 (1983); J. M Supplee, E. A. Whittaker, and W. Lenth, Appl. Opt. **33**, 6294 (1994)

6 N. M. Strickland, P. B. Sellin, Y. Sun, J. L. Carlsten, and R. L. Cone, *Phys. Rev. B* **62,** 1473 (2000)

7 P. B. Sellin, N. M. Strickland, T. Bottger, J. L. Carlsten, R.L. Cone, *Laser Stabilization at 1536 nm Using Regenerative Spectral Holeburning*, Phys. Rev. B, manuscript submitted for review (2000)

8 N. C. Wong and J. L. Hall, J. Opt. Sci. Am. B **2**, 1527 (1985)

9 J. L. Hall and T. W. Hänsch, Opt. Lett. **9**, 502 (1984); M. Zhu and J. L. Hall, J. Opt. Sci. Am. B **10**, 802 (1993)

10 K. D. Merkel, R. D. Peters, P. B. Sellin, W. R. Babbitt, Opt. Lett. **25**, 1627-1629 (2000)

11 B. Boggs, C. Greiner, T. Wang, H. Lin, and T. W. Mossberg, Opt. Lett. **23**, 1906-1908 (1998)

12 M. de Labachelerie, G. Passedat, Appl. Opt. **32**, 269-274 (1993)

13 K. S. Repasky, J. L. Carlsten, Appl. Opt. **39**, 5500-5505 (2000)

14 F. Morgansen, H. Olesen, G. Jacobsen, IEEE Journal of Quantum Electronics **21**, 784-792 (1985)

15 G. L. Abbas, et al, IEEE Journal of Quantum Electronics **24**, 609-617 (1988)

Appendix 3

Randy Reibel, "Spectral filtering of amplitude or phase modulated carriers," graduate project report, Department of Physics, Montana State University (2000)

1 Spectral Filtering of Amplitude or Phase Modulated Carriers

Randy Reibel

Montana State University

5/3/2000

Spectral filtering of amplitude and phase modulated carriers is carried out using fast Fourier techniques. These techniques are used in a real time environment allowing the user to graphically see expected signals and examine the filtering process in step by step detail. Theory relating to the simulations is outlined first and experimental proof of that theory is shown. Results relating to four simulations are then presented and discussed.

1.1 Introduction

Work is in progress to show that photon echoes can be used for practical applications. One such experiment is to design and build a true-time-delay regenerator which works with signals in the 1 to 10Ghz range. A true-time-delay regenerator can be thought of as a device for which you specify a certain delay time, then input a given waveform with information encoded on it. The output of the device should be that waveform and information delayed by your specified time delay. These devices could be especially useful in the steering of phased array radar systems or in any communication system which needed to delay signals before processing.

It was postulated and shown that photon echoes can be used for true-time-delay (TTD) purposes. However, no one has shown that the TTD echoes can carry a 1 to 10GHz range of information encoded upon them. Theoretically this is possible. If this can be done then we will have successfully built a true-time-delay regenerator that works in the 1 to 10GHz range. The way this is done with photon echoes is as follows.

First you must have a medium which will produce photon echoes. We use Thulium doped YAG which must be cooled to liquid helium temperatures in order to produce echoes. Next, you must excite the medium. This is done with a very brief laser pulse. Then you enter in with another pulse at exactly the delay time, τ, you desire for your TTD. This second pulse programs the medium with that time delay. Finally, you input your third information laser pulse. This pulse will have your desired 1 to 10Ghz modulation either amplitude or phase modulated on it. What we hope to see on the output is the photon echo of pulse three with the 1 to 10Ghz modulation delayed by τ. Each of the beams is spatially distinct as it enters the crystal (i.e. the k-vectors are all different). So the echo pulse also is spatially distinct and can be discriminated against the other pulses coming through the crystal.

The complexity of making a TTD device is increased by the fact that the crystal itself acts as a spectral filter. The filter, to first approximation looks like a guassian in frequency space with a full-width half max (FWHM) of approximately 17Ghz and is centered at approximately 790 nm. By modelling this filtering process, we will then be able to predict what to expect on the TTD photon echo. There are three main goals for these simulations. First, the modelling process is a good check on the theory. Second the simulation must answer where we should center the carrier frequency in order to obtain maximum amplitude modulation from the phase modulated signals. This is critical to the experiment since the only way to measure the phase modulation is by passing it through a spectral filter and cause beating between the sidebands. Finally, the overall goal of the experiment, that is to see a TTD modulated echo, can be tested in two ways and the effects due to spectral filtering can be sought out. These final experiments are outlined in the theory section below.

1.2 Theory

Phase and amplitude modulation of optical signals is nearly as old as the laser itself. A standard way to modulate an optical signal is to pass it through a crystal which exhibits a large electro-optic effect. The electro-optic effect is simply a change in the index of refraction with an applied electric field. The change in the index of refraction causes the speed at which the carrier can travel through the medium- either slowing it down or speeding it up. This ultimately turns into a phase shift in the carrier after it passes through the crystal. The total phase change through a given crystal is

$$\Phi = \frac{2\pi r n^3 V}{\lambda} \tag{1}$$

Here r is a material dependent parameter, n is the index of refraction with no field and V is the applied voltage across the crystal. A useful characterization of phase modulators is the voltage needed to apply a phase shift of pi radians, V_π. One can show that the total phase shift can then be written as

$$\Phi = \frac{\pi V}{V_\pi} \tag{2}$$

$$V_\pi = \frac{\lambda}{2rn^3} \tag{3}$$

By simply applying an oscillating voltage one can put an rf signal on the carrier. For the case of the simulations a simple cosine wave is used.

$$V = V_o \cos(\omega_m t) \tag{4}$$

Finally we want to put this total phase change onto our carrier and this can be written as

$$E = E_o \cos[\omega_o t + \Phi] \tag{5}$$

$$E = E_o \cos[\omega_o t + \beta \cos(\omega_m t)] \tag{6}$$

$$\beta = \frac{\pi V_o}{V_\pi} \tag{7}$$

The modulator that we will be using has a V_π of approximately 20 volts. Also, in order to not overdrive the modulator the maximum phase shift attainable is $\beta = 1.8$ radians. Using (7) it can be found that we will need to have $V_o = 11$ volts. In the actual experiment the ratio of the optical frequency to the modulation frequency is on the order of 10^5. However, in order to successfully simulate in a reasonable time this ratio must be around 10^3. As shown in (6) we have a signal that is modulated with an rf frequency. By sending this signal through the crystal we will delay this signal and reduce the amplitude of the field to $E_{eo} \sim 10^{-3} E_o$ to theoretically model the photon echo, E_e.

$$E_e = E_{eo} \cos[\omega_o (t+\tau) + \beta \cos(\omega_m (t+\tau))] \tag{8}$$

We can actually ignore this delay on the optical carrier but it becomes very important to analyze the delay in the phase modulation portion of the above equation. What we see is that the delay of the photon echo has caused a frequency dependant phase shift in the rf signal. This echo can be written as

$$E_e = E_{eo} \cos[\omega_o t + \beta \cos(\omega_m t + \phi_m)] \tag{9}$$

$$\phi_m = \omega_m \tau \tag{10}$$

This last equation is the key element to the experiment since we notice a linear dependence of the phase with the frequency of the modulation. The proportionality constant is exactly the delay of the photon echo. By measuring the phase of the rf signal on the echo for different modulation frequencies one can show that the photon echo is truly obeying the properties of a TTD regenerator. Or, by keeping the frequency fixed, the delay, τ, can be varied and the phase monitored. Thus (10) becomes the central equation to the experiment.

As mentioned above the crystal acts like a spectral filter and thus it is important for us to examine what will happen to this echo as it is acted on by this filter. One can rewrite (9) in terms of exponentials.

$$E_e = \frac{E_{eo}}{2} \left\{ e^{i\omega_o t} e^{i\beta \cos(\omega_m t + \phi_m)} + e^{-i\omega_o t} e^{-i\beta \cos(\omega_m t + \phi_m)} \right\} \tag{11}$$

Using a math relation we can show that the phase modulation produces what are called sidebands on the carrier.

$$e^{iz\cos\delta} = \sum_{k=-\infty}^{\infty} e^{ik\pi/2} J_k(z) e^{ik\delta} \tag{12}$$

$$E_e = \frac{E_{eo}}{2}\left\{e^{i\omega_o t}\sum_{k=-\infty}^{\infty} J_k(\beta)e^{ik(\pi/2+\omega_m t+\phi_m)} + c.c.\right\} \tag{13}$$

Expanding the sums around $k = 0$ we find

$$\begin{aligned}
E_e &= \frac{E_{eo}}{2}\left\{e^{i\omega_o t}\left[\begin{array}{c}\cdots + J_1(\beta)e^{-i(\pi/2+\phi_m)}e^{-i\omega_m t}+\\ J_0(\beta) + J_1(\beta)e^{i(\pi/2+\phi_m)}e^{i\omega_m t}+\cdots\end{array}\right] + c.c.\right\} \qquad (14)\\
E_e &= \frac{E_{eo}}{2}\left\{\left[\begin{array}{c}\cdots + J_1(\beta)e^{-i(\pi/2+\phi_m)}e^{i(\omega_o-\omega_m)t}+\\ J_0(\beta)e^{-i\omega_o t} + J_1(\beta)e^{i(\pi/2+\phi_m)}e^{i(\omega_o+\omega_m t)}+\cdots\end{array}\right] + c.c.\right\}\\
E_e &= \frac{E_{eo}}{2}\left\{\begin{array}{c}\cdots + J_1(\beta)\cos((\omega_o-\omega_m)t-\pi/2-\phi_m)+\\ J_0(\beta)\cos(\omega_o t) + J_1(\beta)\cos((\omega_o+\omega_m)t+\pi/2+\phi_m)+\cdots\end{array}\right\}
\end{aligned}$$

Now we can see that the phase modulation does indeed put sidebands on the optical carrier at integer multiples of the modulation frequency. The crystal, as stated above, acts like a quassian filter in frequency space with a FWHM of 17 GHz. If we center our carrier frequency on the center of the frequency filter, and then let the filter act upon the echo signal we can get an idea of what the filter will do to the true echo signal. A simple approximation of this process can be made by eliminating all but the zero order and first order terms in (14) and then reducing the three terms left by separate constants, A, B, C. The constants A, B, C simply represent the amount the quassian filter acts upon the individual sidebands. If we actually centered the filter on the carrier frequency then $A = C$, $B = 1$. However, we can allow small shifts of the center frequency and still keep this approximation, however in this case the constants are not symmetric. So, after filtering (14) becomes

$$E_{filtered} = \frac{E_{eo}}{2}\left\{\begin{array}{c}AJ_1(\beta)\cos((\omega_o-\omega_m)t-\pi/2-\phi_m)+\\ BJ_0(\beta)\cos(\omega_o t) + CJ_1(\beta)\cos((\omega_o+\omega_m)t+\pi/2+\phi_m)\end{array}\right\} \tag{15}$$

Finally in order to simulate what we will actually see we must find the intensity of the filtered echo signal using

$$I_e = < |E_{filtered}|^2 >_{t'} \tag{16}$$

The intensity is a time averaging process. The detector we use has a bandwidth of 12 GHz. Thus we can see the rf modulation put onto the carrier but are not allowed to see the actual carrier oscillations. Thus t' follows the relation $t_o << t' << t_m$. Here t_o and t_m are the periods of the optical and rf signals respectively. One finds after some algebra that the intensity can be written

$$I_e = E_{eo}^2\left\{\begin{array}{c}J_0J_1\cos(\omega_m t+\pi/2+\phi_m)[AB+BC]+\\ ACJ_1^2\cos(2\omega_m t+\pi+2\phi_m)\end{array}\right\} + I_{const} \tag{17}$$

What the above equation tells us is that there is no phase shift associated directly with the filtering process. But we do notice that there is a doubling of the phase shift associated with the beating between the sidebands themselves. We expect then that if our filter does not appreciably damp out both of the sidebands we could end up with the addition of two waves each with two different phase shifts. It can be seen in the above equation that we want $[AB + BC]$ to be a maximum and AC to be a minimum in order to produce an amplitude modulated signal at the modulation frequency without any higher order harmonics. This can be done by simply moving the center frequency of the filter towards either one of the sidebands. Note that there is a constant term in the intensity, I_{const}. This constant is always greater than the intensity modulation term so that there is never a negative intensity.

1.3 Simulations

1.3.1 Program Testing

The first step in testing the code created was to test it for the inherent properties expected. As shown above, if we were to create a phase modulated carrier we should expect sidebands if we examine the frequency components. In order to do this a waveform first had to be built by the computer. This was done by using (6) and choosing the appropriate values for the amplitudes and frequencies. For the phase modulator used in the lab, the maximum modulation depth is $\beta = 1.8$. Using this β we expect approximately 64% of the power of the carrier to be pushed into the sidebands. In order to not overdrive the signal, the carrier amplitude, A_o, had to be chosen to be greater then the maximum modulation depth. For all the simulations shown, $A_o = 10$. To find the frequency components of the modulated signals, a fast Fourier transform (FFT) was done on the waveforms. In figure 1 we see the power spectrum from the FFT of a 1000 GHz carrier phase modulated at 5 GHz. From the figure the sidebands are clearly evident with the correct proportion of energies in the sidebands. A test was run on a 1000 GHz carrier amplitude modulated at 5 GHz. Theoretically one expects two frequency components at half the modulation frequency below and above the carrier frequency. The power spectrum for this signal is shown in figure 2 and the results are as expected. This means that the simulation program is building the waveforms properly and the FFT algorithm employed is reproducing theoretical expectations.

Next, since the frequency components are being correctly simulated for the phase modulated carriers, the spectral filter can be applied to these frequency components. This was done by simply taking each individual component in the FFT array and multiplying it by a guassian function. This algorithm can be represented by the following formula.

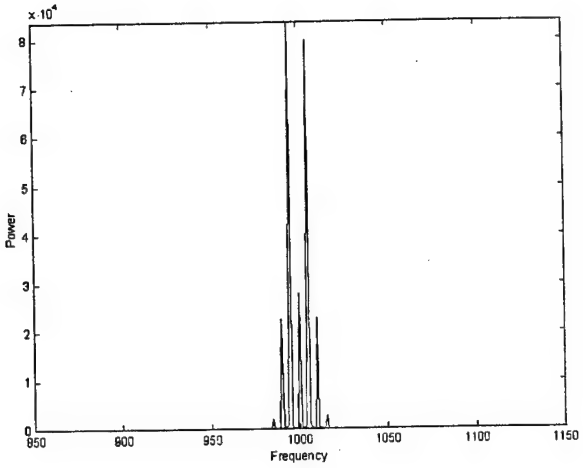

Figure 1: Power spectrum of a 5 GHz phase modulated 1000 GHz carrier.

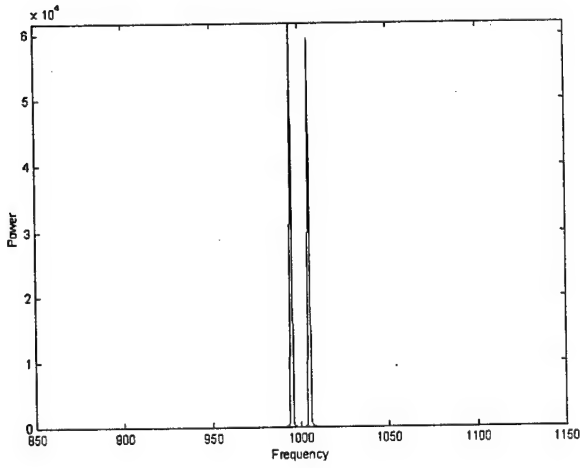

Figure 2: Power spectrum of 5 GHz amplitude modulated 1000 GHz carrier.

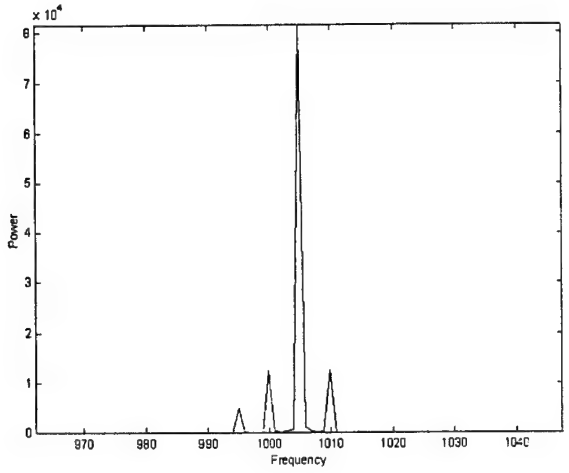

Figure 3: Power spectrum of the 5 GHz phase modulated 1000 GHz carrier spectrally filtered as described in the text.

$$\tilde{E}_{filtered}(\omega) = \tilde{E}_e(\omega) \exp\left(-(\omega - \omega_c)^2/\sigma^2\right) \tag{18}$$

For a given filtering process then, the center frequency, ω_c, and the standard deviation, σ, had to be chosen. Since we wanted to represent our experimental conditions, the standard deviation was chosen to be 8.5 GHz with the assumption that $2\sigma \cong FWHM$. The program then allowed these choices for filtering and then applied the filter once the proper variables were chosen. In the actual experiment, the center frequency of the filter is fixed, however the carrier frequency for the signal can be shifted. To simulate this, instead of rebuilding the waveform with a new carrier frequency and doing another FFT, ω_c of the spectral filter could simply be shifted the appropriate amount in the opposite direction. Figure 3 shows one such spectrally filtered waveform still in frequency space. The center frequency of the filter was centered on the first sideband above the carrier frequency, $\omega_c = 1005$ GHz. This figure demonstrates that the filtering process is occurring as expected.

After the spectral filter has been applied, the waveform is then transformed back into the time domain. This is done by using an inverse fast Fourier transform (IFFT). Once the waveform is back in the time domain, it was then time averaged. This time averaging was done to simulate the process of detecting the signal using the 12 GHz detector in the lab. As discussed above the intensity of the filtered signal is given by (16). In order to simulate this time averaging process, t' was chosen such that $t_o << t' << t_m$. The time domain filtered waveform was then divided into $N_{avg} = t_m/t'$ segments.

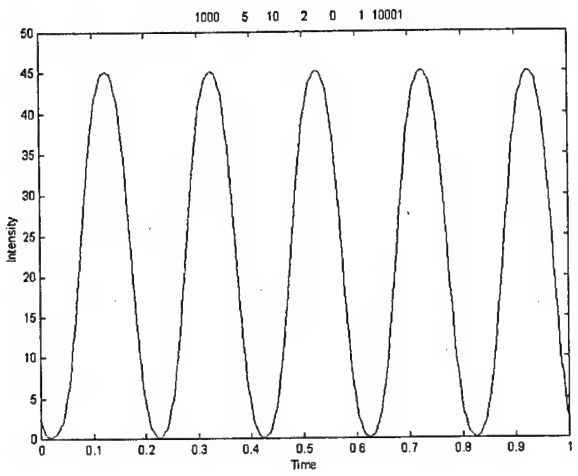

Figure 4: Time averaged time domain filtered signal.

The time averaged value for a given segment was then the average of the time domain filtered waveform within the given segments beginning and end times. Figure 4 shows the time averaged waveform from figure 3. One can notice here that the intensity, I_e, is approximately what one expects from (17). I_{const} is approximately 25 and the amplitude of the cosine function is

$$\begin{aligned} A &\approx A_o^2 J_0(\beta) J_1(\beta)[AB + BC] \\ &= 10^2(.17) \\ &= 17 \end{aligned} \tag{19}$$

The final step in the simulations is to find the phase shift of the time averaged waveform, I_e. This is needed because the actual experiment will measure the phase of the echo signal in reference to the input signal. In the experiment, a mixing measurement is made to get the phase. This means that the phase shift will only be detected on the frequency component for the given rf modulation. In the examples above, this modulation is 5 GHz. So, the phase must be ascertained for just the 5 GHz component and not the phase of the total waveform. In order to measure the phase for the 5 GHz component another FFT must be employed. From the real and imaginary parts at the modulation

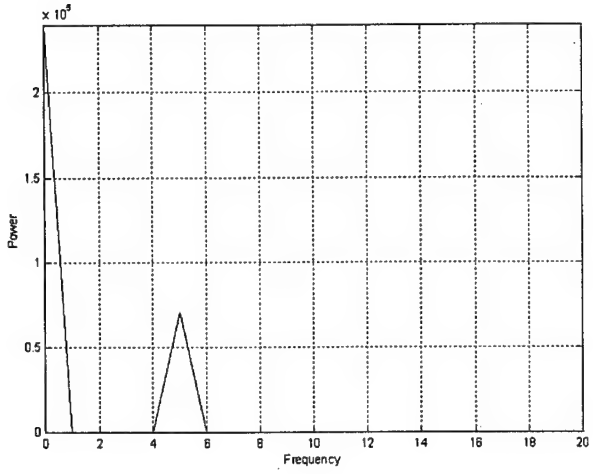

Figure 5: Power spectrum of a time averaged filtered waveform.

frequency, the phase can be found using the following relation

$$\phi_{\text{exp}} = \arctan\left\{\frac{imag\left[\tilde{I}_e(\omega_m)\right]}{\text{real}\left[\tilde{I}_e(\omega_m)\right]}\right\} \tag{20}$$

$$= \pi/2 + \phi_{m\,\text{exp}} \tag{21}$$

The equality in (21) comes from (17). So, essentially, in order to get the true experimental phase shift, $\phi_{m\,\text{exp}}$, we must actually subtract off $\pi/2$ from ϕ_{exp}. In figure 5 a plot of the power spectrum, $\tilde{I}_e$, is shown for the waveform from figure 4.

In order to test whether or not the simulations were capable of picking out the phase shift several different arbitrary phases were added to the modulated signal. This phase then appeared after the filtering and time averaging. Some of the arbitrary phase shifts and the simulation results are shown in table 1. Good agreement was found for the phase shifts.

Given the above demonstrations one can tell that the program behaves as theory expects and can now be used to simulate our actual experimental needs.

1.3.2 Results

As stated in the introduction there were three goals that needed to be met. The first was to see if the program was living up to the theory. This as outlined

$-\phi_m$	ϕ_{exp}	$\phi_{m\,exp}$
$\pi/8 = 0.39$	1.15	-0.46
$\pi/4 = 0.79$	0.76	-0.81
$\pi/2 = 1.57$	-0.03	-1.60
$3\pi/4 = 2.35$	-0.79	2.36

Table 1: Arbitrary phase shifts and simulated values

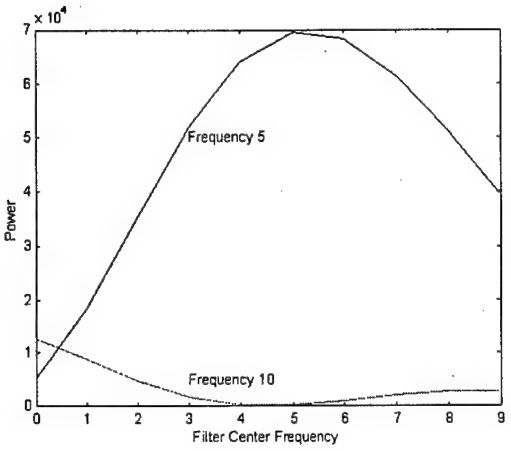

Figure 6: Intensity modulation of the first and second harmonics plotted as a function of filter center frequency.

in the last section is in good agreement. Next, the program was to be used to find an optimal center frequency for the spectral filter. The optimal center frequency would cause the largest beating between the carrier and one of the sidebands. This in turn would give the largest time averaged signal with the rf modulation seen on it. This problem may seem at first glance an easy one. Just choose the center frequency of the filter such that BC in (17) is the largest. However, where that maximum is could depend on many of the variables in the simulation. To find where this maximum intensity modulation is found a set of filters were applied to a 5 GHz phase modulated 1000 GHz carrier. In figure 6, the intensity modulation is plotted as a function of filter center frequency. The intensity for the components was found by taking the peak height off of the FFT of the time averaged signal as in figure 5. Both the first and second harmonics are plotted as a function of center frequency.

One can see that the first harmonic is a maximum and the second harmonic is a minimum when the filter center frequency is placed on the first sideband

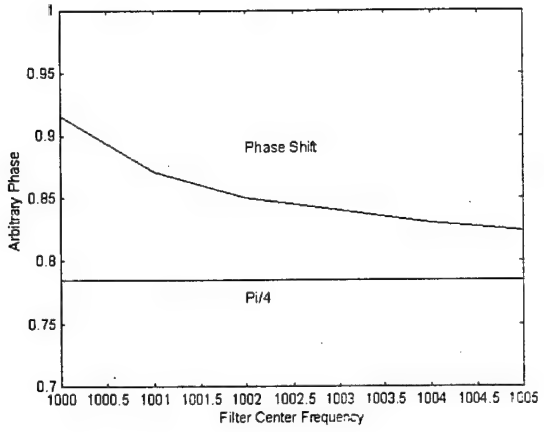

Figure 7: Measured arbitrary phase shift versus center frequency.

at frequency 1005 GHz. It is obvious from figure 6 that the second harmonic plays a role in the intensity of the echo signal when the center frequency is close to the carrier frequency. This means that the first and second harmonic add together to give the echo intensity. Not only that but by the addition of the second harmonic, the phase shift of the first harmonic can be influenced. This dependence is examined in figure 7 which plots the measured phase shift, $\phi_{m\,\mathrm{exp}}$, versus the center frequency. One can see that as the second harmonic is reduced the measured shift more closely approaches the arbitrary phase shift simulated ($\pi/4$ in this case). Notice that when the center frequency of the filter is put on the first sideband, the measured phase shift comes closer to its predicted value.

The final goal of the simulation was to see if the spectral filtering would induce artifacts onto the two actual experiments that are planned. Both experiments want to show that the echo obeys the formula given by (10). There are two ways to exploit the phase shift on the echo experimentally. First, one could set an arbitrary delay time, τ. Then, by scanning the frequency of the rf phase modulation one could measure the phase of the echo signal. By plotting the results a linear trend should be found with a slope of τ. In the actual experiment, the carrier frequency will have to be held constant while the modulation frequency is scanned. This means that to simulate this experiment, the filter center frequency must be held constant and then the phase shift measured for several values of modulation frequency. To carry out this simulation an arbitrary delay time $\tau = 2\pi(0.1)$ was chosen. Then an arbitrary phase shift was added to a given phase modulated wave which obeyed (10). This was done

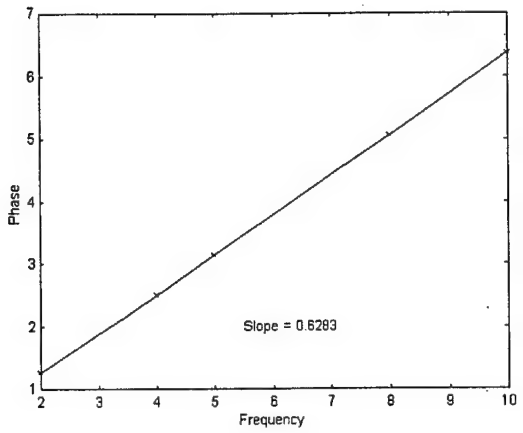

Figure 8: Plot of measured phase versus modulation frequency for the first simulated experiment.

for several different values of the modulation frequency. In (8) , one can see that excellent agreement is found to (10) with a slope very close to τ. From the graph there are no apparent deviations in the linear trend caused by the spectral filtering process.

The other approach to experimentally verify (10) is to pick an arbitrary frequency, ω_m, and then sweep the delay time, τ. The same procedure as for the last experiment was followed. This time the phase modulation was kept at 5 GHz but the arbitrary phase shift was changed as a function of τ. A plot of the phase shift versus the delay time is shown in figure 9. Again, this plot is in excellent agreement to (10), producing a slope equal to that of the arbitrary frequency of 5 GHz. In both plots no artifacts can be seen due to the spectral filtering process.

These results are quite amazing actually. If the crystal did not act like a spectral filter, the phase shift and for that matter the signal could never be seen. Yet no deviations from the linear trends can be seen in either plot. However, as can be seen from figure 7, if the center frequency of the filter is not chosen properly, the phase shifts can be influenced by the second harmonic. And it is also important to note that if the center of the guassian filter is not chosen to overlap well with one of the first sidebands, then the modulation in intensity may be to small to measure. This translates into experimentally choosing a carrier frequency such that in the first experiment, the guassian filter acts on the middle of the swept frequencies. And, for the second experiment, the carrier frequency should be chosen such that the guassian filter acts directly on either of the first sidebands.

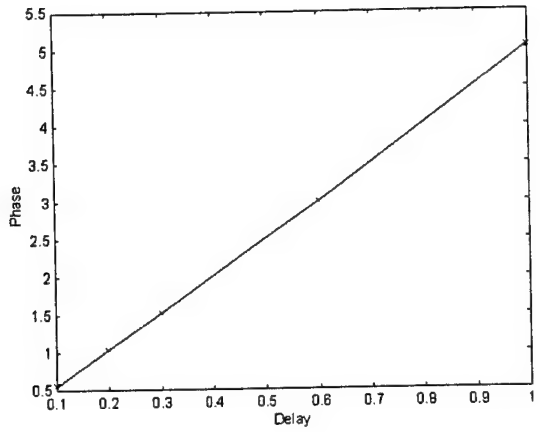

Figure 9: Plot of measured phase versus delay times.

1.4 Conclusion

As stated above the three goals outlined were achieved. The two ways to experimentally verify the linear trends given by (10) appear to be a valid. The simulations have shown that what we hope to measure in the lab will not be influenced in a bad way by the spectral filtering process caused by the crystal. The program also gave insight into where to place the center frequency as hoped. It also withstood the test of theory, performing exactly as it should have in several rigorous tests. What is hard to show in any paper is the ease of use of this code. It is implemented using a GUI which allows for quick input and output of the waveforms. This program will be an excellent tool to have on hand when actually running the experiment and taking the data. One other benefit of the program is its ability to use any periodic arbitrary waveform. The waveforms must be periodic due to the programs use of the FFTs. In this first demonstration a continuous wave was used. However, in the lab, this is usually not the case and pulsed waveforms are usually the norm. This program will be able to treat these pulsed waveforms- which is something that is simply to complex to theoretically analyze and can only be simulated.

Appendix 4

K. D. Merkel, W. R. Babbitt, K. E. Anderson, K. H. Wagner, "Variable-time-delay optical coherent transient signal processing," Optics Letters **24**, 1386-1388 (1999)..

Variable-time-delay optical coherent transient signal processing

K. D. Merkel and W. R. Babbitt

Department of Physics, Montana State University, Bozeman, Montana 59717-3840

K. E. Anderson and K. H. Wagner

Department of Electrical Engineering, University of Colorado, Boulder, Boulder, Colorado 80309

Received June 3, 1999

A technique is proposed and experimentally demonstrated that achieves simultaneous optical pattern waveform storage and programmable time delay for continuous real-time signal processing by use of optical coherent transient technology. We achieve variable-time-delay and broadband signal processing by frequency shifting of two chirped programming pulses, the chirp rate of one being twice that of the other, without using brief reference pulses and without changing the timing of the programming sequence. We demonstrate the technique experimentally in Tm^{3+}:YAG at 5 K for 40-MHz chirps by performing temporal signal convolution with true-time delays that vary over a 250-ns range. © 1999 Optical Society of America

OCIS codes: 070.6020, 060.1660, 190.2640, 320.1590.

An optical coherent transient (OCT) signal processor[1–3] and an OCT variable true-time-delay (TTD) device[4] have been proposed and demonstrated. After a brief review, we propose and experimentally demonstrate a novel method for simultaneously performing programmable time delay and optical signal processing for a continuous optical waveform modulated in amplitude and (or) phase at data rates greater than 10 GHz and with time–bandwidth products greater than 10,000.[2]

Previously proposed OCT devices store the spectral–spatial interference of two optical pulses separated in time as a population grating on an inhomogeneously broadened transition (IBT),[1–6] which can then process, or spectrally filter, a subsequently applied continuous data waveform.[2] One can store a pattern waveform in a grating by interfering it with a brief reference pulse (BRP). For optimal grating efficiency, the duration and intensity of a BRP should be sufficient to excite half of the atoms within the pattern and data bandwidth. To meet this constraint, the intensity of a BRP increases with bandwidth squared, so at wide bandwidths the appropriate intensities [~100 GW/cm^2 for 30 GHz in Tm:YAG (0.1 at.%)] are impractical to produce and can be of the order of the material bulk damage threshold. OCT signal processing can be achieved by an alternative technique in which the BRP is replaced with two frequency-chirped pulses, where the chirp rate of one pulse is twice that of the other.[7] One advantage of chirped-pulse programming is the ability to store an optimally efficient grating with significantly lower pulse intensities than that of a BRP.

For processing received signals in an array of antennas,[8] both variable TTD and signal processing are required. The previously demonstrated OCT TTD device achieved variable delay but not signal processing.[4] In the typical OCT processor, variable delay is achieved only by external generation of a time difference between programming pulses. In this Letter we propose and demonstrate the use of frequency shifting of chirped pulses in an OCT signal processor to achieve variable time delay.

Four methods for achieving OCT signal processing with two frequency-chirped pulses, the chirp rate of one pulse being twice that of the other, in place of a BRP were presented in Ref. 7. We propose that, in all four cases, the use of frequency shifting to vary the stored time delay is possible. Of the two methods that were experimentally demonstrated in Ref. 7, that of reversed dephasing (convolution) is better at minimizing the coherence dephasing time between chirps than that of delayed rephasing (correlation). For this reason, only reversed dephasing is discussed and experimentally demonstrated here, but the analysis of this case can be extended to the other three methods for using frequency shifting to achieve time-delay variations for signal processing.

Programming an OCT processor without chirped pulses is typically achieved with two temporally modulated noncollinear optical pulses separated in time and resonant with an IBT. Each laser pulse has a form $E_n(t - t_n - \eta_n)\cos[\omega_0(t - \eta_n)]$, where the subscript n determines the order of arrival of each pulse, $E_n(\tau)$ is a slowly varying temporal envelope function, $\omega_0 = 2\pi\nu_0$ is the laser center frequency, $\eta_n = (\hat{k}_n \cdot \mathbf{r}/c)$, where $\hat{k}_n$ is the unit wave vector of pulse n, and each pulse reaches the input face of the medium at $\hat{k}_n \cdot \mathbf{r} = 0$ at its arrival time t_n. Programming pulses $E_1(\tau)$ and $E_2(\tau)$, separated by $\tau_{21} = t_2 - t_1$, write a spatial–spectral holographic population grating on the IBT. After a grating is programmed, the atomic absorption is modulated in both frequency and space for subsequently applied optical waveforms. Within the grating lifetime, the application of $E_3(\tau)$ causes a coherent emission $E_S(t - t_S - \eta_S)\cos[\omega_0(t - \eta_S)]$ from the IBT with the temporal envelope of the form

$$E_S(t - t_S - \eta_S) \propto \int_{-\infty}^{\infty} E_1^*(\Omega)E_2(\Omega)E_3(\Omega) \times \exp[i\Omega(t - t_S - \eta_S)]\mathrm{d}\Omega\,, \quad (1)$$

where $t_S = t_3 + t_2 - t_1$, $\eta_S = \eta_3 + \eta_2 - \eta_1$, and $E_n(\Omega)$ is the Fourier transform of the nth applied optical

0146-9592/99/201386-03$15.00/0 © 1999 Optical Society of America

Variable-time-delay optical coherent transient signal processing

K. D. Merkel and W. R. Babbitt

Department of Physics, Montana State University, Bozeman, Montana 59717-3840

K. E. Anderson and K. H. Wagner

Department of Electrical Engineering, University of Colorado, Boulder, Boulder, Colorado 80309

Received June 3, 1999

A technique is proposed and experimentally demonstrated that achieves simultaneous optical pattern waveform storage and programmable time delay for continuous real-time signal processing by use of optical coherent transient technology. We achieve variable-time-delay and broadband signal processing by frequency shifting of two chirped programming pulses, the chirp rate of one being twice that of the other, without using brief reference pulses and without changing the timing of the programming sequence. We demonstrate the technique experimentally in Tm^{3+}:YAG at 5 K for 40-MHz chirps by performing temporal signal convolution with true-time delays that vary over a 250-ns range. © 1999 Optical Society of America

OCIS codes: 070.6020, 060.1660, 190.2640, 320.1590.

An optical coherent transient (OCT) signal processor[1–3] and an OCT variable true-time-delay (TTD) device[4] have been proposed and demonstrated. After a brief review, we propose and experimentally demonstrate a novel method for simultaneously performing programmable time delay and optical signal processing for a continuous optical waveform modulated in amplitude and (or) phase at data rates greater than 10 GHz and with time–bandwidth products greater than 10,000.[2]

Previously proposed OCT devices store the spectral–spatial interference of two optical pulses separated in time as a population grating on an inhomogeneously broadened transition (IBT),[1–6] which can then process, or spectrally filter, a subsequently applied continuous data waveform.[2] One can store a pattern waveform in a grating by interfering it with a brief reference pulse (BRP). For optimal grating efficiency, the duration and intensity of a BRP should be sufficient to excite half of the atoms within the pattern and data bandwidth. To meet this constraint, the intensity of a BRP increases with bandwidth squared, so at wide bandwidths the appropriate intensities [~100 GW/cm^2 for 30 GHz in Tm:YAG (0.1 at.%)] are impractical to produce and can be of the order of the material bulk damage threshold. OCT signal processing can be achieved by an alternative technique in which the BRP is replaced with two frequency-chirped pulses, where the chirp rate of one pulse is twice that of the other.[7] One advantage of chirped-pulse programming is the ability to store an optimally efficient grating with significantly lower pulse intensities than that of a BRP.

For processing received signals in an array of antennas,[8] both variable TTD and signal processing are required. The previously demonstrated OCT TTD device achieved variable delay but not signal processing.[4] In the typical OCT processor, variable delay is achieved only by external generation of a time difference between programming pulses. In this Letter we propose and demonstrate the use of frequency shifting of chirped pulses in an OCT signal processor to achieve variable time delay.

Four methods for achieving OCT signal processing with two frequency-chirped pulses, the chirp rate of one pulse being twice that of the other, in place of a BRP were presented in Ref. 7. We propose that, in all four cases, the use of frequency shifting to vary the stored time delay is possible. Of the two methods that were experimentally demonstrated in Ref. 7, that of reversed dephasing (convolution) is better at minimizing the coherence dephasing time between chirps than that of delayed rephasing (correlation). For this reason, only reversed dephasing is discussed and experimentally demonstrated here, but the analysis of this case can be extended to the other three methods for using frequency shifting to achieve time-delay variations for signal processing.

Programming an OCT processor without chirped pulses is typically achieved with two temporally modulated noncollinear optical pulses separated in time and resonant with an IBT. Each laser pulse has a form $E_n(t - t_n - \eta_n)\cos[\omega_0(t - \eta_n)]$, where the subscript n determines the order of arrival of each pulse, $E_n(\tau)$ is a slowly varying temporal envelope function, $\omega_0 = 2\pi\nu_0$ is the laser center frequency, $\eta_n = (\hat{k}_n \cdot \mathbf{r}/c)$, where $\hat{k}_n$ is the unit wave vector of pulse n, and each pulse reaches the input face of the medium at $\hat{k}_n \cdot \mathbf{r} = 0$ at its arrival time t_n. Programming pulses $E_1(\tau)$ and $E_2(\tau)$, separated by $\tau_{21} = t_2 - t_1$, write a spatial–spectral holographic population grating on the IBT. After a grating is programmed, the atomic absorption is modulated in both frequency and space for subsequently applied optical waveforms. Within the grating lifetime, the application of $E_3(\tau)$ causes a coherent emission $E_S(t - t_S - \eta_S)\cos[\omega_0(t - \eta_S)]$ from the IBT with the temporal envelope of the form

$$E_S(t - t_S - \eta_S) \propto \int_{-\infty}^{\infty} E_1^*(\Omega)E_2(\Omega)E_3(\Omega) \times \exp[i\Omega(t - t_S - \eta_S)]\mathrm{d}\Omega, \quad (1)$$

where $t_S = t_3 + t_2 - t_1$, $\eta_S = \eta_3 + \eta_2 - \eta_1$, and $E_n(\Omega)$ is the Fourier transform of the nth applied optical

0146-9592/99/201386-03$15.00/0 © 1999 Optical Society of America

waveform envelope, $E_n(\tau)$. Relation (1) is based on the Fourier-transform approximation of the input temporal waveforms,[1,5] which is valid for waveforms with bandwidths less than the inhomogeneous linewidth and intensities that ensure a linear response and avoid both coherent and incoherent saturation.[2] Assuming that the input wave vectors are arranged to satisfy the phase-matching conditions, the output propagates with direction $\hat{k}_S = \hat{k}_3 + \hat{k}_2 - \hat{k}_1$.[5] If $E_3(\tau)$ is a data waveform, the operation of correlation (convolution) between the pattern and data is achieved when the first (second) pulse is the pattern and the second (first) pulse is a BRP.

Figure 1 shows the four-pulse input sequence that we use to achieve convolution of a stored pattern waveform with a data waveform, using two chirped reference pulses and the physical process of reversed dephasing.[7] The two chirps $E_{\mathrm{chA}}(\tau)$ and $E_{\mathrm{chB}}(\tau)$ have arrival times of t_{chA} and t_{chB} (defined here as the leading edge), durations τ_{chA} and $\tau_{\mathrm{chB}} = 0.5\tau_{\mathrm{chA}}$, respectively, and the same chirp bandwidth $\delta\nu_{\mathrm{ch}}$. The vertical axes show the electric field amplitude of all pulses and the frequency of the chirped pulses (dashed lines). The pattern waveform is $E_P(\tau)$ at time t_P, and the data waveform is $E_D(\tau)$ at time t_D. In Fig. 1(b), the starting frequencies of the chirped pulses, $\nu_{S_{\mathrm{A}}}$ and $\nu_{S_{\mathrm{B}}}$, respectively, are identical ($\nu_{S_{\mathrm{A}}} = \nu_{S_{\mathrm{B}}} = \nu_0 - \delta\nu_{\mathrm{ch}}/2$) and linearly ramp over $\delta\nu_{\mathrm{ch}}$ (to $\nu_0 + \delta\nu_{\mathrm{ch}}/2$). In Fig. 1(b), the temporal separation between instantaneously identical frequencies is $\tau_{\mathrm{chBA}} = t_{\mathrm{chB}} - t_{\mathrm{chA}}$, and these pulses cause a coherence at time $t_C = t_{\mathrm{chB}} + \tau_{\mathrm{chBA}} = 2t_{\mathrm{chB}} - t_{\mathrm{chA}}$,[9] shown as the intersection of the dotted lines. This rephasing event can be predicted by the optical Bloch equations, the Fourier-transform approximation,[5] the diagrammatic method,[7] or a generalized perturbation theory.[10]

In terms of the traditional three-pulse sequence, the coherence at time t_C acts as $E_1(\tau)$ in Eq. (1), equivalent to a BRP, and the pattern waveform acts as $E_2(\tau)$.[7] Therefore the stored TTD is $\tau_{\mathrm{ttd}} = t_P - t_C$, and the emitted output signal occurs at time $t_S = t_D + (t_P - t_C) \equiv t_D + \tau_{\mathrm{ttd}}$. The direction of the output signal is given by the six-wave mixing condition $\hat{k}_S = \hat{k}_{\mathrm{chA}} - 2\hat{k}_{\mathrm{chB}} + \hat{k}_P + \hat{k}_D$,[7] with the same subscript notation. Even though this is a six-wave mixing process, the efficiency can ideally equal that of the typical OCT processor, which is a four-wave mixing process, when the intensities of the chirped pulses are optimized. Simulation results show that the efficiency is optimized when the Rabi frequencies Ω_{chA} and Ω_{chB} of the first and the second chirped pulses, respectively, are $\Omega_{\mathrm{chA}} \approx 0.27(\delta\nu_{\mathrm{ch}}/\tau_{\mathrm{chA}})^{1/2}$ and $\Omega_{\mathrm{chB}} \approx 4\Omega_{\mathrm{chA}}$. In practice, the effects of propagation, absorption, coherence dephasing, and use of Gaussian beams will affect the optimization conditions, but the six- and four-wave mixing efficiencies should be of the same order.

The desired result is to vary the TTD that is programmed without changing the pulse timings or chirp bandwidths. Arbitrary control of t_C is possible by frequency shifting the chirped pulses. As t_C is determined by the temporal separation of identical frequencies between the two chirped pulses, a change in $\nu_{S_{\mathrm{A}}}$ and $\nu_{S_{\mathrm{B}}}$ ($\delta\nu_{S_{\mathrm{A}}}$ and $\delta\nu_{S_{\mathrm{B}}}$, respectively) or of both translates to changing the effective time delay τ_{chBA} without actually changing $(t_{\mathrm{chB}} - t_{\mathrm{chA}})$. We define $\delta\nu_{S_{\mathrm{BA}}} = \nu_{S_{\mathrm{B}}} - \nu_{S_{\mathrm{A}}}$; then $t_C = (2t_{\mathrm{chB}} - t_{\mathrm{chA}}) - \delta\nu_{S_{\mathrm{BA}}}(\tau_{\mathrm{chA}}/\delta\nu_{\mathrm{ch}})$. A variation in t_C with a fixed t_P translates into a change in τ_{ttd}. As $E_{\mathrm{chA}}(\tau)$ acts to first order and $E_{\mathrm{chB}}(\tau)$ acts to second order, equally opposite values of $\delta\nu_{S_{\mathrm{A}}}$ and (or) $\delta\nu_{S_{\mathrm{B}}}$ have the same net result. For example, if $\tau_{\mathrm{chA}} = 1.0\ \mu\mathrm{s}$ and $\delta\nu_C = 40$ MHz (as in the experiment, below) then $t_C = (2t_{\mathrm{chB}} - t_{\mathrm{chA}}) - 125$ ns by (1) $\delta\nu_{S_{\mathrm{A}}} = -5$ MHz, $\delta\nu_{S_{\mathrm{B}}} = 0$, (2) $\delta\nu_{S_{\mathrm{A}}} = 0$, $\delta\nu_{S_{\mathrm{B}}} = +5$ MHz, or (3) $\delta\nu_{S_{\mathrm{A}}} = -2.5$ MHz, $\delta\nu_{S_{\mathrm{B}}} = +2.5$ MHz. Frequency shifting reduces the spectral overlap of the chirped pulses, so for a processing bandwidth $\delta\nu_{\mathrm{proc}}$ the condition $|\delta\nu_{S_{\mathrm{BA}}}| \le (\delta\nu_{\mathrm{ch}} - \delta\nu_{\mathrm{proc}})$ should be satisfied. Optimally, equal and opposite shifts about ν_0 (or the frequency-shifting device offset) are used. Figure 1(a) [Fig. 1(c)] shows the effect of a shorter (longer) stored delay τ_{ttd}' (τ_{ttd}'') by equal and opposite values of $\delta\nu_{S_{\mathrm{A}}}$ and $\delta\nu_{S_{\mathrm{B}}}$, such that $\delta\nu_{S_{\mathrm{BA}}}$ is negative (positive) without any change in the input sequence timing. The maximum delay tuning range by frequency shifting is $\pm(\delta\nu_{\mathrm{ch}} - \delta\nu_{\mathrm{proc}})(\tau_{\mathrm{chA}}/\delta\nu_{\mathrm{ch}})$.

Frequency-tuned TTD optical signal processing was experimentally demonstrated in a 1.0-mm-long Tm^{3+}:YAG crystal (0.5 at.%), maintained at 5 K. The continuous-wave output of an argon-pumped Ti:sapphire laser, resonant with the 793-nm transition[11] of Tm^{3+}, was crafted into optical pulses by

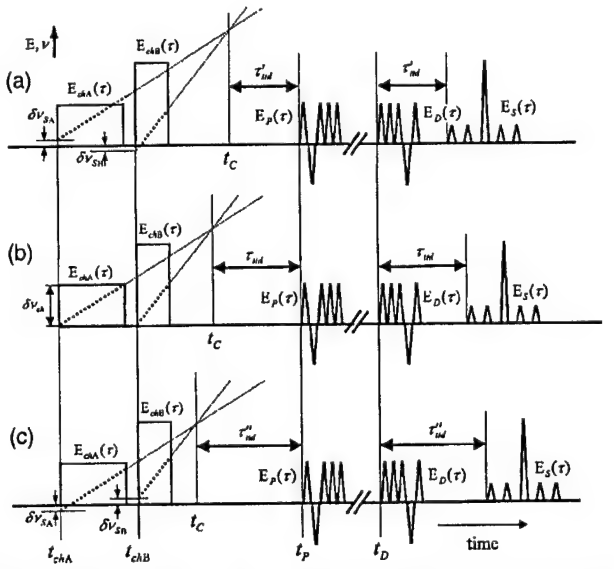

Fig. 1. Four-pulse input sequence to achieve convolution and variable time delay by application of two frequency chirps, a pattern and a data waveform. Vertical axes, electric field amplitude of all pulses and also frequencies of chirped pulses (bold dashed lines). In (b), both starting frequencies of the chirps are identical, causing a coherence at t_C (intersection of the dotted lines). In (a) [(c)] the coherence caused by the two chirps occurs later [earlier] because of frequency shifting. The net result is to vary the time delay stored along with the pattern waveform, $\tau_{\mathrm{ttd}} = t_P - t_C$, without changing the timing of the input sequence. In all three cases the signal $E_S(\tau)$ (not to scale) is the convolution of the pattern and data waveforms emitted after the appropriate delay.

waveform envelope, $E_n(\tau)$. Relation (1) is based on the Fourier-transform approximation of the input temporal waveforms,[1,5] which is valid for waveforms with bandwidths less than the inhomogeneous linewidth and intensities that ensure a linear response and avoid both coherent and incoherent saturation.[2] Assuming that the input wave vectors are arranged to satisfy the phase-matching conditions, the output propagates with direction $\hat{k}_S = \hat{k}_3 + \hat{k}_2 - \hat{k}_1$.[5] If $E_3(\tau)$ is a data waveform, the operation of correlation (convolution) between the pattern and data is achieved when the first (second) pulse is the pattern and the second (first) pulse is a BRP.

Figure 1 shows the four-pulse input sequence that we use to achieve convolution of a stored pattern waveform with a data waveform, using two chirped reference pulses and the physical process of reversed dephasing.[7] The two chirps $E_{\mathrm{chA}}(\tau)$ and $E_{\mathrm{chB}}(\tau)$ have arrival times of t_{chA} and t_{chB} (defined here as the leading edge), durations τ_{chA} and $\tau_{\mathrm{chB}} = 0.5\tau_{\mathrm{chA}}$, respectively, and the same chirp bandwidth $\delta\nu_{\mathrm{ch}}$. The vertical axes show the electric field amplitude of all pulses and the frequency of the chirped pulses (dashed lines). The pattern waveform is $E_P(\tau)$ at time t_P, and the data waveform is $E_D(\tau)$ at time t_D. In Fig. 1(b), the starting frequencies of the chirped pulses, $\nu_{S_{\mathrm{A}}}$ and $\nu_{S_{\mathrm{B}}}$, respectively, are identical ($\nu_{S_{\mathrm{A}}} = \nu_{S_{\mathrm{B}}} = \nu_0 - \delta\nu_{\mathrm{ch}}/2$) and linearly ramp over $\delta\nu_{\mathrm{ch}}$ (to $\nu_0 + \delta\nu_{\mathrm{ch}}/2$). In Fig. 1(b), the temporal separation between instantaneously identical frequencies is $\tau_{\mathrm{chBA}} = t_{\mathrm{chB}} - t_{\mathrm{chA}}$, and these pulses cause a coherence at time $t_C = t_{\mathrm{chB}} + \tau_{\mathrm{chBA}} = 2t_{\mathrm{chB}} - t_{\mathrm{chA}}$,[9] shown as the intersection of the dotted lines. This rephasing event can be predicted by the optical Bloch equations, the Fourier-transform approximation,[5] the diagrammatic method,[7] or a generalized perturbation theory.[10]

In terms of the traditional three-pulse sequence, the coherence at time t_C acts as $E_1(\tau)$ in Eq. (1), equivalent to a BRP, and the pattern waveform acts as $E_2(\tau)$.[7] Therefore the stored TTD is $\tau_{\mathrm{ttd}} = t_P - t_C$, and the emitted output signal occurs at time $t_S = t_D + (t_P - t_C) \equiv t_D + \tau_{\mathrm{ttd}}$. The direction of the output signal is given by the six-wave mixing condition $\hat{k}_S = \hat{k}_{\mathrm{chA}} - 2\hat{k}_{\mathrm{chB}} + \hat{k}_P + \hat{k}_D$,[7] with the same subscript notation. Even though this is a six-wave mixing process, the efficiency can ideally equal that of the typical OCT processor, which is a four-wave mixing process, when the intensities of the chirped pulses are optimized. Simulation results show that the efficiency is optimized when the Rabi frequencies Ω_{chA} and Ω_{chB} of the first and the second chirped pulses, respectively, are $\Omega_{\mathrm{chA}} \approx 0.27(\delta\nu_{\mathrm{ch}}/\tau_{\mathrm{chA}})^{1/2}$ and $\Omega_{\mathrm{chB}} \approx 4\Omega_{\mathrm{chA}}$. In practice, the effects of propagation, absorption, coherence dephasing, and use of Gaussian beams will affect the optimization conditions, but the six- and four-wave mixing efficiencies should be of the same order.

The desired result is to vary the TTD that is programmed without changing the pulse timings or chirp bandwidths. Arbitrary control of t_C is possible by frequency shifting the chirped pulses. As t_C is determined by the temporal separation of identical frequencies between the two chirped pulses, a change in $\nu_{S_{\mathrm{A}}}$ and $\nu_{S_{\mathrm{B}}}$ ($\delta\nu_{S_{\mathrm{A}}}$ and $\delta\nu_{S_{\mathrm{B}}}$, respectively) or of both translates to changing the effective time delay τ_{chBA} without actually changing ($t_{\mathrm{chB}} - t_{\mathrm{chA}}$). We define $\delta\nu_{S_{\mathrm{BA}}} = \nu_{S_{\mathrm{B}}} - \nu_{S_{\mathrm{A}}}$; then $t_C = (2t_{\mathrm{chB}} - t_{\mathrm{chA}}) - \delta\nu_{S_{\mathrm{BA}}}(\tau_{\mathrm{chA}}/\delta\nu_{\mathrm{ch}})$. A variation in t_C with a fixed t_P translates into a change in τ_{ttd}. As $E_{\mathrm{chA}}(\tau)$ acts to first order and $E_{\mathrm{chB}}(\tau)$ acts to second order, equally opposite values of $\delta\nu_{S_{\mathrm{A}}}$ and (or) $\delta\nu_{S_{\mathrm{B}}}$ have the same net result. For example, if $\tau_{\mathrm{chA}} = 1.0\ \mu$s and $\delta\nu_C = 40$ MHz (as in the experiment, below) then $t_C = (2t_{\mathrm{chB}} - t_{\mathrm{chA}}) - 125$ ns by (1) $\delta\nu_{S_{\mathrm{A}}} = -5$ MHz, $\delta\nu_{S_{\mathrm{B}}} = 0$, (2) $\delta\nu_{S_{\mathrm{A}}} = 0$, $\delta\nu_{S_{\mathrm{B}}} = +5$ MHz, or (3) $\delta\nu_{S_{\mathrm{A}}} = -2.5$ MHz, $\delta\nu_{S_{\mathrm{B}}} = +2.5$ MHz. Frequency shifting reduces the spectral overlap of the chirped pulses, so for a processing bandwidth $\delta\nu_{\mathrm{proc}}$ the condition $|\delta\nu_{S_{\mathrm{BA}}}| \le (\delta\nu_{\mathrm{ch}} - \delta\nu_{\mathrm{proc}})$ should be satisfied. Optimally, equal and opposite shifts about ν_0 (or the frequency-shifting device offset) are used. Figure 1(a) [Fig. 1(c)] shows the effect of a shorter (longer) stored delay τ_{ttd}' (τ_{ttd}'') by equal and opposite values of $\delta\nu_{S_{\mathrm{A}}}$ and $\delta\nu_{S_{\mathrm{B}}}$, such that $\delta\nu_{S_{\mathrm{BA}}}$ is negative (positive) without any change in the input sequence timing. The maximum delay tuning range by frequency shifting is $\pm(\delta\nu_{\mathrm{ch}} - \delta\nu_{\mathrm{proc}})(\tau_{\mathrm{chA}}/\delta\nu_{\mathrm{ch}})$.

Frequency-tuned TTD optical signal processing was experimentally demonstrated in a 1.0-mm-long Tm^{3+}:YAG crystal (0.5 at.%), maintained at 5 K. The continuous-wave output of an argon-pumped Ti:sapphire laser, resonant with the 793-nm transition[11] of Tm^{3+}, was crafted into optical pulses by

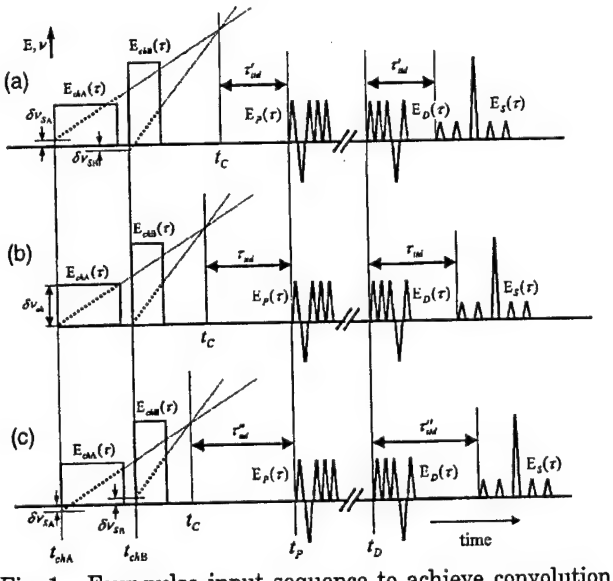

Fig. 1. Four-pulse input sequence to achieve convolution and variable time delay by application of two frequency chirps, a pattern and a data waveform. Vertical axes, electric field amplitude of all pulses and also frequencies of chirped pulses (bold dashed lines). In (b), both starting frequencies of the chirps are identical, causing a coherence at t_C (intersection of the dotted lines). In (a) [(c)] the coherence caused by the two chirps occurs later [earlier] because of frequency shifting. The net result is to vary the time delay stored along with the pattern waveform, $\tau_{\mathrm{ttd}} = t_P - t_C$, without changing the timing of the input sequence. In all three cases the signal $E_S(\tau)$ (not to scale) is the convolution of the pattern and data waveforms emitted after the appropriate delay.

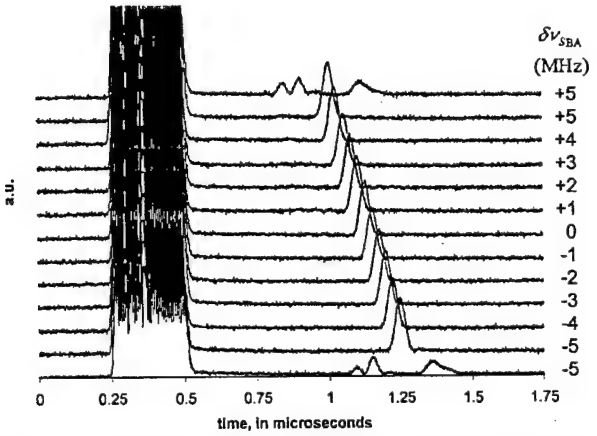

Fig. 2. Experimental output data showing variable time delay and signal processing by frequency tuning of the chirped pulses. With reference to the data waveform (left), the time delay of the emitted signal (0.75–1.0 μs) varies with the offsets of the chirp frequencies $\delta\nu_{S_{BA}}$. The 11 peaks are the detected intensity of the emitted signals representing the autocorrelation of the code; in addition, two other signals are shown, at $\delta\nu_{S_{BA}} = \pm 5$ MHz, representing the autoconvolution of the code.

a 40-MHz acousto-optic modulator driven by a 1-GHz arbitrary waveform generator that controlled the amplitude, frequency, and phase of all the input pulses. Two identical acousto-optic modulators deflected different portions of this pulse sequence onto separate beams, preserving the frequency relationships between pulses. The two beams were focused (100-μm $1/e^2$ diameter spot) and crossed in the crystal. The output waveforms were incident onto an 800-MHz avalanche photodetector and were captured single shot (every 50 ms) by a 1.0-GHz digitizing oscilloscope.

A standard programming waveform sequence was chosen to maximize the amplitude of the emitted signal without saturating the transition of interest within the experimental constraints. The two frequency-chirped pulses had peak powers of 70 and 100 mW (power limited) and durations of 1.0 and 0.5 μs, respectively, and each was chirped over 40 MHz. The first chirp was on beam 1, and the second chirp was on beam 2. The timing ($t_{chB} - t_{chA}$) between the chirps was 1.368 μs. Both the pattern pulse and the data stream occurred on beam 2 and were 5-bit biphase nonreturn-to-zero codes, each bit of duration 50 ns with power 100 mW. The pattern occurred 1.4 μs after the second chirp ended, and the data occurred 6.4 μs after the pattern ended.

Figure 2 shows the experimental results that we achieved by keeping the timing of the input sequence fixed. For all cases we changed ν_{S_B} and ν_{S_A} in equal and opposite amounts of 0.5 MHz, so each increment of $\delta\nu_{S_{BA}}$ was 1 MHz (25 ns). Delay tuning of $\pm$125 ns was achieved for $\delta\nu_{S_{BA}}$ over a range of -5 to $+5$ MHz. The emitted output was detected along beam 1, and the maximum power of these signals was approximately 0.15 mW. Along beam 1 a small fraction (0.25%) of the data waveform (scattered from beam 2) was also detected and served as a reference, showing that the signal was emitted after a variable programmed delay in each case. The operation in all cases was the convolution of the pattern and data waveforms. In the 11 peaks shown, the programmed pattern was a time-reversed replica of the data {+, +, +, −, +}, so the emitted output is the autocorrelation of the code. Two additional output signals are shown at $\delta\nu_{S_{BA}} = \pm 5$ MHz, where the programmed pattern was identical to the data, resulting in the autoconvolution of the code.

These results show the emitted signal occurring at different times for the application of a common waveform applied to each channel at the same time. In a typical TTD receiver processor device a common data waveform arrives at different times (i.e., an angled wave front), and a frequency-tuned delay on each channel compensates for that difference while simultaneously correlating the wave front with the stored patterns. Additionally, continuous programming of the pattern and time delay[12] permits continuous processing by a steady-state grating or adaptive learning for varying incoming signals.

In summary, we have demonstrated a novel technique for programming a variable true-time delay and pattern waveform as a spectral–spatial population grating. Delays that varied over a 250-ns range were demonstrated without changes in the timing of the input pulse sequence. The demonstrated bandwidth was limited by the acousto-optic modulators, representing ~0.1% of the available 17-GHz bandwidth in Tm^{3+}:YAG. Chirped-pulse programming of optical coherent transient processors permits the design of a versatile, all-optical device for transmitting and processing of received signals in broadband array antennas.

We gratefully acknowledge the support of this research by the U.S. Army Research Office under Defense Experimental Program to Stimulate Competitive Research grant DAAG55-98-1-0244.

References

1. Y. S. Bai, W. R. Babbitt, N. W. Carlson, and T. W. Mossberg, Appl. Phys. Lett. **45,** 714 (1984).
2. W. R. Babbitt and J. A. Bell, Appl. Opt. **33,** 1538 (1994); M. Zhu, W. R. Babbitt, and C. M. Jefferson, Opt. Lett. **20,** 2514 (1995).
3. X. A. Shen, Y. S. Bai, and R. Kachru, Opt. Lett. **17,** 1079 (1992).
4. K. D. Merkel and W. R. Babbitt, Opt. Lett. **21,** 1102 (1996); **23,** 528 (1998).
5. T. W. Mossberg, Opt. Lett. **7,** 77 (1982).
6. M. Mitsunaga, R. Yano, and N. Uesugi, Opt. Lett. **16,** 1890 (1991).
7. K. D. Merkel and W. R. Babbitt, Appl. Opt. **35,** 278 (1996).
8. B. Widrow and S. D. Stearns, *Adaptive Signal Processing* (Prentice-Hall, Englewood Cliffs, N.J., 1985).
9. Y. S. Bai and T. W. Mossberg, Appl. Phys. Lett. **45,** 1269 (1984); Opt. Lett. **11,** 30 (1986).
10. M. Mitsunaga and R. G. Brewer, Phys. Rev. A **32,** 1605 (1985).
11. R. M. Macfarlane, Opt. Lett. **18,** 1958 (1993).
12. K. D. Merkel and W. R. Babbitt, Opt. Lett. **24,** 172 (1999).

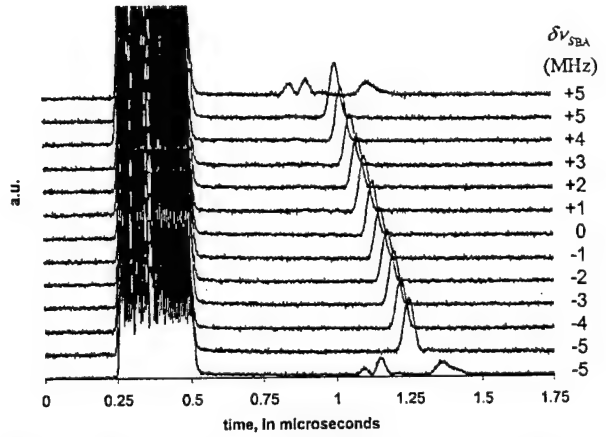

Fig. 2. Experimental output data showing variable time delay and signal processing by frequency tuning of the chirped pulses. With reference to the data waveform (left), the time delay of the emitted signal (0.75–1.0 μs) varies with the offsets of the chirp frequencies $\delta\nu_{S_{BA}}$. The 11 peaks are the detected intensity of the emitted signals representing the autocorrelation of the code; in addition, two other signals are shown, at $\delta\nu_{S_{BA}} = \pm 5$ MHz, representing the autoconvolution of the code.

a 40-MHz acousto-optic modulator driven by a 1-GHz arbitrary waveform generator that controlled the amplitude, frequency, and phase of all the input pulses. Two identical acousto-optic modulators deflected different portions of this pulse sequence onto separate beams, preserving the frequency relationships between pulses. The two beams were focused (100-μm $1/e^2$ diameter spot) and crossed in the crystal. The output waveforms were incident onto an 800-MHz avalanche photodetector and were captured single shot (every 50 ms) by a 1.0-GHz digitizing oscilloscope.

A standard programming waveform sequence was chosen to maximize the amplitude of the emitted signal without saturating the transition of interest within the experimental constraints. The two frequency-chirped pulses had peak powers of 70 and 100 mW (power limited) and durations of 1.0 and 0.5 μs, respectively, and each was chirped over 40 MHz. The first chirp was on beam 1, and the second chirp was on beam 2. The timing ($t_{chB} - t_{chA}$) between the chirps was 1.368 μs. Both the pattern pulse and the data stream occurred on beam 2 and were 5-bit biphase nonreturn-to-zero codes, each bit of duration 50 ns with power 100 mW. The pattern occurred 1.4 μs after the second chirp ended, and the data occurred 6.4 μs after the pattern ended.

Figure 2 shows the experimental results that we achieved by keeping the timing of the input sequence fixed. For all cases we changed ν_{S_B} and ν_{S_A} in equal and opposite amounts of 0.5 MHz, so each increment of $\delta\nu_{S_{BA}}$ was 1 MHz (25 ns). Delay tuning of ± 125 ns was achieved for $\delta\nu_{S_{BA}}$ over a range of -5 to $+5$ MHz. The emitted output was detected along beam 1, and the maximum power of these signals was approximately 0.15 mW. Along beam 1 a small fraction (0.25%) of the data waveform (scattered from beam 2) was also detected and served as a reference, showing that the signal was emitted after a variable programmed delay in each case. The operation in all cases was the convolution of the pattern and data waveforms. In the 11 peaks shown, the programmed pattern was a time-reversed replica of the data {+, +, +, −, +}, so the emitted output is the autocorrelation of the code. Two additional output signals are shown at $\delta\nu_{S_{BA}} = \pm 5$ MHz, where the programmed pattern was identical to the data, resulting in the autoconvolution of the code.

These results show the emitted signal occurring at different times for the application of a common waveform applied to each channel at the same time. In a typical TTD receiver processor device a common data waveform arrives at different times (i.e., an angled wave front), and a frequency-tuned delay on each channel compensates for that difference while simultaneously correlating the wave front with the stored patterns. Additionally, continuous programming of the pattern and time delay[12] permits continuous processing by a steady-state grating or adaptive learning for varying incoming signals.

In summary, we have demonstrated a novel technique for programming a variable true-time delay and pattern waveform as a spectral–spatial population grating. Delays that varied over a 250-ns range were demonstrated without changes in the timing of the input pulse sequence. The demonstrated bandwidth was limited by the acousto-optic modulators, representing ~0.1% of the available 17-GHz bandwidth in Tm^{3+}:YAG. Chirped-pulse programming of optical coherent transient processors permits the design of a versatile, all-optical device for transmitting and processing of received signals in broadband array antennas.

We gratefully acknowledge the support of this research by the U.S. Army Research Office under Defense Experimental Program to Stimulate Competitive Research grant DAAG55-98-1-0244.

References

1. Y. S. Bai, W. R. Babbitt, N. W. Carlson, and T. W. Mossberg, Appl. Phys. Lett. **45,** 714 (1984).
2. W. R. Babbitt and J. A. Bell, Appl. Opt. **33,** 1538 (1994); M. Zhu, W. R. Babbitt, and C. M. Jefferson, Opt. Lett. **20,** 2514 (1995).
3. X. A. Shen, Y. S. Bai, and R. Kachru, Opt. Lett. **17,** 1079 (1992).
4. K. D. Merkel and W. R. Babbitt, Opt. Lett. **21,** 1102 (1996); **23,** 528 (1998).
5. T. W. Mossberg, Opt. Lett. **7,** 77 (1982).
6. M. Mitsunaga, R. Yano, and N. Uesugi, Opt. Lett. **16,** 1890 (1991).
7. K. D. Merkel and W. R. Babbitt, Appl. Opt. **35,** 278 (1996).
8. B. Widrow and S. D. Stearns, *Adaptive Signal Processing* (Prentice-Hall, Englewood Cliffs, N.J., 1985).
9. Y. S. Bai and T. W. Mossberg, Appl. Phys. Lett. **45,** 1269 (1984); Opt. Lett. **11,** 30 (1986).
10. M. Mitsunaga and R. G. Brewer, Phys. Rev. A **32,** 1605 (1985).
11. R. M. Macfarlane, Opt. Lett. **18,** 1958 (1993).
12. K. D. Merkel and W. R. Babbitt, Opt. Lett. **24,** 172 (1999).

Appendix 5

Manuscript: Randy Reibel, Zeb Barber, Mingzhen Tian and Wm. Randy Babbitt, "Temporally overlapped linear frequency chirped programming for true-time delay amplification," submitted to Optics Letters

Temporally Overlapped Linear Frequency Chirped Programming for True Time Delay Applications

R. Reibel, Z. Barber, M. Tian, W. R. Babbitt

Department of Physics, Montana State University, Bozeman,

MT, 59717

A novel technique for programming a true time delay grating into an inhomogeneously broadened absorber is discussed. This technique uses two frequency offset temporally overlapped linear frequency chirps to produce spatial-spectral true time delay gratings. Advantages of this technique include the ability to use chirps longer than the coherence time of the crystal, less stringent frequency stability for grating accumulation, and delay tuning with frequency offset. © 2001 Optical Society of America

High bandwidth spatial-spectral holography has been proposed as a realistic platform for many optical devices such as low latency computer memory systems, signal correlators, continuously programmed-continuous processors and broadband true-time delay (TTD) systems for phased array radar. Many of these applications have been developed and shown for low bandwidths using acousto-optic modulators.[1,2] However several problems must be surmounted as higher bandwidths are reached. One of these is the ability to program an efficient high bandwidth grating. Because of laser power limitations or crystal damage thresholds, accumulation of spectral gratings using low power optical brief pulses has been proposed and demonstrated at low and high bandwidth.[3,4] However, brief pulse accumulation requires stringent frequency tolerances and thus a need for either a stabilized laser, optical delay lines, or short time delays.

Another common way to program TTD gratings is to use linear frequency chirps (LFC). This method uses two LFC's separated by a time delay. One advantage of this technique is that the time delay can be tuned by simply adjusting the start frequency of one of the LFC's.[5] Chirped external cavity diode lasers (CECDL) can produce linear frequency chirps in the high bandwidth range, however output powers from these devices remains limited to less than 10 mW. This limitation requires that either accumulation be used to produce efficient TTD gratings or a high bandwidth amplifier be used. Injection locking, used as an amplifier for LFC's has recently been explored, but output powers still remain lower than 100 mW, which would still lead to a need for accumulation of large bandwidths with short chirps.[6] Due to the lack of significant stabilizing technologies for CECDL's, a new method must be employed in order to program TTD gratings using CECDL's.

In this paper we present a novel technique for programming a TTD grating into an inhomogeneously broadened absorber (IBA). This technique uses two frequency offset temporally overlapped linear frequency chirps (TOLFC's). This frequency offset translates directly into a time delay. Advantages of this technique include the ability to use chirps longer than the coherence time of the crystal, shorter delay times for grating accumulation, and easier experimental setup. Experiments were performed using the $^3H_6$ - $^3H_4$ transition in Tm^{3+}:YAG. Experimental verification of the TTD grating is shown using different temporal lengths for low bandwidth ($\sim$40 MHz) linear frequency chirps. The dynamics of accumulated gratings using this technique are also studied.

As briefly discussed in the introduction, LFC's have been used to program TTD gratings in the past. However in all of these cases, the LFC's have no temporal overlap. To set up a TTD grating, two LFC's act as the programming pulses, each with the same chirp rate, γ, as seen in figure 1(a). These LFC's, each of temporal length τ_C and bandwidth B, are separated by some time delay, denoted τ_{21}. Note that the chirp rate is then defined as $\gamma = \frac{B}{\tau_C}$. In the simple case that both LFC's start out with the same frequency, the delay programmed, τ_D, is equal to τ_{21}. However, if

there is an offset in the start frequency between the two chirps then the delay can be shifted. The programmed time delay is then given by

$$\tau_D = \tau_{21} + \frac{\Delta B}{\gamma} . \tag{1}$$

Here ΔB is defined as the start frequency of the first LFC minus the start frequency of the second LFC. Of course, the bandwidth of the probe pulse signal can not be greater than the overlap of the two LFC's chirped bandwidths. This technique has great promise for TTD applications since the time delay can be shifted simply by changing the offset between the start frequencies of the LFC's. Delay times of several microseconds can be programmed with delay accuracies on the order of a hundred picoseconds or better.[5]

There are two drawbacks to this approach for high bandwidth TTD. First is that the two chirps of the programming sequence must be completed within the coherence time, T_2, of the IBA. Because of this constraint, time lengths of the LFC's must be on the order of a microsecond. For high bandwidth chirps, this means that extremely fast chirp rates be employed putting larger demands on chirp driver circuitry and possible distortions of the spectral characteristics of the chirps. The second drawback comes from the fact that in a typical experiment $\Delta B \ll B$ and thus the shortest delay times are limited to approximately the temporal length of the chirps (typically microseconds). In order to accumulate a spectral grating a constant phase relationship must exist between each programming sequence. This requires that the frequency jitter of the laser, Δf, satisfy $\Delta f \ll \frac{1}{2\tau_D}$. In the case of CECDL's, $\Delta f \approx 300 - 500$kHz, thus, time delays need to be much shorter than a microsecond in order to accumulate an efficient grating.[3]

By setting τ_{21} equal to zero, we can temporally overlap the two LFC's as shown in figure 1(b). We can still set up a delay using (1). By changing the frequency offset, we can effectively change the delay a probe signal will experience. This offset in frequency can be made by low bandwidth AOM's and depending on the diffraction limit, can be spatially overlapped. This allows for collinear

programming of the LFC's and probe pulse, making the experimental arrangement very simple. However, this need not be the case. In fact, for a useful device, the two LFC's will be spatially distinct, allowing the delayed signal to be isolated completely from the input beams.

Because of the temporal overlap we can now make delays shorter than the chirp length τ_C. Along with this, the chirp rate constraint is relaxed using this method. All that is required is that the chirp length must be kept much shorter than the total upper state lifetime (tens of milliseconds for Tm^{3+}:YAG) and that the delay which is programmed be shorter than T_2. Using this approach, delay times of hundreds of picoseconds to microseconds is achievable with spatially distinct delayed signals.

Experiments were carried out using an injection locking setup that has been described elsewhere.[7] The master laser was a homemade external cavity diode laser (ECDL) with a tuning range from 780nm to 810nm and outputs of approximately 10 mW. In these experiments, the light from the master laser passes through a 40 MHz bandwidth acousto-optic modulator operating at 125 MHz center frequency. This AOM was used to linear frequency chirp the master laser with $B = 40$MHz for all experiments. The chirp bandwidth was centered around the 125 MHz center frequency of the AOM and when the AOM was not chirping the output was kept constant at the center frequency so the probe pulse carrier would equal the center of the chirp. The light from the master laser is then injected into the slave laser with injection powers just outside the slave laser of approximately 2 mW. The slave laser, an anti-reflection coated 100 mW single mode diode laser is then locked to the master laser and reproduces an amplified version of the chirped signals with output powers after optical isolation of $\sim$ 70 mW. After isolation, the light is directed towards another AOM which creates the dual frequency pulses and the probe pulse for the experiment. This AOM is driven by an arbitrary waveform generator with 200MHz of bandwidth. The dual frequency is programmed using the voltage

$$V = A\left[\cos\left(\left(\omega_m - {}^{\Delta B}/_{2}\right)t\right) + \cos\left(\left(\omega_m + {}^{\Delta B}/_{2}\right)t\right)\right]$$

Here ω_m is the drive frequency of the AOM, ΔB the offset frequency, and A is the amplitude. The light was focused tightly into this AOM keeping the angle between the two frequencies close to the diffraction limit ensuring spatial overlap of the two frequency pulses. During the probe pulse $\Delta B = 0$, and thus the probe pulse's frequency remains centered between the frequency offset of the LFC's. The pulses were then focused into a Tm^{3+}:YAG crystal with an absorption length, αL, of 1.4 cooled to 4K. The power measured before the crystal was approximately 35 mW and the beam waist inside the crystal was $\sim$ 35 μm . The output from the crystal was incident on a silicon photodiode with a bandwidth of 1 GHz and recorded on a digitizing oscilloscope with bandwidth of 300 MHz. The dephasing time, T_2, of the Tm^{3+}:YAG crystal was measured using brief pulses and also by chirps, and was found to be 18 μs and 13 μs respectively. This indicates that there is an increase in spectral diffusion using the LFC approach.

For all single shot experiments, the TOLFC's are followed 35 μs later by a 50 ns probe pulse. The echo output was observed at the expected delay time, τ_D, as given in (1). τ_D was tuned by changing the frequency offset ΔB for different τ_C's to demonstrate the wide tunability of the TTD. In figure 2, the observed delay of the echo, τ_D, is plotted versus the offset frequency, ΔB, for several different temporal chirp lengths, τ_C =0.5, 1, 3, 5, 15, 30, and 100 μs. The lines are calculated delays from (1). Excellent agreement is found between the calculated and measured delays. It is important to note that echo outputs were observed for $\tau_C = 30$ and 100 μs, both temporal lengths which are much longer than the LFC dephasing time of 13 μs. This clearly shows the relaxation on chirp rate since the chirp can now be allowed to have temporal lengths over hundreds of μs. Figure 3 shows the results of TTD for an amplitude modulated data sequence. The data sequence, a binary coding of 101011001 at a rate of 20 Mbit/s, was sent into the crystal 40 μs after a $\tau_c = 100\mu$s TOLFC with

$\Delta B = 0.25$ MHz. The echo signal is found at the expected $\tau_D = 625$ ns after the input sequence. Good signal fidelity as well as strong echo efficiency ($\sim 2.5\%$) have been achieved. The above results show that this method is indeed a reliable and simple approach to programming TTD gratings and will be very applicable to programming high bandwidth TTD gratings using chirped lasers.

As discussed in the introduction, accumulation is a way to strengthen a spectral grating using weak programming pulses. To demonstrate accumulation using the TOLFC method, we first used a frequency stabilized Ti:Sapphire laser as the laser source. This laser has been locked using a regenerative spectral hole giving a laser jitter of approximately a few kHz.[3] By attenuating the optical power, we chose a series of weak programming strengths that would show the dynamics of the accumulated gratings. The programming pulses are characterized by an individual LFC's Rabi frequency, which were $\Omega = 0.37$, 0.48, 0.72, 1.04, 1.30, and 1.67 MHz for this experiment. Following the standard approach for accumulation, we repeated programming TOLFC's with a repetition time, τ_r, of 31 μs, for N times. After the N programming sequences, the grating was probed using a 50 ns brief pulse as in the single shot experiments. Figure 4 details the echo peak power as a function of N for the set of weak programming pulses. For this figure, $\tau_C = 1$ μs and $\Delta B = 10$ MHz giving a delay time for the echo of $\tau_D = 250$ ns. As can be seen from the figure, the various gratings accumulate quite well. Because of the population dynamics, the larger programming strengths, $\Omega > 0.9$ MHz, are too strong and saturate the medium leading to inefficient gratings. The weaker programming strengths, $\Omega < 0.65$ MHz, are not strong enough and can not accumulate an efficient grating before population decay wipes them out. Between these two regimes the best accumulation can be found such as the $\Omega = 0.72$ MHz programming strength.

We also accumulated gratings using the original injection locked ECDL laser system. For these experiments, another set of Rabi frequencies had to be chosen as the systems intensities and spot size were slightly different. The results were similar to the locked laser results discussed above

indicating that indeed the injection locked laser could produce efficient accumulated gratings. As the lasers ability to accumulate a grating rests directly on the lasers stability and the programmed τ_D, we changed the time delay to discover the largest τ_D we could accumulate reasonably well. We found that τ_D's < 250 ns accumulated quite well however the results were noisier than the frequency stabilized laser results. These accumulation results will have a direct impact upon our ability to use affordable non-stabilized external cavity diode laser systems to program efficient high bandwidth gratings.

In this letter we have shown that by temporally overlapping linear frequency chirps and using an offset frequency we can program efficient TTD gratings. The demonstrated echoes showed the expected characteristics for delay time, which was easily tuned using the frequency offset. Using this approach, the chirp rate constraint is relaxed, and chirp programming sequences much longer than T_2 have been demonstrated. Good signal fidelity and excellent efficiency have been found on data sequences. Along with this, the TOLFC method accumulated gratings according to theory. All of these results combine to make the TOLFC programming method an attractive solution for high bandwidth programming. This work was supported in part by Dr. William Miceli of ONR, Dr. Steve Pappert of SPAWAR, and the Office of the Secretary of Defense DDR&E through the MURI program grant number N00014-97-1-1006 and Army Research Office Defense Experimental Program to Stimulate Competitive Research under grant DAAG55-98-1-0244 and by the Spectrum Lab of Montana State University.

References

1. K. Merkel, Z. Cole, and W. Babbitt, "Signal correlator with programmable variable time delay based on optical coherent transients," J. Lumin. **86,** 375–82 (2000).

2. W. Babbitt and T. Mossberg, "Time-domain frequency-selective optical data storage in a solid-state material," Opt. Commun. **65,** 185–8 (1988).

3. K. Merkel, R. Peters, P. Sellin, K. Repasky, and W. Babbitt, "Accumulated programming of a complex spectral grating," Optics-Letters **25,** 1627–9 (2000).

4. M. Tian, J. Zhao, Z. Cole, R. Reibel, and W. R. Babbitt, "Dynamics of Broadband Accumulated Spectral Gratings in Tm^{3+}:YAG," J. Opt. Soc. Am. B **18,** 673–78 (2001).

5. K. Merkel and W. Babbitt, "Chirped-pulse programming of optical coherent transient true-time delays," Optics-Letters **23,** 528–30 (1998).

6. K. Repasky, P. Roos, L. Meng, and J. Carlsten, "Amplified Output of a Frequency Chirped Diode Source Via Injection Locking," Optical Engineering To be published (2001).

7. R. Reibel, Z. Barber, M. Tian, W. R. Babbitt, Z. Cole, and K. D. Merkel, "Amplification of High Bandwidth Phase Modulated Signals at 793 nm," Submitted to JOSA B (2001).

Figures

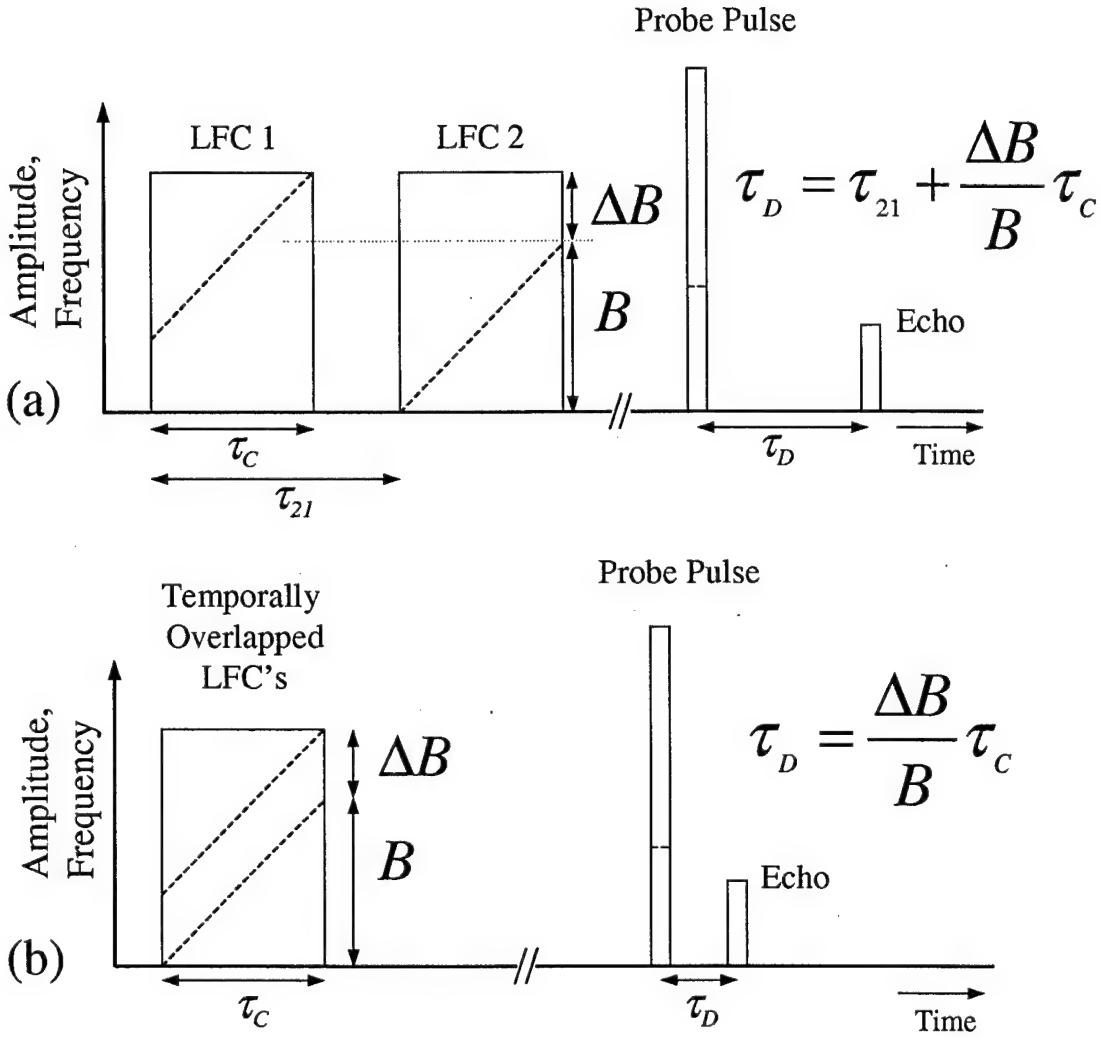

Fig. 1. Input sequences and expected echo for (a) Two LFC's separated by a delay τ_{21} (b) Two temporally overlapped LFC's. Solid lines represent intensity and dashed lines represent frequency.

Figure 1, R.Reibel et. al.

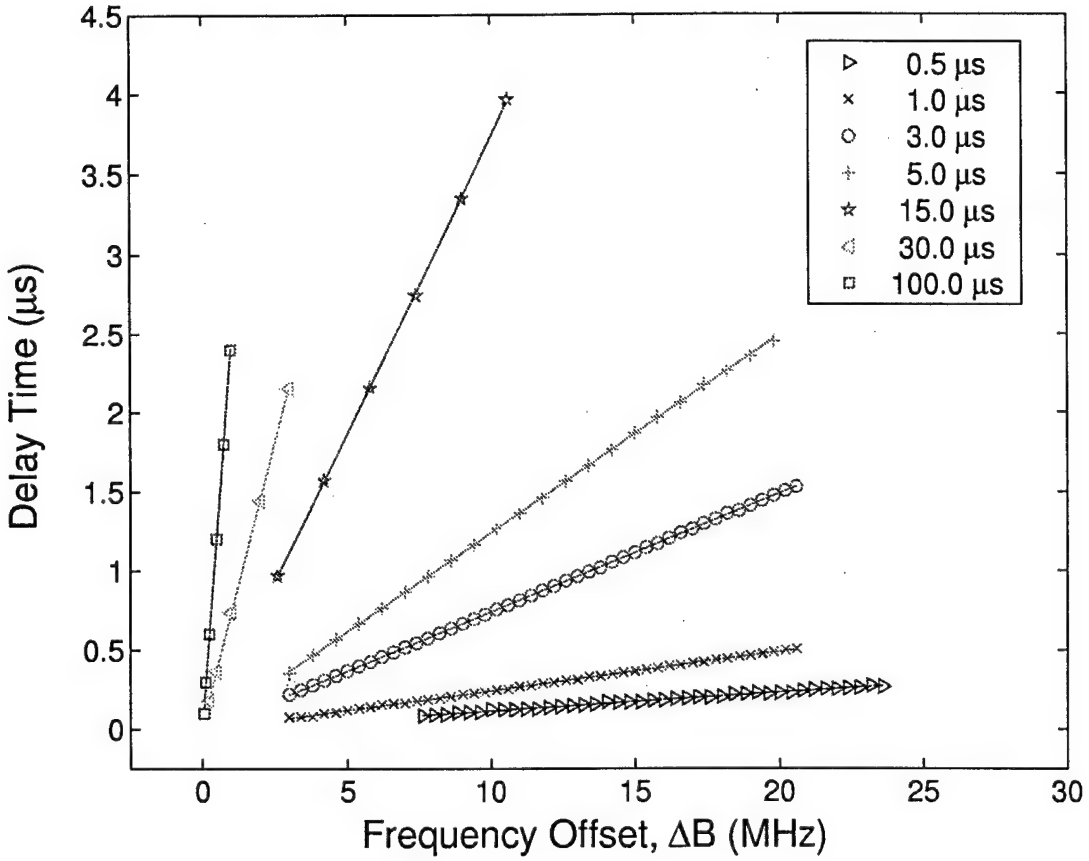

Fig. 2. Measured echo delays vs. frequency offset for several different τ_C's with solid lines calculated from (1). Note also the lines for $\tau_C = 30$ and 100 μs which alleviate the chirp rate requirements.

Figure 2, R.Reibel et. al.

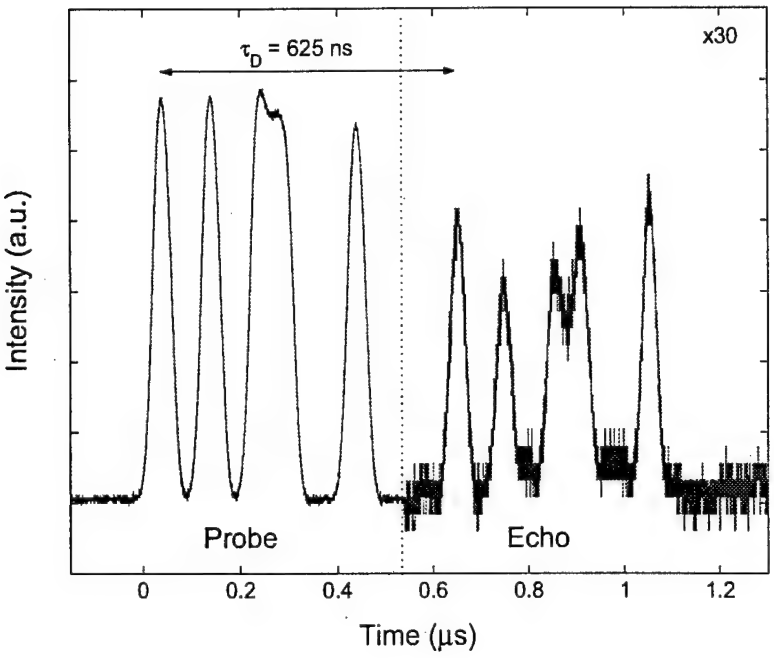

Fig. 3. An example of a data sequence true time delayed. Here $\tau_c = 100\ \mu s$ with a programmed time delay of 625 ns. The data sequence is 101011001 at a data rate of 20 Mbit/s.

Figure 3, R.Reibel et. al.

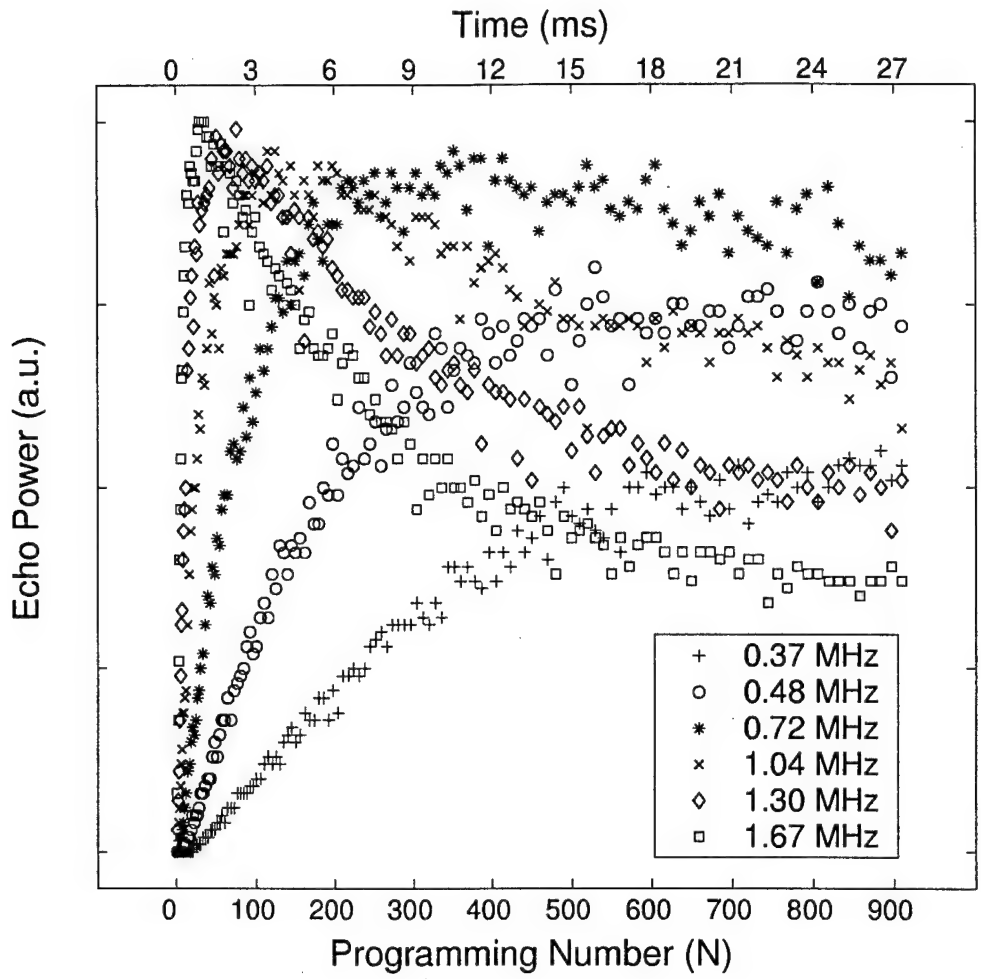

Fig. 4. Echo intensities vs. programming number (lower axis) or time (upper axis) for a frequency stabilized Ti:Saphire laser system. The different plots are various programming strengths (Rabi frequency, Ω) as shown in the legend. Here $\tau_c = 1\ \mu s$, $\tau_D = 250\ ns$, and $\tau_r = 36\ \mu s$.

Figure 4, R.Reibel et. al.

Appendix 6

University of Colorado subcontract final report.

Photon Echo Adaptive Array Processing

A subcontract by the University of Colorado to
Montana State University as part of Prof. Randall Babbit's DEPSCoR program

Final Report

October 2, 2001

Submitted by :	The University of Colorado
duration :	24 months
no cost extension	12 additional months
cost :	$80,000
CU matching	$40,000

Contact :	Professor Kelvin Wagner
	University of Colorado
	Dept of ECE
	Campus Box 425
	Boulder, Colorado 80309-0425
Phone :	(303)492-4661
FAX :	(303)492-3674
email :	kelvin@optics.colorado.edu
Attention :	Prof. Randall Babbit
	Associate Professor of Physics
	Montana State University
	Bozeman, MT 59717-3840
Phone :	(406) 994-6156
FAX :	(406) 994-4452
email :	babbitt@physics.montana.edu

1 University of Colorado Statement of Work

1.1 Year 1: Algorithms for Photon Echo Processing

We will investigate the implementation of adaptive beamforming using the photon echo response function, and specifically will examine approaches to mitigate the restrictions of causality and the limits of integration through the incorporation of additional programming delay. In addition, we will examine more sophisticated algorithms such as the generalized sidelobe cancellor, P-vector passive beamforming, and other constrained algorithms for implementation using photon echoes. Detailed numerical simulations will be utilized to examine the applicability and performance limitation of these various algorithms using the photon echo array processing techniques in the presence of nonidealities such as noise.

1.2 Year 2: Experimental Demonstration of Beamforming

To validate the numerical modelling and gain experience with the strengths and weaknesses of this technology we will undertake a preliminary experimental demonstration of beamforming towards a desired signal of interest. This first step towards the full adaptive closed loop system will be demonstated at low frequency (100 MHz) at the University of Colorado, and the lessons learned will be applied to subsequent demonstrations at higher frequencies at MSU. As part of this demonstration it will be necessary to extend our previous work in which we built an optical phased array simulator to allow for the simulation of true time delay array environmenmts by using acousto-optic devices and variable magnification optical systems. We will build up the laser system, cryostat, modulators, and detectors necessary to undertake these initial demonstrations, and transfer the resulting technology to MSU for further higher frequency experiments.

2 Tasks Completed in Year 1

In the first year of the University of Colorado DEPSCOR funding, we have done extensive investigation into the implementation of an adaptive beam former (ABF) using optical coherent transients (OCT's). We have worked through the theory to show the response to be consistent with what is required by the Least Mean Squared (LMS) algorithm and published a paper with the results (see Published Papers Section). In addition, we have built computer simulations of the system that allows us to investigate noise effects and will allow us to investigate different algorithms for performing beamforming within an OCT material. To enable us with the capability to do experimental investigation into coherent transients, we are in the process of building a state of the art laboratory capable of doing high bandwidth experiments.

2.1 Investigation of ABF using OCT

In year one, we investigated the implementation of adaptive beam forming using optical coherent transients (OCT) and proposed an architecture (see Figure 1) which utilizes the capabilities of the OCT as the central component of a true-time-delay adaptive beamforming algorithm which is used to dynamically steer the gain of large RF phased array antenna towards a signal of interest while simultaneously recognizing unwanted interference signals and minimizing their effects. In this architecture, a RF wavefront is detected with a phased array antenna where each antenna

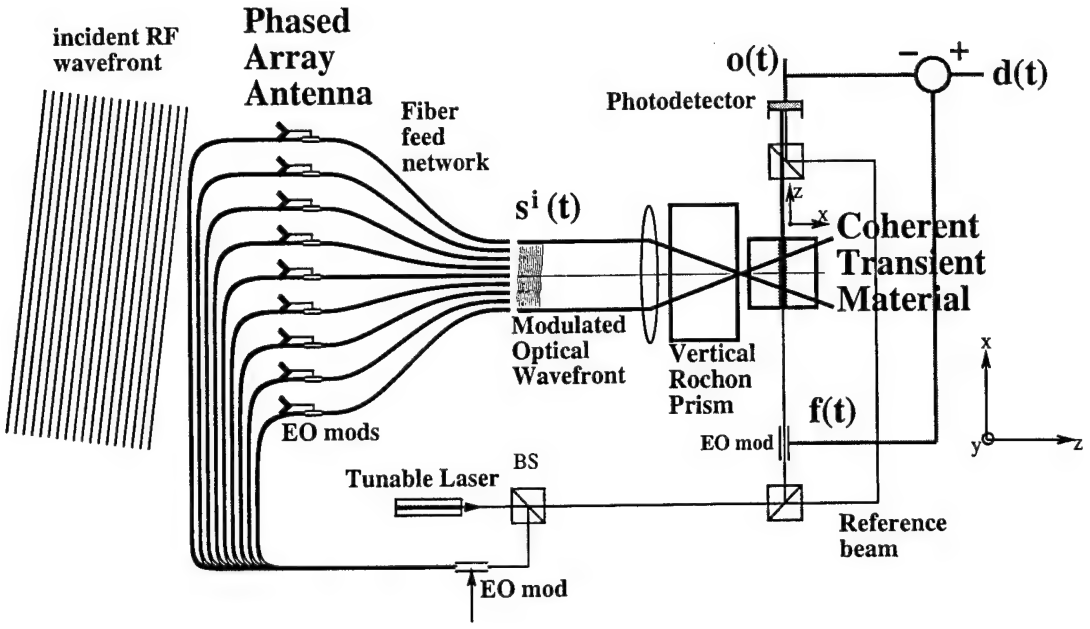

Figure 1: Optical coherent transient adaptive beamforming system that nulls jammers through the TTD correlation-cancellation loop.

element is the driving signal for an electro optic modulator which puts the incident RF signal onto an optical carrier. The optical signals are then carried by fiber to a central location and then are simultaneously imaged in free space through a rochon prism onto the OCT material which is contained in a cryostat. The Rochon prism splits each signal vertically and introduces it into the OCT material at a slight angle in the direction of Bragg degeneracy into the OCT medium. Interference with the feedback reference beam $f(t) = d(t) - o(t)$ yields OCT output signals from all the simultaneous correlations (i.e. for all j) that will co-propagate in the same and be coherently summed.

Our approach uses the intrinsic delay processing capabilities of OCT materials to avoid the use of any time delay lines (TDLs), as required in other time-delay-and-sum adaptive beamformers. The similarity between OCT and the time-delay-and-sum ABF algorithm:

$$o(t) = \sum_{j=0}^{M-1} \sum_{i=1}^{N} s_i(t - j\tau) \int_{-\infty}^{t} s_i^*(t_1 - j\tau) \left(d(t_1) - o(t_1)\right) dt_1$$

becomes apparent if we examine the generalized OCT propagating along $\vec{k}_4 = \vec{k}_3 + \vec{k}_2 - \vec{k}_1$ direction which has an output

$$o(t) = A \int_{-\infty}^{t} dt_3 E_3(t_3, \vec{r}) \int_{-\infty}^{t_3} E_2(t_2, \vec{r}) E_1^*(t_2 + t_3 - t, \vec{r}) e^{\frac{-2(t-t_3)}{T_2} \frac{-(t_3-t_2)}{T_1}} dt_2, \quad (1)$$

where T_1 and T_2 are the longitudinal and transverse relaxation times, which act as windowing functions on the integrations.

Making the following substitutions into Equation 1

$$\begin{aligned} E_1(t_1,\vec{r}) &= \sum_{j=1}^{N} s_j(t)e^{-i\vec{k}_j\cdot\vec{r}}(1+e^{-i\vec{k_y}\cdot\hat{y}}), \\ E_2(t_2,\vec{r}) &= f(t_2)e^{-i\vec{k}_f\cdot\vec{r}}, \\ E_3(t_3,\vec{r}) &= \sum_{j'=1}^{N} s_{j'}(t-T)e^{-i\vec{k}_{j'}\cdot\vec{r}}(1+e^{-i\vec{k_y}\cdot\hat{y}}), \end{aligned} \tag{2}$$

in which $E_1(t_1,\vec{r})$ represents the array of write signals, $E_2(t_2,\vec{r})$ represents the feedback signal, and $E_3(t_3,\vec{r})$ represents the next waveform arriving on the array one pulse repetition interval T later. The Rochon prism produces the beam split in y, $(1+e^{-i\vec{k_y}\cdot\vec{y}})$, which produces a Bragg degenerate diffraction when $\vec{k_y}\cdot(\vec{k}_j-\vec{k}_f)=0$. Bragg matching enforces $j=j'$. The echoed output is spatial filtered to isolate the desired output waveform and interferometrically detected giving

$$o(t) = A\sum_{j=1}^{N}\int_0^{\infty} d\tau s_j(t-T-\tau)\int_{-\infty}^{t-\tau} dt_2 f(t_2)S_j^*(t_2-\tau)e^{-i(\vec{k}_f+\vec{k_y}\cdot\vec{y})\cdot\vec{r}}e^{\frac{-2(\tau+T)}{T_2}-\frac{(t-t_2-\tau-T)}{T_1}}. \tag{3}$$

This shows that the OCT output is in the form of the desired spatio-temporal adaptive filter except for the limits of integration. This difference can be compensated by adjusting T_1 and T_2 to effectively vary the integration window. Utilizing a subsequent RF pulse as readout signal 3 produces the appropriate correlation cancellation loop output. Thus, OCT can perform all the necessary TTD adaptive processing for an entire array in parallel without any TDLs.

In addition, to address the causality issues associated with OCT's, it has been determined that a proper delay be implemented in the feedback loop such that for repetitive signals, repetition N will be sufficiently delayed with respect to repetition N-1 that causality will be not be violated for the response signal output.

2.2 Computer Simulations

We have worked extensively to build a set of computer simulation tools which will allow us to analyze phased array beamforming algorithms under varying conditions. One of the key concerns of implementing a practical system of ABF is performance in the presence of noise. The results of a simulation that was performed to quantify the effects of noise is shown in Figure 2

2.3 Laboratory setup

Additional work accomplished which was accomplished includes building up the lab facilities in order to perform OCT experiments. The first step of this included studying and becoming familiar with techniques for stabilizing laser diodes since highly stable lasers are needed for optimum performance of OCT experiments. Once this was accomplished, we designed and built two frequency stabilized semiconductor lasers which have stabilities of less than 50KHz over 100us time intervals. Due to thermal drifts in the stabilization system, the laser frequency drifts over 23MHz; however, the linewidth over a 40 microsecond interval is less than 48kHz. This result is significant since coherent transient experiments are effected more by the short term linewidth (10's of microseconds) than about the long term linewidth (¿100 microseconds). This is due to the fact that the coherence time of the resonant atoms is on the order of 10's of microseconds. A linewidth much narrower than

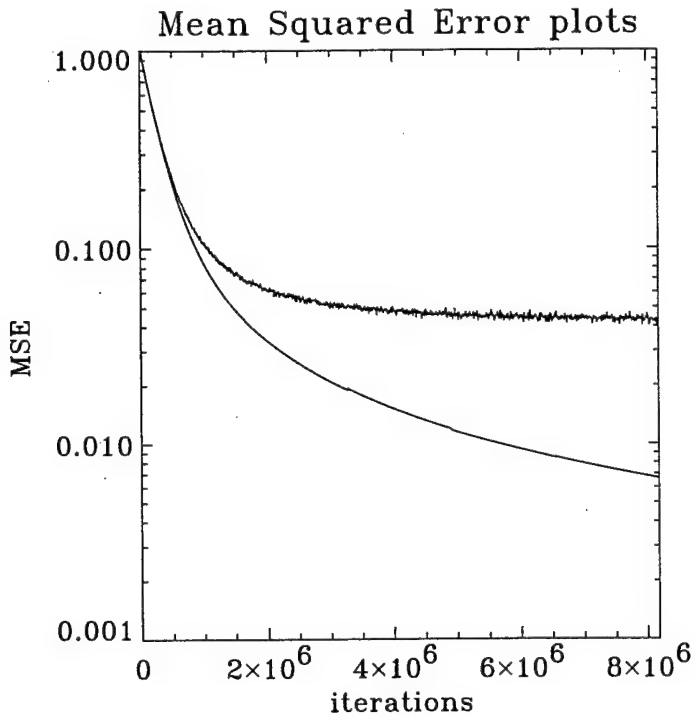

Figure 2: The learning curve during beamforming when the noise (gaussian white, zero mean) is 10dB above signal power (upper trace) and 60dB below signal power (lower trace). The effect of noise is monotonic: the higher the noise the higher the MSE, at all times for a given convergence rate.

this wouldn't contribute significantly to the processing capabilities of the system, whereas a much larger linewidth would significantly reduce the potential time-bandwidth product of the system. One laser was built using optical feedback from a custom designed thermally compensated confocal fabry perot cavity. The second laser was built using optical feedback from an external diffraction grating in the Littman configuration. Once we had implemented these lasers, it was necessary to test their performance which necessitated measurement instruments with far more sensitivity that that available commercially. We thus investigated and became familiar with techniques for measuring highly stable lasers. The first measurement device we build included a self-heterodyning linewidth measuring interferometer to measure laser stability on the order of sub-100Khz. The second device built was a cross-heterodyning linewidth measuring interferometer to measure relative stability between two lasers. The next step in setting up an OCT laboratory included the specification and purchase of a large number of high performance pieces of equipment including a high speed oscilloscope, spectrum analyzer, arbitrary waveform generators, acousto-optic devices, electro-optic devices, cryostats, and near infrared optics. Once the equipment was obtained, we began building the laboratory setups necessary for performing OCT experiments. Currently, the lab is capable of running low bandwidth photon echo experiments (40MHz) in co-linear or crossed beam configurations.

3 Tasks completed in Year 2

Optical signal processing using coherent transients promises to significantly enhance phased array antenna adaptive beam forming (ABF) due to the large potential processing bandwidths ($> 17GHz$) and time-bandwidths ($> 10^5$) that are made available with this technology. The goal of this research is to investigate and design novel processing architectures which can take full advantage of the utility of these spatial-spectral holographic recording devices in their application to phased array beamforming.

3.1 Year 2 Objectives

The objectives for the past year have been to further our efforts in photon echo phased array beamforming. These efforts have been sub-divided into the areas of 1) Establishing laboratory facilities at CU capable of demonstrating and investigating photon echo techniques, 2) Develop techniques for utilizing photon echo processors for a variety of phased array processing scenarios, 3) Investigating the use of photon echo processing techniques to the new area of dispersion compensation in fiber communications, and 4) Make further enhancements to the long term stabilization of laser diodes for use in a beam forming system.

3.2 Year 2 Highlights

During the second year (April 99 - April 00) of this DEPSCOR subcontract at the University of Colorado, we have built a state of the art coherent transient laboratory capable of demonstrating high bandwidth optical signal processing architectures. With the assistance of Dr. W.R. Babbit, we have demonstrated the first photon echo two and three pulse experiments using these facilities and have gained a strong familiarity with the laboratory techniques necessary to perform efficient coherent transient experiments. In addition, we have further developed our facilities in the area of laser stabilization. We have built a Pound-Drever-Hall frequency locking system using a external confocal fabry perot cavity as a reference and are currently characterizing its performance.

In the process of developing the coherent transient technology for adaptive phased-array beam forming, we have discovered that the same time delay compensation techniques that we have been developing for beam forming can be applied to compensating wavelength dispersion effects in high bandwidth fiber communications.

We plan to experimentally demonstrate the principles of the time delay compensation utilized in the coherent transient beam forming system by showing the capability for multimode fiber dispersion compensation. The technologies are very similar in that they both simultaneously compensate the time delay of a large number of beams and give coherent recombination. In the case of beam forming, the beams are individual antenna's each receiving the same signal at a slightly different delay based on the incident angle of the incoming signal. In the case of multimode fiber communications, the beams are the modes of the multimode fiber which travel at different velocities with respect to each other thereby impart a net time delay unique to each mode giving a similar effect to that of an array of antennas.

We are currently pursuing a patent based on this technology. Several optical signal processing architectures have been designed to demonstrate this application and these will be demonstrated shortly.

3.3 Laser Stabilization

To optimally process high bandwidth optical signals using coherent transients, it is necessary that the laser source that is being modulated is tunable and has frequency stability (linewidth) better than hundred kilohertz over a time interval of several milliseconds. This laser stability is required because the material frequency resolution (also known as homogeneous broadening) is on the order of several hundred kilohertz. In order to realize the full potential of these materials, it is necessary to use a laser with a linewidth equal to or less than the material resolution.

We decided to use semiconductor laser diodes since they are less expensive, have the correct wavelength, and are easy to work with. Since typical single-mode laser diodes have linewidths on the order of tens of megahertz and are not smoothly tunable, it is necessary to stabilize diodes using frequency selective feedback which allows tunability and linewidth narrowing. Over the past two years, we have developed several semiconductor laser systems capable of smooth tuning and a significant narrowing in linewidth. Several methods have been implemented including the optical feedback techniques of external gratings and external Fabry-Perot cavities. In addition, we have implemented an electronic stabilization technique known as Pound-Drever-Hall frequency locking that uses an external reference (such as a Fabry-Perot cavity or an atomic vapor cell resonance) to produce an error signal which can be used to make rapid corrections to the laser frequency by current injection thereby correcting laser frequency jitter and narrowing long term linewidth. We are currently in the process of fully characterizing the effects of electronic locking on the laser frequency stability.

In addition to frequency locking to an atomic vapor cell or Fabry-Perot cavity, our desire is to use a spectral hole as a reference source and lock the laser frequency to it. The next step of stabilizing lasers will be building an apparatus for obtaining frequency locking to a spectral hole using Tm:YAG crystal. In this way, arbitrary wavelengths within the inhomogeneous distribution (17GHz) of frequencies can be chosen as a frequency reference as opposed to the approach of using a separate atomic vapor cell as a reference which limits the potential wavelengths that a laser can be locked to. Each different crystal into which Tm^{3+} is doped has a slightly different shift of the inhomogeneously broadened absorption band making the selection of an appropriate atomic reference problematic. It is preferable to use the resonance structure of the coherent transient materials as the reference. This can be done by locking to the entire inhomogeneous band (whose width is 17GHz), but sub-megahertz stability is unlikely with this technique. Another approach is to first write a spectral hole inside the inhomogeneous linewidth which can be on the order of 100kHz. Using this self-made feature as the reference, one should be able to obtain frequency stability on the order of tens of hertz.

3.4 Coherent Transient signal processing

The coherent transient laboratory facilities at the University of Colorado has been built over the past year and is currently capable of processing optical information at bandwidths up to 30MHz with a time bandwidth of up to 400. High bandwidth electro-optic modulators and acousto-optic deflectors (AOD) have been ordered which will increase the potential processing bandwidth to the hundreds of megahertz level.

With the current lab setup, we have performed experiments with one beam (collinear) and two beam geometries. Upon receiving the AOD, we will have the potential of. building architectures which can process up to 500 channels of information simultaneously.

Thanks to a collaborative visit from Drs. Randy Babbitt and Kris Merkel, we performed our first two and three pulse echoes at CU in July 1999. The results of these experiments are illustrated in figures 3- 6.

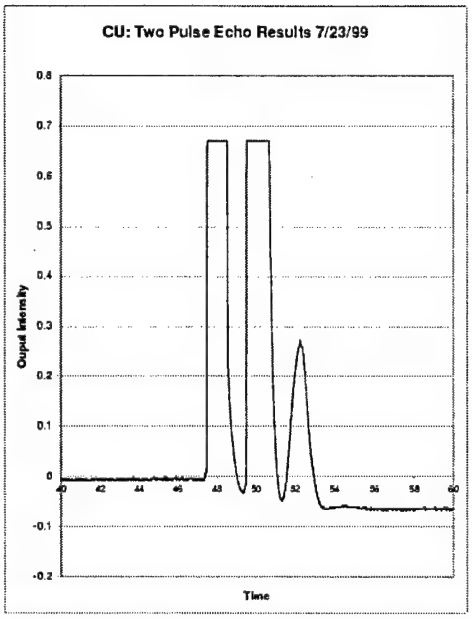

Figure 3: First two pulse echo experimental demonstration at CU

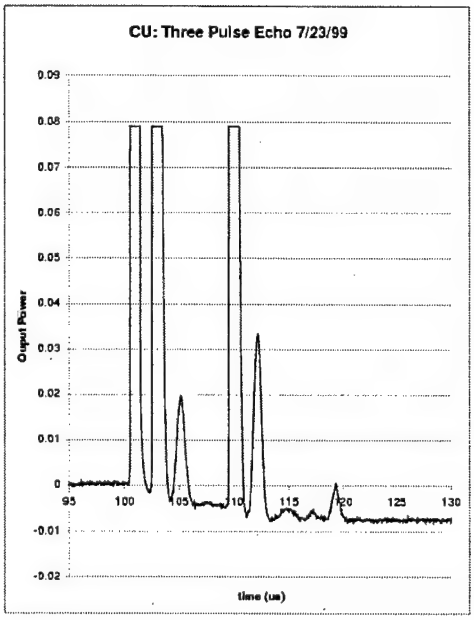

Figure 4: First three pulse echo experimental demonstration at CU

Since this time, we have been studying the material characteristics of several samples and have been optimizing the overall architectural performance of the system to maximize the potential time-bandwidth product that can be achieved in future experiments.

In addition, we are currently building an optical signal processing setup which will allow us to demonstrate a raster correlator. Demonstrating this will be a stepping stone towards building efficient signal processing systems using coherent transient effects.

4 Year 3 Additional Progress: Dispersion Compensation

Much of the modern research and development in fiber optics emphasizes the use of wavelength division multiplexing (WDM) to increase the capacity of single mode fiber communication systems, which are limited to about 128 channels. A revolutionary breakthrough would be a technique that could encode information on the different spatial modes of a multimode fiber, because this would allow multiplexing of up to 10^4 signals, dramatically increasing communication capacity. With current approaches, however, this appears totally infeasible because of the complexity of launching individual modes. The inevitable coupling of modes due to enormous modal dispersion, perturbations, and the intractability of separating out the superposition of modes at the multimode fiber output. However, during the past year we have extended our work on phased array beamforming

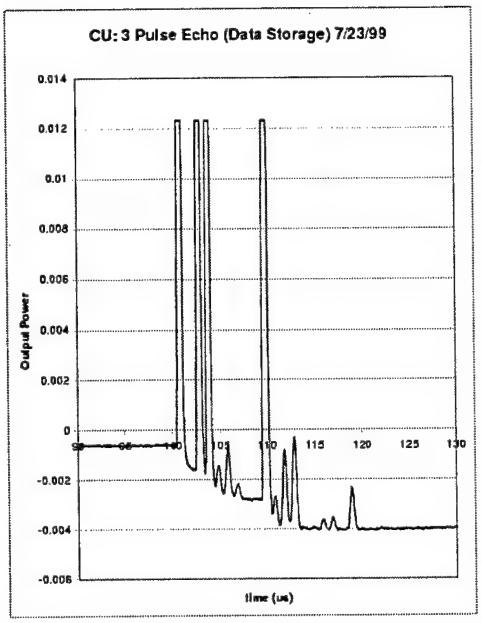

Figure 5: First two bit "data storage" experimental demonstration at CU

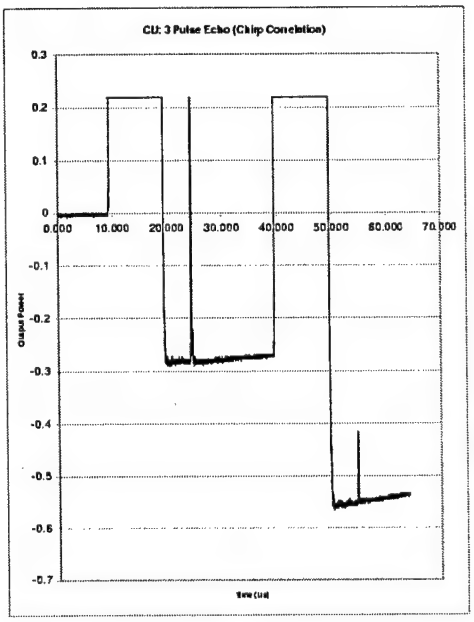

Figure 6: First Chirp correlation experimental demonstration at CU

using optical coherent transients to solve all of these issues and potentially provide the next evolution of fiber capacity. The multi-channel multimode Dispersion (MCMD) compensator system is shown in figure 7. Using one multimode fiber, a spatial-spectral hologram is first used to record the impulse response of each communications channel. This programming step is accomplished by sequentially modulating each of the NxN modulators with an impulse of light. The impulse having bandwidth equal to or large than the desired throughput of the system once it is transmitting data. Each impulse, $f_m(t) = \delta(t)$, is coupled into a multimode fiber as a unique input beam, $\bar{u}(\vec{r}_t)$, and is spatially decomposed into M spatial eigenmodes within the fiber. During propagation through the system, the impulse will encounter various other linear perturbations due to chromatic dispersion, modal dispersion, modal coupling, polarization decomposition, and polarization mode dispersion. At the output of the fiber the signal can be written:

$$\bar{E}_0^m(\vec{r},\omega) = \sum_{l=1}^{M} a_{l,m}\bar{H}_l(\vec{r}_t,\omega)F(\omega) \tag{4}$$

where m is the mth channel, $\bar{H}_l(\vec{r}_t,\omega)$ is the transfer function of the l_{th} mode of the multimode fiber,

$$\bar{H}_l(\vec{r}_t,\omega) = \bar{M}_l(\vec{r}_t)e^{i(k_z(\omega,l)\cdot d-\omega t)}, \tag{5}$$

$\bar{M}_l(\vec{r}_t)$ is the spatial mode profile of mode l, $F(\omega) = \mathcal{F}\{\delta(t)\}$ is the spectrum of the impulse of modulator m, and $a_{l,m}$ is the amplitude and phase of the mode l after being coupled in to the fiber and is a result of projecting the vector field onto mode l using the projection operator

$$a_{l,m} = \int E_m\bar{u}_m(\vec{r}_t)\cdot\bar{M}_l(\vec{r}_t)d\vec{r}_t. \tag{6}$$

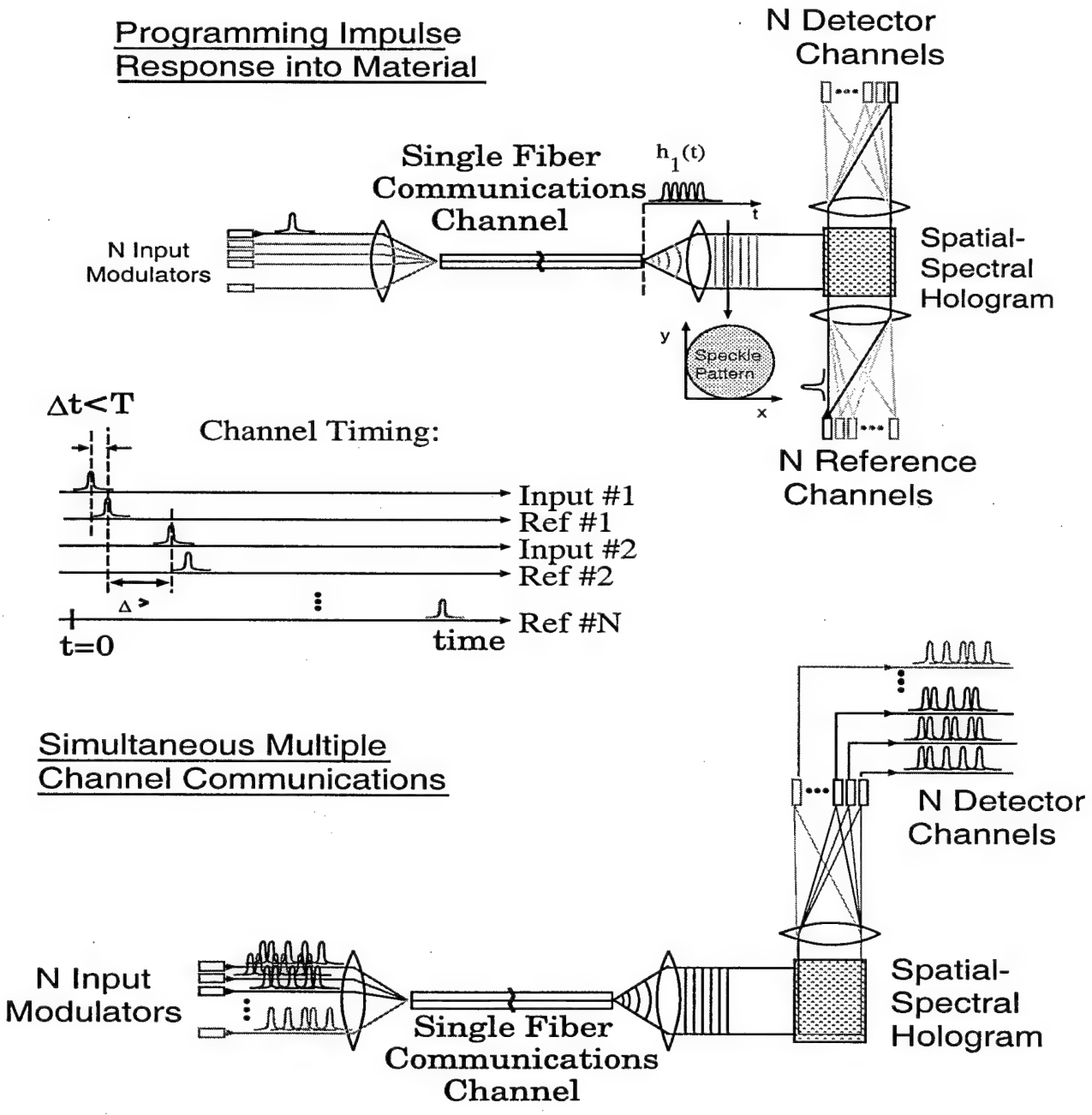

Figure 7: Multichannel-multimode fiber dispersion compensation

The field from the mth modulator is focussed onto the fiber end face with profile $\bar{u}_m(\vec{r}_t)$ and amplitude E_m, and since the modulators are separated in space

$$\int \bar{u}_m(\vec{r}_t)\bar{u}_n(\vec{r}_t)d\vec{r}_t = \delta_{nm} \tag{7}$$

After the field leaves the fiber, it propagates through an imaging system and into the crystal. This propagation can be written as a linear field imaging operator, $\mathcal{L}_z$, which takes into account imaging and fresnel propagation of the output plane of the fiber into the crystal at depth z. The

field throughout the crystal can be represented as

$$\bar{E}_1^m(\vec{r},\omega) = \mathcal{L}_z\left\{\bar{E}_0^m(\vec{r}_t,\omega)\right\} \tag{8}$$

where $\vec{r}$ spans the extent of the crystal, and $\vec{r}_t$ is a 2-D transverse position vector of the fiber end face.

The m_{th} reference beam is used to illuminate the crystal with a plane wave and can be represented as

$$\bar{E}_2^m(\vec{r},\omega) = R(\omega)e^{i\left(\vec{k}_r^m\cdot\vec{r}-\omega t\right)}e^{-i\omega\tau_2}\hat{e}_2 \tag{9}$$

where $r(t) = S(t-\tau_2)$ and $R(w) = e^{-i\omega\tau_2}$ is the spectrum of the reference impulse that is delayed with respect to the channel impulse by a time τ_2. τ_2 must be longer than the fiber delay in order to set up the desired material response.

The fields E_1^m and E_2^m form a spatial-spectral interference pattern which is recorded inside the crystal. After this recording has been completed, the impulse response of the next channel is recorded using the same technique. In this manner, a separate spatial-spectral grating is recorded for each of the m channels. Upon recording all of the channel impulse responses, the system is ready to be used. Each of the m channels can now be simultaneously modulated, propagated down the fiber and imaged into the crystal where it is modulated by the spatial spectral grating. The field in the crystal is similar to that of the impulse response; although, instead of an impulse, the full spectrum of channel m, $S_m(\omega)$, is multiplied by the transfer function of the system and imaged into the crystal.

$$\bar{E}_3^m(\vec{r},\omega) = \mathcal{L}_{z'}\left\{\sum_{l'}\sum_{m'} a_{l',m'}\bar{H}_{l'}(\vec{r}_t,\omega)e^{-i\omega\tau_3}S_{m'}(\omega)\right\} \tag{10}$$

The crystal response can then be represented as the interaction of the m channels of modulated information $\sum_{m'}\bar{E}_3^m$ with the prerecorded interference patterns that were stored in the crystal $\sum_m(\bar{E}_1^{m*}\bar{E}_2^m)$ and can be written

$$o(\vec{k}_r^{m''},t) = \eta\int_{-\infty}^{\infty} e^{-i\left(\vec{k}_r^{m''}\cdot\vec{r}\right)}\int e^{i\omega t}\sum_m(\bar{E}_1^{m*}\bar{E}_2^m)\sum_{m'}\bar{E}_3^{m'}\,d\omega d\vec{r} \tag{11}$$

where the response is Fourier transformed into the time domain and integrated over the volume of the crystal to give an output propagating in the direction $veck_r^{m''}$. Substituting in for $\bar{E}_1^m$,$\bar{E}_2^m$, and $\bar{E}_3^{m'}$ gives

$$\begin{aligned} o(\vec{k}_r^{m''},t) = \eta\sum_l\sum_{l'}\int_{-\infty}^{\infty} e^{-i\left(\vec{k}_r^{m''}\cdot\vec{r}\right)}\int a_{lm}^*\mathcal{L}_z^*\left\{\bar{H}_l(\vec{r}_t,\omega)\right\}F^*(\omega)R(\omega)e^{i(\vec{k}_r^{m'}\cdot\vec{r}-\omega t)} \\ a_{l'm'}\mathcal{L}_z^*\left\{\bar{H}_{l'}(\vec{r}_t,\omega)\right\}S(\omega)e^{i\omega(t-\tau_2-\tau_3)}d\omega d\vec{r} \end{aligned} \tag{12}$$

At this point, several simplifications are necessary. The spectrums of $R(\omega)$ and $F(\omega)$ can be simplified to unity since they are a result of impulses. The orthogonality of the eigenmodes of a multimode fiber gives

$$\int M_l^*(\vec{r}_t)M_{l'}(\vec{r}_t)d\vec{r}_t = \delta_{ll'}, \tag{13}$$

the non-overlapping input modulators and the non-overlapping reference beam modulators gives

$$\int e^{i\vec{k}_r^m \cdot \vec{r}} e^{i\vec{k}_r^{m'} \cdot \vec{r}} dz = \delta_{\vec{k}_r^m - \vec{k}_r^{m'}} = \delta_{mm'} \tag{14}$$

so that

$$\int H_l^*(\vec{r}_t) H_{l'}(\vec{r}_t) d\vec{r}_t = \int M_l^*(\vec{r}_t) e^{-i(k_z(\omega,l')\cdot d - \omega t)} M_{l'}(\vec{r}_t) e^{i(k_z(\omega,l)\cdot d - \omega t)} d\vec{r}_t = \delta_{ll'}.. \tag{15}$$

Therefore, equation 13 becomes

$$o(\vec{k}_r^{m''}, t) = \eta \sum_l |a_l|^2 \int S^{m'}(\omega) e^{i\omega(t-\tau_2-\tau_3)} dw \int_0^L dz = S^{m'}(t - \tau_2 - \tau_3). \tag{16}$$

The result shows that the original signal is restored with all the effects of fiber modal dispersion, coupling and even PMD removed while each of the m' input signals is diffracted towards a unique output detector.

To demonstrate multiple channel dispersion compensation, we have designed and analyzed a system which is outlined in Figure 8. This architecture utilizes the 80MHz pulse repetition rate from a picosecond pulsed laser to generate high enough bandwidth signals to demonstrate the full bandwidth processing potential of the Tm:YAG spatial-spectral holographic programming medium. Gate 1 and Gate 2 are used to pull out bits (pulses) from the 80MHz stream of pulses. This gives us the first impulses of each channel followed by two separately programmable streams of data in some predetermined information bearing capacity. Each channel is then coupled into a kilometer of multimode step-index fiber which gives about 1 microsecond of delay with a total dispersion on the order of 25ns. Thus, each individual bit or pulse with be broadened from being picoseconds in duration to about 25 nanoseconds. Upon exiting the multimode fiber, all of the channels are then imaged through the Spatial-Spectral Holographic recording medium. The reference arm of the demonstration device is composed of a kilometer long single mode fiber (used to ensure proper coherence between the interfering bits of data) and two gates which pick off reference pulses from the 80MHz stream and, with the proper timing, these reference pulses are steered such that they spatially overlap both communication channels inside the material and write a spatial-spectral impulse response grating. The subsequent bit streams from both channels then interacts with this recorded impulse response grating to produce a deconvolved signal with all linear perturbations removed including any dispersional effects (chromatic and modal) that caused pulse spreading in the communications channel. Reprogramming of the spatial-spectral impulse response grating only occurs when the grating has deteriorated due to natural material relaxation processes which can range on order of milliseconds to many hours in rare earth materials.

Building an optimal demonstration system will require gigahertz AO modulators (used as gates), high bandwidth detectors (50GHz), a picosecond laser system, and several kilometers of multimode fiber that, at this point, we don't currently have in our laboratory facilities.

5 Scientific Personnel working on the project

- Eric Hoyte - undergraduate student, BS earned, MS in Progress
- Ken Anderson - graduate student, PhD earned
- Kelvin Wagner - Advisor

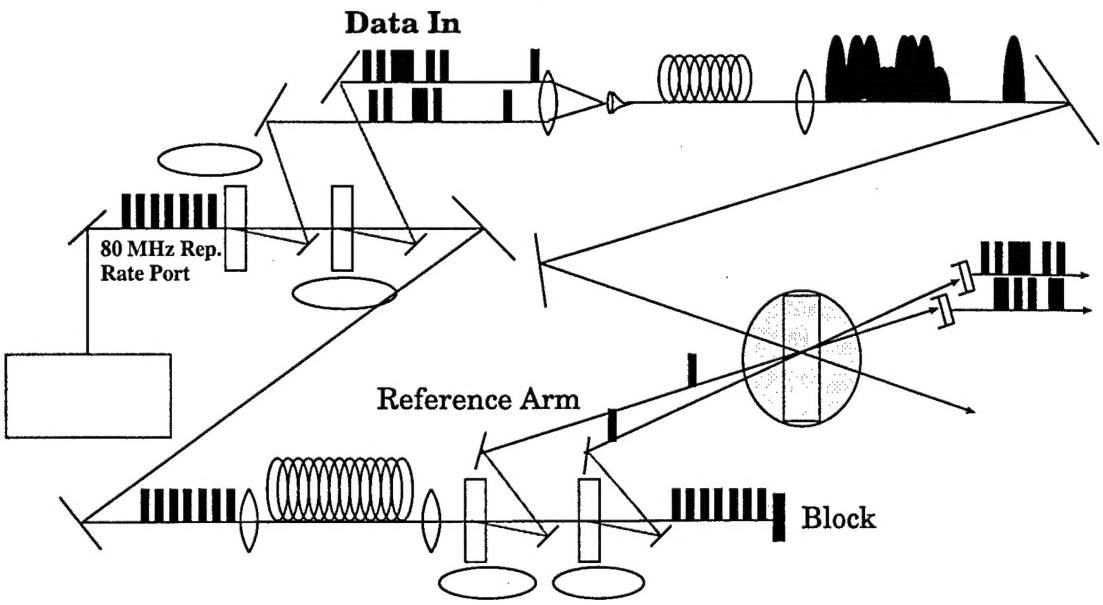

- **20 picosecond Pulses @ 80MHz Repetition Rate**
- **1Km Multimode fiber = 25nm Disperion/pulse**
- **50GHz Detectors**
- **Singlemode Fiber Transmits Reference Pulses**
- **Built in Crossbar Switching**

Figure 8: Two Channel Demonstration Setup of Multichannel Dispersion Compensation

6 Papers, Talks, and Patents

6.1 Thesis supported by DEPSCoR

1. Kenneth E. Anderson, Multidimensional optical signal processing using optical coherent transient spatial-spectral holography, PhD Thesis, Dept of Electrical and Computer Engineering, University of Colorado, Boulder, CO, May 31, 2001.

6.2 Papers Published

1. K.D. Merkel, W.R. Babbitt, K.E. Anderson, K.H. Wagner, "Variable-time-delay optical coherent transient signal processing", Optics Letters, **24**, 1386, 1999.

6.3 Conference Papers Published

1. K.E. Anderson, K.H. Wagner, "Multidimensional Photon Echo Optical Processing", OSA Optics in Computing 1997 - Postdeadline paper.

2. K.E. Anderson, K.H. Wagner, "Optical Coherent Transient True-Time-Delay Beamforming Processor", OSA Optics in Computing 1999.

3. K. H. Wagner, K. Anderson, W.R. Babbitt, and K. D. Merkel, Multidimensional photon echo processing, (Invited Paper) Proceedings of the SPIE, Optical Science, Engineering, and Instrumentation, Denver, CO, July 18-23, 1999, Algorithms, devices, and systems for optical information processing II, Vol. 3804, paper 3804-03 (1999).

4. K. H. Wagner, K. E. Anderson, K. D. Merkel, and W. R. Babbitt, Photon Echo Adaptive Array Processor, (Invited Paper) presented at 6th Int. Meeting of Hole Burning and Related Spectroscopies: Science and Applications (HBRS'99), September 18-23, 1999, Hourtin, France.

5. Ken E. Anderson, K.W. Wagner, "Chromatic and Polarization Mode Dispersion Compensation Using Spectral Holography", OFC 2001, Anaheim CA, Mar 2001.

6. Ken E. Anderson and Kelvin H. Wagner Demonstration of Chromatic Dispersion Compensation Using Spectral Holography, Persistend Spectral Hole Burning 2001 - PSHB 2001, Taiwan, Nov 2001.

6.4 Talks Given

1. K.E. Anderson, K.H. Wagner, "Multidimensional Photon Echo Optical Processing", OSA Optics in Computing 1997.

2. K.E. Anderson, K.W. Wagner, "Multidimensional Optical Signal Processing Architectures Utilizing Photon Echoes", Spectral Holeburning 1998 Annual Conference.

3. K.E. Anderson, K.H. Wagner, "Optical Coherent Transient True-Time-Delay Beamforming Processor", OSA Optics in Computing 1999.

4. K.E. Anderson, K.W. Wagner, "Spatial-Temporal Dispersion Compensation for High Bandwidth Communications", OSA Annual 1999 talk.

5. K.E. Anderson, K.W. Wagner, "Spatial-Temporal Dispersion Compensation Utilizing Photon Echoes" , Spectral Holeburning 1999 Annual Conference.

6. K.E. Anderson, K.W. Wagner, "System Issues in Simultaneous Space-Time Coherent Transient Optical Signal Processing", Spectral Holeburning 2000 Annual Conference.

7. K.E. Anderson, "Optical Data Storage", Undergraduate class lecture series in Magnetic Data Storage 2000.

6.5 Patent Applications

1. K. E. Anderson, K.D. Merkel, W.R. Babbitt, K.H. Wagner, "Method and Apparatus for Variable Time Delay Optical Coherent Transient Signal Processing", Patent Pending, #60/152,611

2. K.E. Anderson, "Spatial-Temporal Linear Compensator", Patent Pending, #60/123,346.

3. K.E. Anderson, K.W. Wagner, "Method of Polarization Mode Dispersion Compensation using dispersive element and spatial holography", Patent Application in Progress.

4. K.E. Anderson, "Polarization Mode Dispersion Compensation using spectral decomposition and Polarization Rotation", Patent Application in Progress

5. K.E. Anderson, "Simultaneous Polarization Mode Dispersion Compensation and wavelength routing", Patent Application in Progress.

6.6 Papers in progress related to DEPSCoR

1. K.E. Anderson, F. Schlotta, K. Wagner, J.L. Legouet, I. Logere, Photon Echo based coherent scanners, to be submitted to Applied Optics.

2. K.E. Anderson, F. Schlotta, K. Wagner, Multimode fiber adaptive mode multiplexing, routing, and dispersion compensation using spatial-spectral holography, to be submitted to Applied Optics.

3. K.E. Anderson, F. Schlotta, K. Wagner, Raster correlators with high TB photon echoes, to be submitted to Applied Optics.

4. F. Schlotta, K. Wagner, J. Bregman, Correlation Based Array Imaging with Photon Echoes, to be submitted to Applied Optics.

5. F. Schlotta, K. Wagner, W.R. Babbitt, K. Merkel, Range-Doppler processing using accumulated spectral gratings, to be submitted to Applied Optics.